NUMERICAL AND EXPERIMENTAL PERFORMANCE ANALYSIS OF PCM BASED PHOTOVOLTAIC THERMAL SYSTEM

FAYAZ HUSSAIN

INSTITUTE FOR ADVANCED STUDIES
UNIVERSITY OF MALAYA
KUALA LUMPUR

2019

NUMERICAL AND EXPERIMENTAL PERFORMANCE ANALYSIS OF PCM BASED PHOTOVOLTAIC THERMAL SYSTEM

FAYAZ HUSSAIN

THESIS SUBMITTED IN FULFILMENT OF THE REQUIREMENTS FOR THE DEGREE OF DOCTOR OF PHILOSOPHY

INSTITUTE FOR ADVANCED STUDIES
UNIVERSITY OF MALAYA
KUALA LUMPUR

2019

UNIVERSITY OF MALAYA

ORIGINAL LITERARY WORK DECLARATION

Name of Candidate: **Fayaz Hussain**

Registration/Matric No: **HHD140003**

Name of Degree: **Doctor of Philosophy**

Title of Thesis ("this work"): **Numerical and Experimental Performance Analysis of PCM Based Photovoltaic Thermal System**

Field of Study: **Energy**

I do solemnly and sincerely declare that:

(1) I am the sole author/writer of this Work;
(2) This Work is original;
(3) Any use of any work in which copyright exists was done by way of fair dealing and for permitted purposes and any excerpt or extract from, or reference to or reproduction of any copyrighted work has been disclosed expressly and sufficiently and the title of the Work and its authorship have been acknowledged in this Work;
(4) I do not have any actual knowledge nor do I ought reasonably to know that the making of this work constitutes an infringement of any copyrighted work;
(5) I hereby assign all and every right in the copyright to this Work to the University of Malaya ("UM"), who henceforth shall be owner of the copyright in this Work and that any reproduction or use in any form or by any means whatsoever is prohibited without the written consent of UM having been first had and obtained;
(6) I am fully aware that if in the course of making this Work I have infringed any copyright whether intentionally or otherwise, I may be subject to legal action or any other action as may be determined by UM.

Candidate's Signature   Date:

Subscribed and solemnly declared before,

Witness's Signature   Date:

Name:

Designation:

NUMERICAL AND EXPERIMENTAL PERFORMANCE ANALYSIS OF PCM BASED PHOTOVOLTAIC THERMAL SYSTEM

ABSTRACT

Climate change due to global warming is the major on-going concern among the scientists and governments. Fossil fuels play the major role in both global warming and world's mainstream energy resources on which global economy is almost fully dependent. However, these harmful fossil fuels are fast depleting, creating the situation of low supply and high demand along with environmental pollution. Therefore, many researchers from all over the world have researched new energy sources, which are clean and non-depleting. Abundantly available solar energy is the best option of harnessing clean and non-depleting energy among the other renewable energy resources. Irradiations incident on the photovoltaic module are not fully converted into electrical energy as PV modules convert only 15-20% with the rest are lost into heat conversion. Incorporation of thermal collectors into photovoltaic panels has two-fold advantages of increasing PV module efficiency through highest irradiations and hot water for different applications. However, low heat transfer from PV module to the thermal collector and other technical complications result in the overall reduced performance of the system. There is still need of research numerically based on 3D models to understand and investigate their performance thoroughly. Heat transfer of the system greatly depends on the design and material of the thermal collector and flow path of working fluid along with its method/technic of contact with PV module. To deal with these problems, a new design of thermal collector has been introduced for increasing the efficiency of the photovoltaic system regarding electrical energy as well as thermal. Nanofluid as multi-walled carbon nanotubes/water (MWCNT/water) is also used as working fluid to additionally investigate the performance of PVT with nanofluids. Furthermore, phase change materials (PCM) are added in the photovoltaic thermal system for studying enhanced low cell temperature and stable thermal management as compared to the photovoltaic thermal system. COMSOL Multiphysics® has been used for 3D numerical investigation of the proposed systems based on the finite element method. Numerical optimum results are validated with indoor and outdoor experimental data of fabricated PV, PVT and PVT-PCM systems with aluminium heat exchanger simultaneously with the indoor controlled environment and outdoor natural weather. Effect of parameters such as irradiation level and mass flow rates are thoroughly examined in numerical and experimental studies. For indoor case, the maximum overall efficiency of PVT and PVT-PCM systems is obtained as 92.24% and 88.32% at 200 W/m^2 and 0.5 LPM with ambient and inlet water temperatures of 27°C experimentally. For outdoor case, the maximum overall efficiency of PVT and PVT-PCM systems is obtained as 88.95% and 85.53% at 200 W/m^2 and 0.5 LPM with ambient and inlet water temperatures of 32°C experimentally. It has been found that PVT-PCM system is efficient in electrical performance. However, PVT system is efficient in thermal energy gain into water. For electrical efficiency requirements, PVT-PCM is a better candidate, whereas, PVT system is suitable where higher thermal energy is required as compared to electrical energy.

Keywords: Energy; Photovoltaic; Thermal; Phase change materials; Finite element analysis.

ANALISIS PRESTASI NUMERIK DAN EKSPERIMEN PCM BERASASKAN SISTEM FOTOVOLTAIK HABA

ABSTRAK

Perubahan iklim akibat pemanasan global adalah kebimbangan utama yang berterusan di kalangan saintis dan kerajaan. Bahan api fosil memainkan peranan penting dalam pemanasan global dan sumber tenaga arus utama dunia di mana ekonomi global hampir bergantung sepenuhnya kepada sumber tersebut. Walau bagaimanapun, bahan api fosil yang berbahaya ini semakin berkurangan, mewujudkan kadar bekalan yang rendah serta permintaan yang tinggi dan juga mengakibatkan pencemaran. Oleh itu, ramai penyelidik di seluruh dunia telah mengkaji sumber tenaga baru, yang bersih dan tidak berkurangan. Di antara sumber tenaga yang boleh diperbaharui yang lain adalah tenaga solar yang banyak tersedia ada dan ia adalah pilihan terbaik untuk memanfaatkan sumber tenaga bersih dan tidak berkurangan. Kejadian penyinaran pada modul fotovoltaik tidak diubah sepenuhnya kepada tenaga elektrik kerana modul PV hanya menukar 15-20% sahaja. Justeru, sisa peratusan yang berubah menjadi tenaga panas menurunkan kecekapan elektrik modul. Penggabungan pengumpul haba ke panel fotovoltaik mempunyai kelebihan dua kali ganda peningkatan tenaga elektrik pada modul PV dan digunakan untuk penyediaan air panas untuk aplikasi yang berbeza. Walau bagaimanapun, pemindahan haba yang rendah dari modul PV kepada pengumpul haba dan juga komplikasi-komplikasi teknikal yang lain mengakibatkan prestasi keseluruhan sistem berkurangan. Terdapat penyelidikan secara numerik berdasarkan model 3D untuk memahami dan menyiasat prestasi tersebut dengan teliti. Sistem pemindahan haba adalah sangat bergantung pada reka bentuk dan bahan pengumpul haba atau aliran-aliran cecair kerja bersama dengan kaedah / teknik hubungan dengan modul PV. Untuk menangani masalah ini, dalam kajian ini, satu reka bentuk pengumpul haba yang novel telah diperkenalkan untuk meningkatkan kecekapan sistem fotovoltaik

mengenai tenaga elektrik serta haba. Cecair nano sebagai MWCNT/air juga digunakan sebagai cecair kerja untuk mengkaji prestasi PVT dengan cecair nano. Selain itu, bahan-bahan perubahan fasa ditambah ke dalam sistem terma fotovoltaik untuk mengkaji suhu sel yang dapat dipertingkatkan dan menjamin pengurusan haba yang stabil berbanding dengan sistem terma fotovoltaik. Perisian berasaskan elemen infiniti COMSOL Multiphysics telah digunakan untuk penyiasatan berangka 3D untuk sistem yang dicadangkan. Keputusan optimum berangka disahkan melalui data eksperimen dalaman dan luaran PV, PVT dan sistem PVT-PCM yang direka dengan penukar haba aluminium serentak dengan persekitaran terkawal dalaman dan cuaca semula jadi luaran. Kesan parameter seperti tahap penyinaran dan kadar aliran jisim diperiksa dengan teliti dalam kajian berangka dan eksperimen. Untuk kes kondisi tertutup secara eksperimen, kecekapan keseluruhan maksimum PVT dan sistem PVT-PCM yang diperolehi adalah 92.24% dan 88.32% pada 200 W/m^2 dan 0.5 LPM dengan suhu air ambien sebanyak 27°C. Untuk kes kondisi luaran secara eksperimen, kecekapan keseluruhan sistem PVT dan PVT-PCM maksimum yang diperolehi adalah 88.95% dan 85.53% pada 200 W/m^2 dan 0.5 LPM dengan suhu air sekitar 32°C. Penyelidikan ini telah mendapati bahawa sistem PVT-PCM adalah cekap dalam prestasi elektrik, manakala sistem PVT adalah cekap dari segi keuntungan tenaga haba. Untuk keperluan kecekapan elektrik, PVT-PCM adalah calon yang lebih baik, sedangkan sistem PVT adalah sesuai sekiranya tenaga haba yang tinggi diperlukan berbanding dengan kecekapan elektrik.

Kata kunci: Tenaga; Fotovoltaik; Terma; Bahan perubahan fasa; Analisis elemen terhad.

ACKNOWLEDGEMENTS

First of all, I exhibit the gratitude to Almighty Allah, who gave me the strength to complete the thesis successfully. I fully got the esteem, inspiration and sacrifices of all of my family during the period of my candidature. I am pleased to confer my gratitude and respect to my supervisors **Prof. Dr Nasrudin Abd Rahim** and **Dr Md. Hasanuzzaman** for their sincere, encouraging and dedicated support and exploration throughout my candidature.

I express my gratitude to the IPS and the UMPEDAC staff who helped me kindly and sincerely to conduct my research and complete with success. I am thankful to the UMPEDAC for kind financial support as well as the financial support from the University Malaya IPPP fund to carry out this research project successfully.

TABLE OF CONTENTS

LIST OF FIGURES

LIST OF TABLES

LIST OF SYMBOLS AND ABBREVIATIONS

A	:	Total PV cell area (m^2)
A_{sc}	:	Area of each solar cell (m^2)
B	:	Bias error
C_p	:	Specific heat at constant pressure (J/kg.K)
E_c	:	Total solar energy rate into the cell (W)
E_{el}	:	Electrical energy rate (W)
Ep	:	Module's electrical power (W)
E_t	:	Thermal power in the system (W)
E_{th}	:	Thermal energy rate extracted by water (W)
g	:	Accelaration due to gravity (m/s^2)
G	:	Solar irradiance (W/m^2)
h	:	Heat transfer coefficient ($W/m^2.K$)
k	:	Thermal conductivity (W/m.K)
L	:	Length (m)
m	:	Mass flow rate (kg/s)
N	:	Number of data
Nu	:	Nusselt number
p	:	Pressure (Pa)
P_c	:	Packing factor
Pe	:	Perimeter (m)
Pr	:	Prandtl number
q	:	Inward heat flux (W/m^2)
R	:	Solar irradiance (W/m^2)
R_x	:	Precision

Ra	:	Rayleigh number
Re	:	Reynolds number
S_F	:	Standard deviation
T	:	Temperature (^oC/K)
t	:	Time (s)
u,v,w	:	Velocity components along axes x, y and z
U	:	Overall heat transfer coefficient (W/m^2.K)
U_o	:	Inlet water velocity (m/s)
U_x	:	Measurement uncertainty
V	:	Wind speed (m/s)
t_λ	:	Estimate of the precision error
X'	:	True value
$\bar{X}$	:	Mean value

Greek symbols:

α	:	Absorptivity
β_{ref}	:	Temperature coefficient at reference temperature of 25^{o}C
μ	:	Dynamic viscosity (Pa.s)
v	:	Kinematic viscosity (m^2/s)
ρ	:	Density (kg/m^3)
η	:	Efficiency (%)
$\overline{\eta_{el}}$	:	Average electrical efficiency (%)
τ	:	Transmissivity
ε	:	Emissivity
σ	:	Stefan-Boltzmann constant W/(m^2.K^4)

δ	:	Thickness (m)
λ	:	Degree of freedom

Subscripts:

amb	:	Ambient
c	:	PV cell
ch		Channel
el	:	Electrical
d	:	Duct
f	:	Fluid
g	:	Glass
in	:	Inlet
out	:	Outlet
pcm,s	:	Phase change material, solid form
pcm,l	:	Phase change material, liquid form
ref	:	Reference
s	:	Sky
S	:	Solid/Surface
sc	:	Solar cell
t	:	time
td	:	Tedlar
th	:	Thermal
tol	:	Total
w	:	Water

Abbreviations:

Al	:	Aluminium
BE	:	Boundary element
BV	:	Boundary volume
BIPV	:	Building integrated photovoltaic
BIPV/T	:	Building integrated photovoltaic thermal
CFD	:	Computational fluid dynamics
CHP	:	Combined heat and power
CHT	:	Conjugate heat transfer
CPC	:	Compound parabolic collector
CPV	:	Concentrator photovoltaic
CPV/T	:	Concentrator photovoltaic thermal
CSP	:	Concentrating solar power
Cu	:	Copper
DC	:	Direct current
DSWH	:	Domestic solar water heater
EIA	:	Energy information administration
ESTELA	:	European Solar Thermal Electricity Association
EVA	:	Ethyl vinyl acetate
FD	:	Finite difference
FE	:	Finite element
FEM	:	Finite element method
FV	:	Finite volume
GHG	:	Greenhouse gas
GWEC	:	Global Wind Energy Council
HTF	:	Heat transfer fluid

IEA	:	International Energy Agency
IHA	:	International Hydropower Association
LPM	:	Liter per minute
MWCNT	:	Multi-walled carbon nanotubes
PV	:	Photovoltaic
PVF	:	Polyvinyl fluoride
PV/T	:	Photovoltaic thermal
REN21	:	Renewable Energy Policy Network for the 21st Century
STC	:	Standard testing condition

CHAPTER 1: INTRODUCTION

1.1 Background

The need for comfort and dependence of humans on technology has started the race among the nations to grow the economy. The economy of any nation depends totally on low cost and reliable source of energy demand and supply balance. The scenario of current energy sources has caused the environmental pollution, climate change and depletion. The reason behind climate change is the greenhouse gases especially CO_2 emitted form majorly used fossil fuels. To solve this issue, alternative sources of energy are under investigation and practically are harnessed to some level (Ahmed et al., 2013; Fayaz et al., 2011). Solar energy is one of the important and main resources of renewable energy abundantly available all over the world (N. Anderson et al., 2008). Solar energy is the world's most unrestricted continuous sources of energy, which is significant and environment-friendly power source (Daghigh et al., 2011).

There is a long history of harnessing thermal energy from the sun for cooking, drying etc. with multiple other applications. Since a few decades, research has broadly been carried out and industrial scale products e.g. photovoltaic technology has been commercially produced. However, photovoltaic panels have low electrical efficiency not more than 10-20%. Therefore, research on different methods is being carried out to enhance the electrical performance of photovoltaic panels. Thermal energy is obtained by using solar thermal collector whereas electrical power is achieved through PV cells. Usually, both systems are independently used. Comparatively, small electrical efficiency of PV cells is obtained. However, almost all of the solar irradiations are absorbed by the cells, which lead to conversion of almost all of the rest solar radiation absorbed into heat, which increases cell temperature following decreased electrical efficiency. For an efficient method to capture the heat produced in PV cells, combined system like PV-thermal collectors (PVT), can be used which also will increase PV efficiency. (Bertram et al., 2012; Dupeyrat et al., 2014). The collectors with a small area and installation costs are better candidates for solar energy applications (Othman et al., 2007). Some easy and inexpensive ways to eliminate heat from PV modules are forced or natural air convections, however, these are not as much of affectivity higher ambient temperatures than 20◦C (Chen et al., 2013; Hosenuzzaman et al., 2015; Kalogirou and Tripanagnostopoulos, 2006). However, the water-based thermal collector can be used to avoid this issue. PV/T system run on water as circulating fluid is capable to attain efficient thermal energy output per unit collector area. Further, the efficiency of PVT systems can be increased as compared to water when nanofluids based on water or other base are used (Ji et al., 2008).

Another method to reduce the temperature of cells is to introduce phase change materials (PCM) attached with PV panels, which in result absorb and store heat from PV cells. These materials have the ability to absorb great amount of heat in the form of latent heat by changing the phase from solid to liquid. Thermal energy is absorbed by PCM in the form of latent heat at the temperature constant phase change. It can be used along with an appropriate phase transition temperature to control the temperature of PV cells (Hasan et al., 2014; Huang et al., 2006) thus, sustaining increased efficiency of PV cells. In comparison to different ways of regulating temperature, its usage has added benefits of storing heat energy which can be used for extended time (Browne, M. et al., 2015). An ideal PCM should contain a huge latent heat of fusion, large thermal conductivity, a melting temperature lying in the practical variety of process, it should also liquefy congruently with least amount of sub-cooling, must be chemically firm, little cost, harmless and non-corrosive (Farid et al., 2004). Thus, incorporating PCM with PVT system increases the efficiency of PV panels.

1.2 Scope of Research

Malaysia is located on the equatorial area by way of solar irradiation of 400 MJ/m^2 to 600 MJ/m^2 on average per month. The country has good potential to create solar energy on a massive scale (Mekhilef et al., 2012). Photovoltaic panels provide electrical energy whereas solar thermal collectors provide thermal energy from solar radiations. However, if both systems can be combined to give a hybrid solar energy system that provides both electrical as well as thermal energy with many benefits as compared to separate PV and thermal collectors. Further, incorporation of PCMs and use of nanofluids as working fluid in the PVT systems can enhance the system performance.

The main scopes of this investigation are given in the following points:

- To introduce novel aluminium pipe design of thermal part of the system with a larger length of pipe will help enhance thermal and electrical efficiencies.
- To investigate indoor and outdoor electrical and thermal performance of the systems at different working conditions and the environment of University of Malaya, Kuala lumpur, Malaysia to understand in-depth performance behaviour of the systems.
- To apply the paraffin PCMs of the suitable temperature range to the PV panel with the thermal collector for reducing PV temperature and possible improvement in the overall performance of the systems.

1.3 Research Objectives

The study aims to investigate new thermal collector design of aluminium material of greater length water flow passage to enhance the heat transfer and output working fluid temperature. Moreover, application of PCMs will provide new information on heat transfer from PV to flowing water in the pipe and then PCM. It covers the main issues of PV efficiency, heat transfer, temporary heat storage in the PCM and overall heat gain in the tropic weather.

- To design and develop a model of solar PVT and PVT-PCM systems.
- To develop experimental PVT and PVT-PCM systems.
- To investigate the effect of different operating parameters on PV, PVT and PVT-PCM systems.
- To analyse and compare the overall performance of PV, PVT and PVT-PCM systems.

Standard procedures for the completion of these objectives are carried out. Numerical modelling of the proposed new design of thermal collector assembled in PV module with and without PCM is prepared in COMSOL Multiphysics®. The simulations are executed with indoor and outdoor working environment. Meshing and execution of models with required physical laws and governing equations are carried out. The proposed systems are separately assembled for achieving electrical and thermal data from all systems simultaneously with higher comparison accuracy. Operating parameters effect and the corresponding performance behaviour of the systems is investigated. All the necessary instrumentation and data acquisition processes are achieved to get experimental results in the desired parameters with minimum errors.

1.4 Thesis Outline

There are total five chapters in this thesis. Details of all thesis chapters are provided as below;

Chapter 2: This chapter is about the review of the previous literature. In this chapter, a review of solar energy technologies with their types, photovoltaic and photovoltaic thermal is conducted. Literature of phase change materials with and their prospects of incorporation into photovoltaic thermal technology is given. Furthermore, mathematical modelling of the current project and use of FEM software COMSOL Multiphysics are introduced.

Chapter 3: This is a methodology chapter, which presents the numerical and experimental methodology of the thesis project. Firstly, numerical investigation procedure, equations, boundary conditions, computational methods and mesh generations for PV, PVT and PVT-PCM are described. Secondly, experimental indoor and outdoor setups are demonstrated with all necessary instrumentation required for data acquisition.

Chapter 4: In this chapter, all the necessary results are provided for the investigation carried out on designed systems. Under indoor and outdoor working conditions, numerical temperature distribution over the systems and post-processed results of electrical as well as the thermal performance of the systems is presented. Results for indoor and outdoor experiments are also given in accordance with numerical ones for the validation.

Chapter 5: In this chapter, all the main essential findings of the present investigation are presented precisely. Future expected research gaps are introduced to carry on further research in the field and fulfil the gaps for advanced findings for the reliable and high-performance solar systems.

CHAPTER 2: LITERATURE REVIEW

2.1 Introduction

For the development of socio-economy of the nations, energy is an important and primary factor. Unfortunately, almost 80% of the fuel used all over the world is fossil-based (Luna-Rubio et al., 2012; Müller-Fürstenberger and Wagner, 2007). Furthermore, the worst form of fossil fuel, which emits a huge amount of carbon dioxide, is coal and its share in electricity generation is about 42% as compared to other fuels. In additions, it will continue to be a a major shareholder in energy supply till coming few decades (Sieminski, 2014). It may decline to 37% of electricity generation by 2035. In addition, the consumptions of energy worldwide will rise 50% more by the year 2030 if the pattern of energy demand remains the same (Suganthi and Samuel, 2012). The fossil fuels usage creates many challenges including environmental issue and its depletion. Thus, there is a need for green energy, which can have positive impacts on the environment and human's health and lifestyle. Clean energy with the advancement of its technology can satisfy the energy demand to some extent and keep the environment by reducing global warming. Recently, clean energy technology is getting mature and its share is rising day by day (Hinrichs-Rahlwes, 2013).

Amongst the clean energy sources, the most abundant and freely available source of energy is solar, which converts solar irradiations into thermal and electrical energy and is eco-friendly with minimum to zero emissions. The technology used for such solar irradiation conversion into thermal and electricity is called solar thermal and photovoltaic collectors. These solar collectors have many uses such as drying, heating and cooling etc. (Kumar et al., 2015). For electrical conversion, the photovoltaic panels are used, which is the most convenient and clean sophisticated technology with minimum maintenance. The first practical PV panels with 6% electrical efficiency were produced in 1954 at the Bell Telephone Laboratories by researchers using a p–n junction type solar cell (Chapin et al., 1954; Zondag et al., 2006). Further progress in silicon-based solar cells with increased efficiency was observed due to expanding space programs, where these are used to power satellites (Chapin et al., 1954; Grant et al., 2002). For dual purpose of solar energy production in terms of thermal as well as electrical, single system of PV and thermal collector called as a a photovoltaic thermal system (PVT) is introduced by researchers. Such design which contains both solar cells and thermal collector has become a logical idea to carry on research for the development of such devices (Tyagi et al., 2012).

2.2 Solar Energy Technologies

Solar energy technologies used commercially for various purposes such as domestic and industrial are briefly explained in this section.

2.2.1 Solar Thermal Collectors

The solar energy absorbed by the system designed for producing thermal energy is called solar thermal collector. There are a few types of such collector used commonly, such as unglazed, glazed flat plate collectors, evacuated tube and solar concentrating collectors. Solar thermal collectors when connected with a properly designed system including piping, storage tank etc. which provides hot water is called a solar hot water system (SHW). SHW is a well-established technology and commonly used all over the world commercially. (Morrison, 1997; UFC, 2004). This chapter deals with relevant types of solar collectors and solar water heating systems in extensive format.

2.2.2 Solar Collectors Technologies

The continuous research on the development of solar thermal technology is still underway for its improved performance. The performance of the collector depends on various factors including the material, design and arrangement of the components. There are many types of solar thermal collectors commercially manufactured and used globally. Some of them which are commonly and successfully used for the domestic hot water purpose are presented in the following sections (Abdunnabi, 2012).

2.2.2.1 Glazed flat plate collectors

Glazed flat-plate collectors are commonly known as liquid-based and air-based collectors. Moderate weather is ideal for such collectors and for the winter season, the required heat for such applications is 30-70°C. Liquid working fluid based glazed flat plate collectors are used for the domestic, swimming pools and commercial hot water for different applications (Kreider and Kreith, 2011).

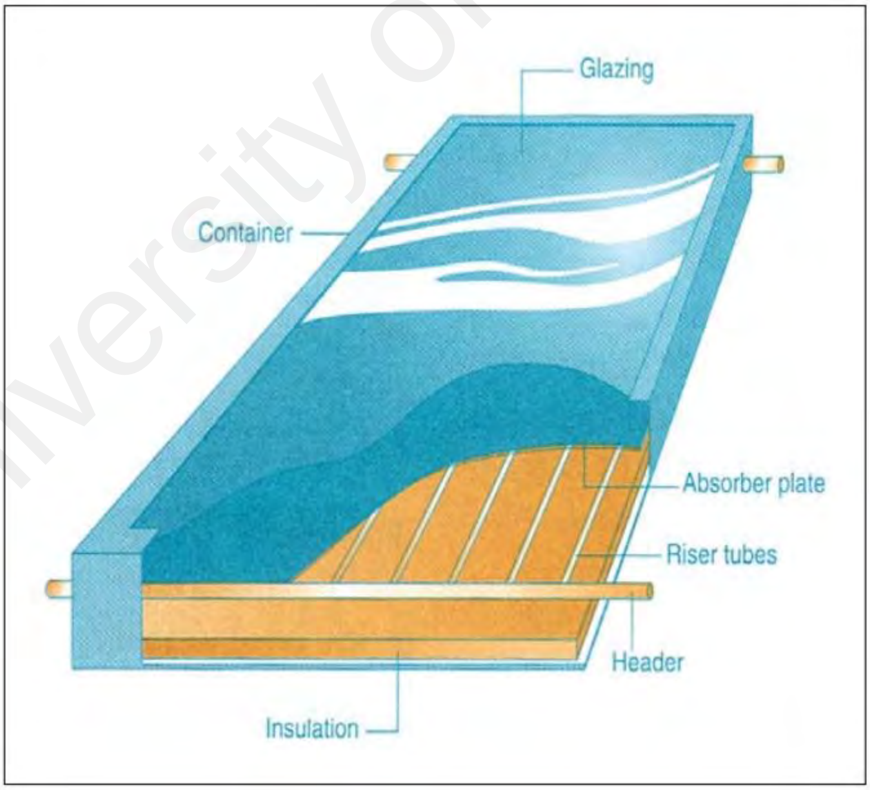

Figure 2.1: Glazed flat plate collector (RETScreen, 2011)

Sunlight is efficiently transformed into heat by using a flat absorber in such kind of collectors. A plate is used between the glazing and an insulating panel to minimise heat loss. The glazing is selected to pass maximum sunlight through and reach the absorber.

2.2.2.2 Unglazed flat plate solar collectors

These collectors are made very simple without any insulation or glazing and are used for low-temperature requirements. Unglazed flat plate collectors are more in number than any other solar collector installed in North America. The market for these collectors is primarily for outdoor swimming pools heating along with seasonal indoor swimming pools, water used in fish farming and preheating water for car wash. For these collectors, there is some other market potential such as summer camps at remote and seasonal locations (Watson, 2011).

Figure 2.2: Unglazed flat-plate collectors (RETScreen, 2011)

These collectors are usually made of ultraviolet light that are absorbed by black plastic. Therefore without glazing a big part of the solar energy is absorbed. Conversely, a great portion of the absorbed energy is dissipated into the environment on cold windy days due to no insolation. These collectors are sensitive to lose and capture heat from the atmosphere. Therefore, these collectors lose heat in the daytime when overheated and capture the heat from the air at nighttime.

2.2.2.3 Evacuated tube collectors

These collectors are used for higher temperatures in domestic applications for heating of water. It works on the principle that when heat enters the outer tube made of glass, it is absorbed by the high conducting material tube. That absorbed heat is carried out by circulating working fluid. The pattern of the tube allows air to evacuate from the space that is generated between the two tubes. In this way, both conductive and convective heat losses are extinguished (Chong et al., 2012).

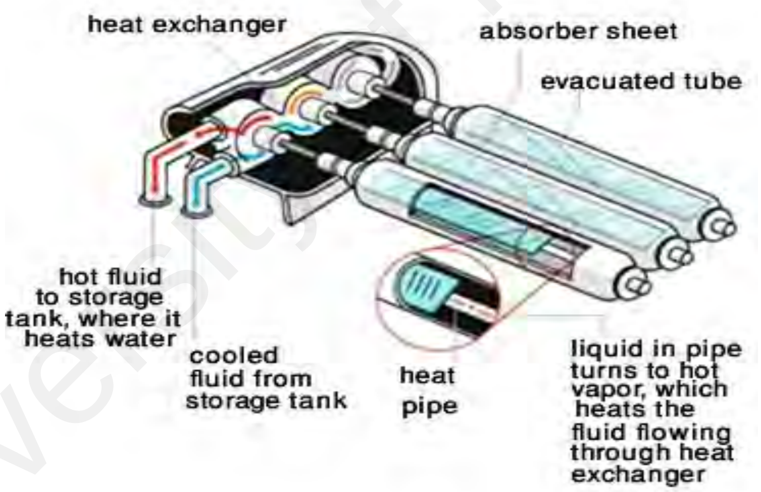

Figure 2.3: Evacuated-tube collector (RETScreen, 2011)

There is a variety of evacuated-tubes collectors. Few of collectors used a third glass tube inside the absorber tube, where some of them contain the configuration of heat transfer fins and fluid tubes. To get more irradiations, the reflectors are used behind evacuated tubes. This way collector works more efficient and offering better performance in both diffuse and beam radiation. Its shape also impacts positively as the circular shape of glass intakes solar irradiations all the time (NREL 1996). The drawback of using such tube is that such collectors are expensive compared to a flat plate (Budihardjo and Morrison, 2009).

2.2.2.4 Concentrating collectors

These collectors concentrate the solar irradiations on a receiver. In the presence of direct sunlight, these collectors can achieve high temperature. The small absorber has the ability to collect sun's energy on large scale to achieve high temperature. Two different ways can be adopted by concentrating collectors. The most advantageous is called" focal line" in that solar energy is concentrated along a line. Furthermore, in the other way it gathers irradiation on a point to create higher temperatures

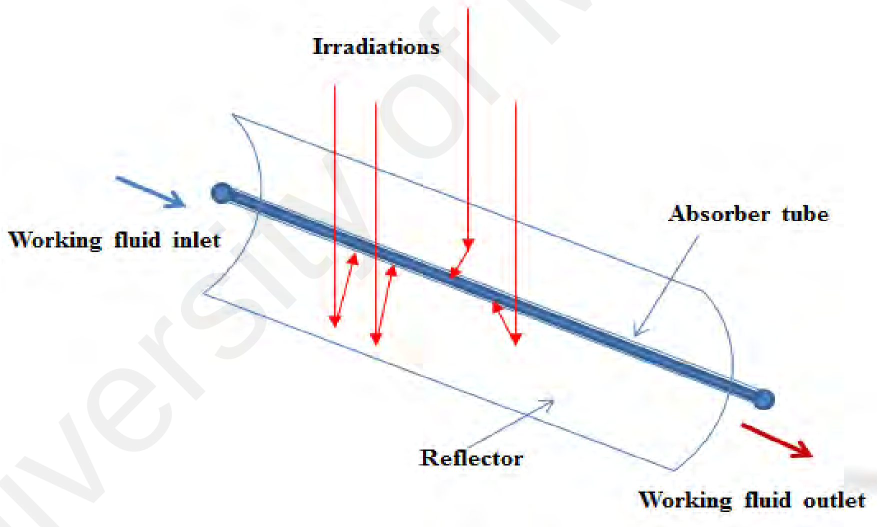

Figure 2.4: Concentrating solar collector

Usually, these types of collectors produce high temperature due to the high intensity of irradiations. In cloudy weather, however, their performance is affected due to the only focus on direct radiation.

2.2.3 Solar Photovoltaic Modules/Collectors

Photovoltaic technology is one of the most expensive amongst the other renewable energy sources, however, maintenance and operational expenses are quite low (Sharma, 2011). The cost effectiveness of PV is calculated by the module lifetime, its degradation of power and power output because the PV modules comprise of 70% of the capital costs in a photovoltaic thermal system (Parida et al., 2011). About 13% to 20% of solar irradiations are converted into electrical energy by a crystalline silicon PV while the rest cause the heat production in the module. The reason behind this is the infrared radiations do not create the photovoltaic effect and their energy converts into heat only (Armstrong and Hurley, 2010). Because of the packing factor and other losses in series connections of solar cells, PV efficiency is lesser than the efficiency of an individual cell (Joshi et al., 2009; Santbergen, 2008). Normally the solar spectrum between 400 nm to 1100 nm is absorbed by the crystalline silicon photovoltaic cell (Anderson et al., 2008; Bergene and Løvvik, 1995; Carriere, 2013; Dupeyrat et al., 2011; Lu and Yao, 2007). As the rest solar radiations cause heat generation in the PV module, therefore, the temperature of PV can rise up to 110°C on the peak sunshine day, which causes the drop in electrical efficiency of about 43%. However, at normal conditions PV modules work at 50°C above ambient temperature, which causes a decrease in electrical efficiency up to 25%, further, more efficiency is reduced when the PV operates in warmer climatic conditions. Besides, other operating factors such as ambient temperature, wind speed and levels of solar irradiations have a great effect on the PV module overall temperature (Hollick and Barnes, 2007; Lu and Yao, 2007; Tyagi et al., 2012). The open circuit voltage decreases when the temperature increases, therefore making PV temperature very important to be in controlled range (Tiwari et al., 2011; Zhangbo et al., 2009).

2.3 Photovoltaic Thermal Systems

The system combined with photovoltaic and solar thermal collector is called PVT systems, which can produce electrical energy and thermal energy simultaneously (Slimani et al., 2017). The temperatures can reach up to 150°C in the PVT system using a typical PV module depending on the operating and environmental conditions (Sandnes and Rekstad, 2002). The working fluid inside the PVT system cools the PV module by carrying the heat out of the PV module and is stored in the tank for different applications. However, the cooling of the PV module causes the efficiency increase of the module (Meyer and Busiso, 2012). The cooling capacity of the PV achieved by the working fluid is determined by the working conditions especially the inlet water temperature and thermal design of the collector (Sandnes and Rekstad, 2002). A typical PVT with its main parts such as the PV panel, the thermal collector is shown in Figure 2.5.

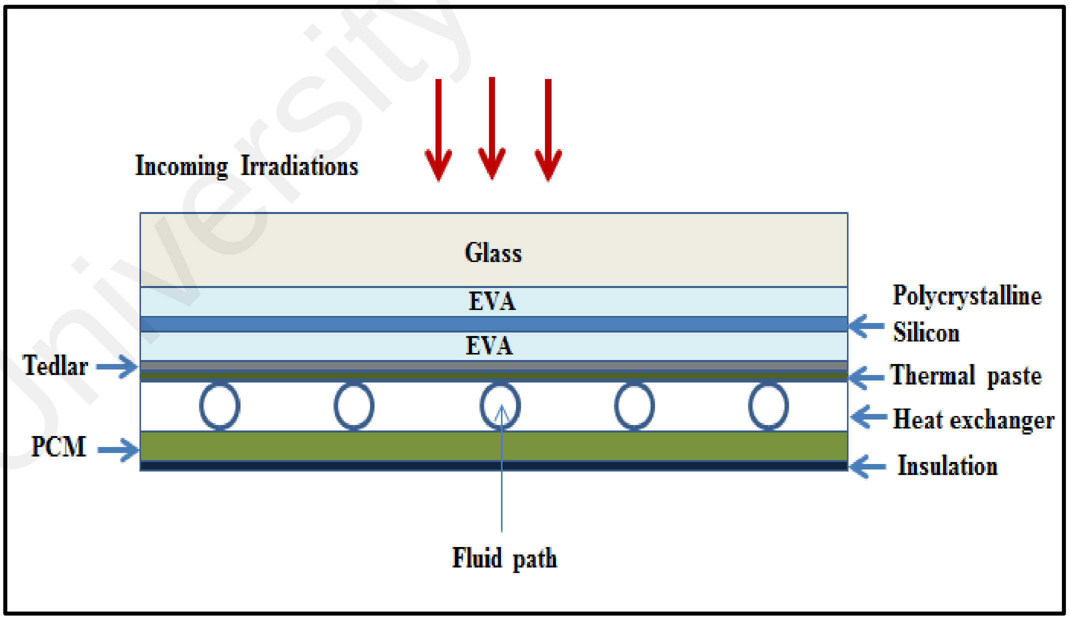

Figure 2.5: The typical PVT systems (Othman et al., 2007)

The area of the PVT system cools faster and at a lower temperature as compared to the area of the system near the outlet of the water because water gets hotter with the passage as it's temperature keeps transferring from PV module to water (Zakharchenko et al., 2004). However, the average temperature of the PV module depends on different parameters such as area and design of the thermal collector and solar irradiations incident on the system (Lausanne, 2000).

2.4 Phase Change Materials

These materials absorb a huge amount of heat latently at the stage of changing their phase from solid to liquid. When the PCM gets heat, at first it heats up sensibly but after a certain temperature point which is its phase change or transition temperature, it starts to store heat latently until it remains in the liquid form as shown in Figure 2.6 (Günther et al., 2009). Mass and thermal conductivity of the PCM along with any heat transfer elements within them determines the range and duration of temperature at which phase of the PCM changes. The research has been carried on the types of PCMs and their physical properties along with their applications (Sarı et al., 2004; Sharma et al., 2009; Zalba et al., 2003).

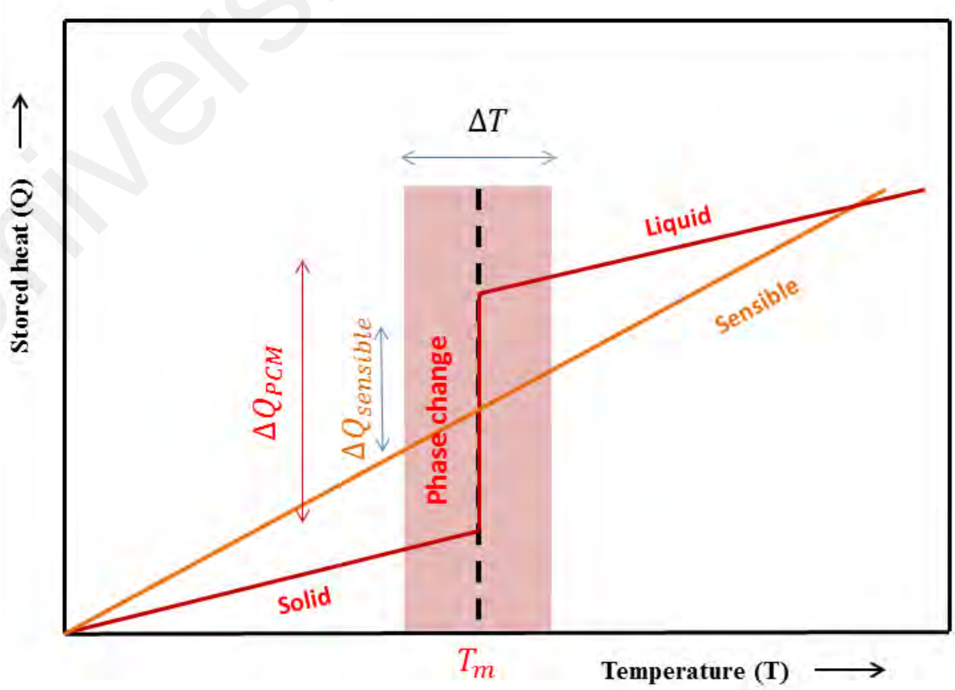

Figure 2.6: Behavior of PCM for storing heat with respect to temperature (Günther et al., 2009)

Extensive research has been carry out on the on the thermal management of PV modules. However, the thermal management of the PV with PCM is for cooling only and heat stored in the PCM is not used. Therefore, recently, more focus is being given to the integration of PCM with PVT systems for cooling the PV panel and use the thermal energy achieved from the cooling of the PV module. PVT-PCM system is simulated and analyzed in a one dimensional energy balance model, where it is shown that 9% of the PV power can be enhanced as compared to only PV module alone with 20ºC of water temperature increment (Aelenei et al., 2014; Browne, M.C. et al., 2015; Malvi et al., 2011).

2.5 Prospects of PCM Incorporated Photovoltaic Systems

In this era of digital technology, the scientists are giving more attention towards the use of renewable energy resources to utilize them to gain and store energy. Therefore, due the environmental issues awareness and depletion of the fossil fuel resources, renewable energy has achieved significant importance (Qazi et al., 2015). To meet with this growing energy demand, solar energy is most abundantly utilized at domestic and industrial scale. To collect the solar energy many types of solar systems are used. These collectors convert solar irradiations into thermal and electrical energy and is a combination of Photovoltaic and solar thermal systems into a hybrid form known as PVT solar collectors (Tian and Zhao, 2013). Figure 2.7 shows the schematic diagram of PVT-PCM system with its parts.

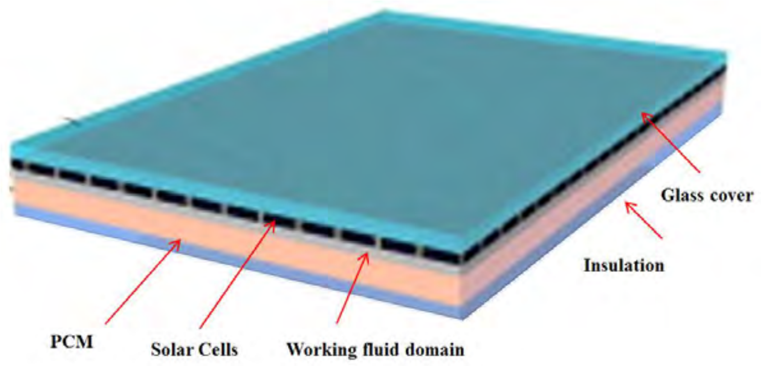

Figure 2.7: Schematic diagram of PVT-PCM system

To enhance the efficiency of PVT, the phase change material (PCM) is mostly used along with PVT in storing thermal energy (Cabeza et al., 2011). The standalone PVT and with the combination of PCM e.g. PVT-PCM both together gives many benefits to the future of digital world.

2.5.1 Applications of Photovoltaic Thermal-PCM Systems

Fiorentini et al. (2015a) has developed a novel (HVAC) system run on solar energy. Prior to practical building management system, analytical models were developed for the PVT and PCM units for better understanding. It is claimed by the authors for good agreement between simulation and experimental results. Stritih (2016) carried out the simulations and experimental setup for PV panel temperature flow using TRANSYS software. Phase change material RT28HC was attached to PV panel Canadian Solar CS6P-M. In the experimental results, 35.6°C temperature difference was achieved in between PV without PCM and PV with PCM.

Al Imam et al. (2016) carried out a performance comparison in winter between a clear day and semi-cloudy day. The reading for overall efficiency of the system was achieved as 55% and 63% for clear-day and about 46–55% for semi-cloudy day

Ni et al. (2016) proposed solar thermal system and PCM unit solar-assisted air source heat pump (PCM-SAHP) system with phase change material (PCM) is proposed. The experimental results show that ambient temperature has a great effect on the performance of the system in the cooling mode. Conversely, the subtle effect of cooling water mass flow rate through the PCM on the efficiency is observed.

Lin et al. (2014) presents the numerical evaluation of the performance of the novel ceiling ventilation system connected with PVT and PCM. The results indicate that the 23.1°C of maximum air temperature is achieved from the PVT collectors for improvement of indoor comfort in the winter conditions. Table 2.1 shows the studies on PVT PCM systems for different applications.

Table 2.1: Studies on PVT PCM systems for different applications

Reference	**Location**	**Dataset/ Experimental setup**	**Applications**	**Operating time**	**Efficiency**
(Hosseinzadeh et al., 2018)	Iran	PVT and PVT-PCM system	PV cooling and hot water	Summer	13.61% exergy efficiency
(Fiorentini et al., 2015b)	China	PVT collector and PCM unit	novel solar-assisted HVAC system servicing	winter & summer	Achieved 6.5 coefficient of performance
(Stritih, 2016)	Ljubljana	PV-PCM panel with TRNSYS software.	PV panel	One year	Achieved by 7.3%
(Kazemian et al., 2018)	Iran	PVT and PVT-PCM system	PV cooling and hot water	One year	4.22% electrical efficiency
(Al Imam et al., 2016)	Bangladesh	PVT solar collector with combined parabolic concentrator	photovoltaic thermal (PVT) collector system	Clear day & semi-cloudy day	Achieved by 55% & 63% for clear-day and around 46–55% for semi cloudy
(Ni et al., 2016)	China	PCM-SAHP system	solar-assisted air source heat pump s	cooling and heating modes	Achieved
(Lin et al., 2014)	Australia	Solar Decathlon house using TRNSYS. The	ceiling ventilation system	Winter	Achieved by 0 to 0.9823 & 0.0060 to 0.9921

2.6 Conclusion

In this chapter, solar energy technologies and systems are reviewed along with phase change materials. The literature shows that there are two separate technologies have been used commercially for solar energy systems, e.g. photovoltaic panels and solar thermal collectors. For enhancing the electrical efficiency of PV modules, PCMs are used for its thermal management. To extract solar thermal energy, solar thermal systems with different types, e.g. flat, evacuated, parabolic and concentrating are used with suitable thermal collector attached to irradiation absorbing materials. Previous research work is evaluated by the researcher on PVT and PVT-PCM systems. PCM uses in the PVT are also reviewed. Furthermore, research gaps of PCMs, thermal collector design and PCM configuration inside the PVT systems with 3D numerical analysis are found.

CHAPTER 3: METHODOLOGY

The investigation on the performance of the proposed solar systems with the newly designed thermal absorber and the introduction of phase change materials is carried. For this purpose, numerical modelling and experimental investigations are done. In this way, the methodology is carried out into two parts: numerical and experimental investigations. Numerical modelling of the systems is done through FEM based software COMSOL Multiphysics. The results obtained are validated with an experimental setup which is carried out in indoor and outdoor environmental and working conditions of Kuala Lumpur, Malaysia. The numerical and experimental methodology is presented in details in the following subsections.

3.1 Numerical Analysis

In this section, all the numerical methodology for a photovoltaic module, photovoltaic thermal and photovoltaic thermal with phase change materials is described in details.

3.1.1 Numerical Investigation

The following equations are presented for the data reduction of the data achieved.

Total energy is shown in equation (3.1) (Nishioka et al., 2003).

$$E_r = \tau_g \alpha_{sc} p_{sc} G A \tag{3.1}$$

Heat lost;

$$E_l = U_{sc}\left(T_{sc} - T_{amb}\right) A \tag{3.2}$$

Electrical power;

$$E_p = \eta_{sc} p_{sc} \tau_g \alpha_{sc} G A \left[1 - \mu_{sc}\left(T_{sc} - T_r\right)\right] \tag{3.3}$$

Equation for conduction through the PV.

$$E_t = U_t \left(T_{sc} - T_{td}\right) A \tag{3.4}$$

Energy balance equation.

$$E_r = E_l + E_t + E_e \tag{3.5}$$

Solar cell temperature equation (Nasrin et al., 2018a).

$$T_{sc} = \frac{p_{sc} G\left(\tau_g \alpha_{sc} - \eta_{sc}\right) + (U_{sca} T_a + U_t T_{td})}{\left(U_{sca} + U_t\right)} \tag{3.6}$$

Thermal energy equation.

$$E_t = mC_{pf}\left(T_{out} - T_{in}\right) \tag{3.7}$$

For electrical efficiency;

$$\eta_e = \frac{E_p}{E_{in}} \tag{3.8}$$

Equation 3.9 is for thermal efficiency;

$$\eta_t = \frac{E_t}{E_{in}} \tag{3.9}$$

For overall efficiency;

$$\eta_o = \frac{E_p + E_t}{E_{in}} \tag{3.10}$$

Amount of stored energy in PCM material can be calculated (Dwivedi et al., 2016) as;

$$Q = m[c_p(T_i - T_m) + L + c_p(T_m - T_f)] \tag{3.11}$$

Under the regular conditions, 3D numerical simulation is carried out. The test conditions are as follows: Transmission quality of ethyl vinyl acetate (EVA) is approximately 100%, the flow is laminar and cannot be compressed, and temperature inconsistencies along the thickness can be ignored. Thermo-physical characteristics of the absorber duct are consistent with the operating temperature.

3.1.2 Numerical Procedure for PVT System

The numerical procedure has been depicted through the equations given below in the numerical simulations conducted thought the COMSOL Multiphysics®. In depth details can be found at (Fayaz et al., 2018; Fayaz et al., 2019; Nasrin et al., 2018a; Nasrin et al., 2018b):

Solid layers equations;

$$-\left(\frac{k}{\rho C_p}\right)\left(\frac{\partial^2 T}{\partial x^2}+\frac{\partial^2 T}{\partial y^2}+\frac{\partial^2 T}{\partial z^2}\right)=0 \qquad (3.12)$$

For the fluid domain

$$\frac{\partial u}{\partial x}+\frac{\partial v}{\partial y}+\frac{\partial w}{\partial z}=0 \qquad (3.12)$$

$$\rho\left(u\frac{\partial u_i}{\partial x}+v\frac{\partial u_i}{\partial y}+w\frac{\partial u_i}{\partial z}\right)=-\frac{\partial p}{\partial x_j}+\mu\left(\frac{\partial^2 u_i}{\partial x^2}+\frac{\partial^2 u_i}{\partial y^2}+\frac{\partial^2 u_i}{\partial z^2}\right) \qquad (3.13)$$

$$\left(\rho C_p\right)\left(u\frac{\partial T}{\partial x}+v\frac{\partial T}{\partial y}+w\frac{\partial T}{\partial z}\right)=k\left(\frac{\partial^2 T}{\partial x^2}+\frac{\partial^2 T}{\partial y^2}+\frac{\partial^2 T}{\partial z^2}\right) \qquad (3.14)$$

3.1.3 PVT-PCM Numerical Procedure

For the schematic drawing of PVT-PCM system shown in Figure 3.10 (a) & (b), the enthalpy-based method is adopted. The governing equation for the numerical prodcudere are given in details below. Further details can be achived at (Bonyadi et al., 2018; Fayaz et al., 2018; Fayaz et al., 2019; Nasrin et al., 2018b)

$$k_{pcm,s}\left(\frac{\partial^2 T_{pcm,s}}{\partial x^2}+\frac{\partial^2 T_{pcm,s}}{\partial y^2}+\frac{\partial^2 T_{pcm,s}}{\partial z^2}\right)=U_{ch}\left(T_{ch}-T_{pcm,s}\right) \tag{3.15}$$

$$k_{pcm,l}\left(\frac{\partial^2 T_{pcm,l}}{\partial x^2}+\frac{\partial^2 T_{pcm,l}}{\partial y^2}+\frac{\partial^2 T_{pcm,l}}{\partial z^2}\right)=U_{pcm}\left(T_{pcm,l}-T_{ch}\right) \tag{3.16}$$

Equations (3.15) and (3.16) repersent the PCM liquification and solidification process with and without irradiations respectively. Equation (3.17) represents the liquid fraction value.

$$\rho_{pcm,s}=\theta\rho_l+(1-\theta)\rho_s;\quad C_{p,pcm,s}=\frac{1}{\rho_{pcm,s}}\left[\theta\rho_l C_{p,l}+(1-\theta)\rho_s C_{p,s}\right];\quad k_{pcm,s}=\theta k_l+(1-\theta)k_s \tag{3.17}$$

Following relationships shows a normalised pulse parameter, D (K^{-1}) (Bonyadi et al., 2018).

$$C_{p,l}=C_{p,l,phase}+DL_{fu}\quad;\quad C_{p,s}=C_{p,s,phase}+DL_{fu}$$

$$C_{p,s}=C_{p,s,phase}+DL_{so}\quad;\quad C_{p,l}=C_{p,l,phase}+DL_{so}$$

Boundary conditions for the numerical model can be approached at (Bonyadi et al., 2018; Fayaz et al., 2018; Fayaz et al., 2019; Nasrin et al., 2018b)

3.2 Numerical Technique

FEM method is used for the proposed model in this study (Chandrasekar et al., 2013).

3.2.1 Mesh Generation and Grid Check

Figure 3.1, 3.2 and 3.3 show the successfully achieved meshing of proposed systems. Details of the meshing standards are depicted in Table 3.1.

Table 3.1: Grid sensitivity check at 1000 W/m^2 irradiation

System type	Type of meshing	Extra Coarse	Coarser	Coarse	Normal
PVT-PCM	Elements	15,51,566	20,98,558	37,09,748	78,54,851
	Cell temperature (°C)	63.01413	63.01458	63.01479	63.01491
	Time of solution (s)	6918	9546	16379	32932
PVT	**Type of meshing**	**Extra Coarse**	**Coarser**	**Coarse**	**Normal**
	Elements	14,99,353	20,33,676	36,64,990	74,00,382
	Cell temperature (°C)	67.00529	67.00559	67.00582	67.00593
	Time of solution (s)	6650	9102	15021	31541
PV	**Type of meshing**	**Normal**	**Fine**	**Finer**	**Extra fine**
	Elements	59,636	1,87,601	11,66,206	79,50,780
	Cell temperature (°C)	69.52532	75.12827	75.12881	75.12890
	Time of solution (s)	26	69	789	5028

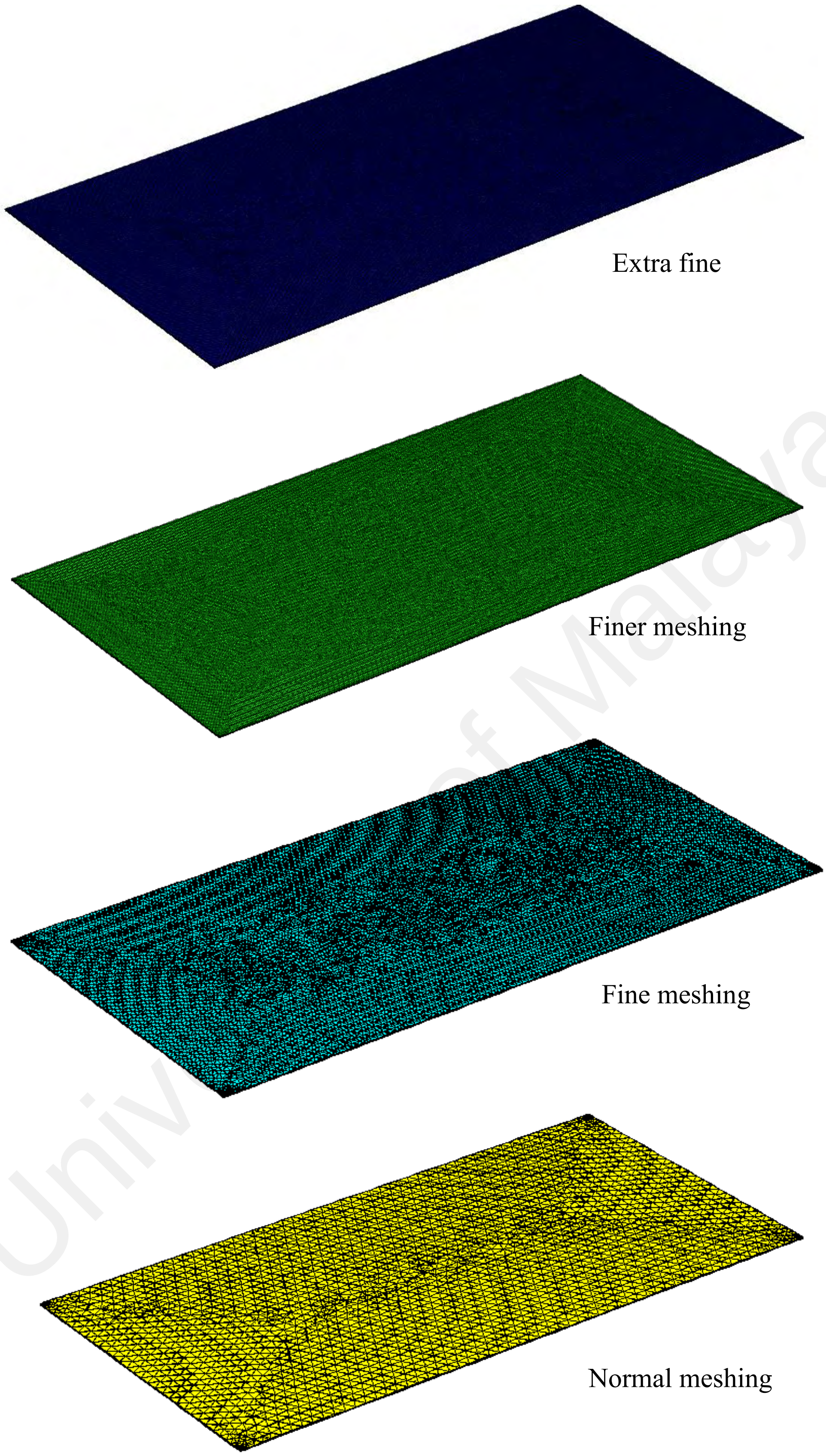

Figure 3.1: Finite element mesh generation for the PV module

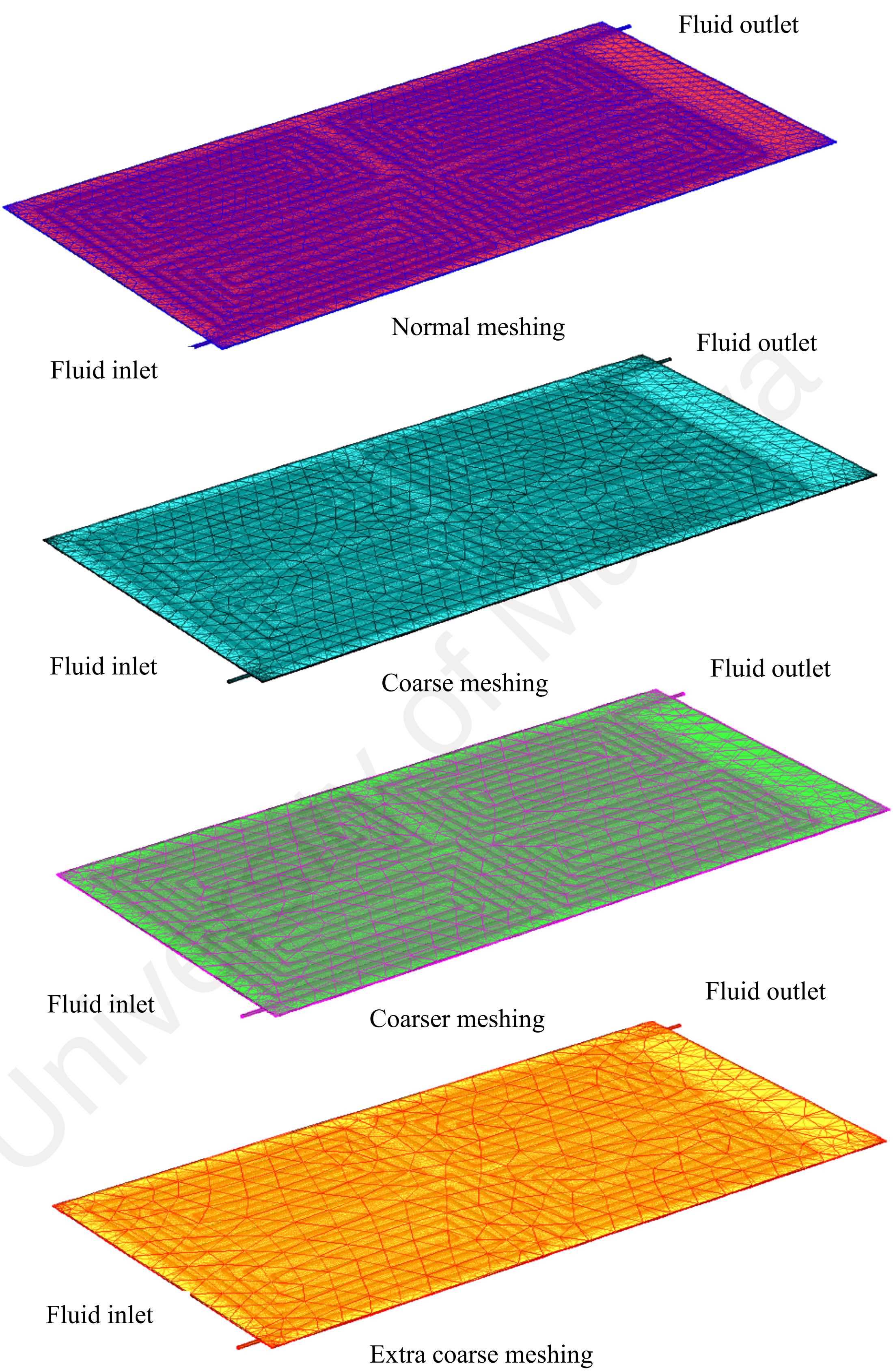

Figure 3.2: Finite element mesh generation for PVT module

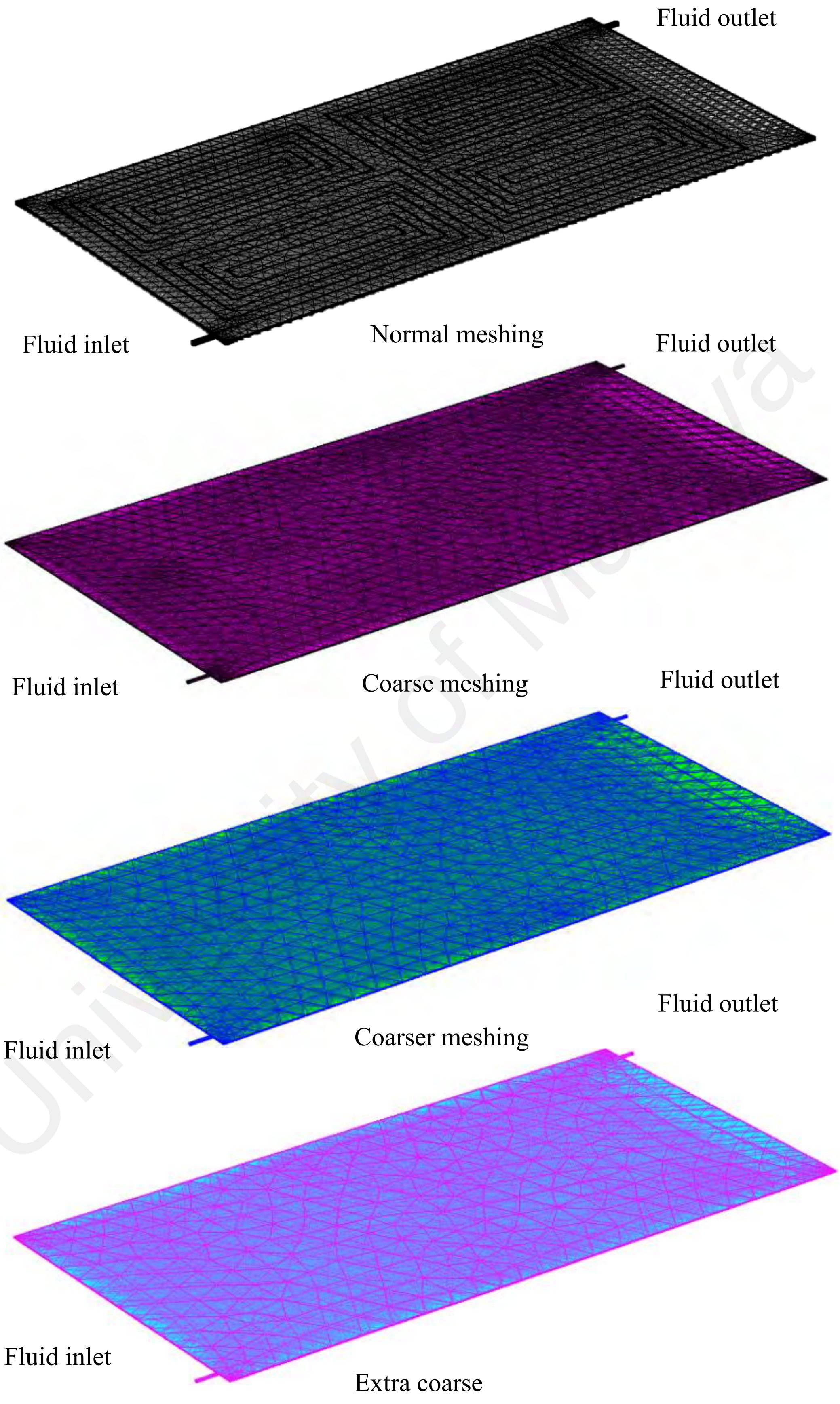

Figure 3.3: Finite element mesh generation for the PVT-PCM system

3.2.2 Thermo-physical Properties and Characterization of PCM

Properties of the PCM used in the photovoltaic thermal management are presented in the following table 3.2.

Table 3.2: PCM properties used in the present investigation (PCMPRODUCTS, 2018)

Layer	Solid phase	Liquid phase	Units
Temperature of transition	44	44	^{o}C
Specific heat at constant pressure	2150	2458	J/kgK
density	805	805	kg/m^3
Latent heat	-242kj	242	kJ
Thermal conductivity	0.18	0.1	W/mK
Transitional interval	1	1	^{o}C

Phase change material A44-PCM is a paraffin group material, which is used for this investigation. Figures 3.4 and 3.5 are presented for the differential calorimetry (DSC) and thermal gravimetric analysis (TGA) results. A44-PCM satisfies the working parameters proposed for the investigation as are evident from the results.

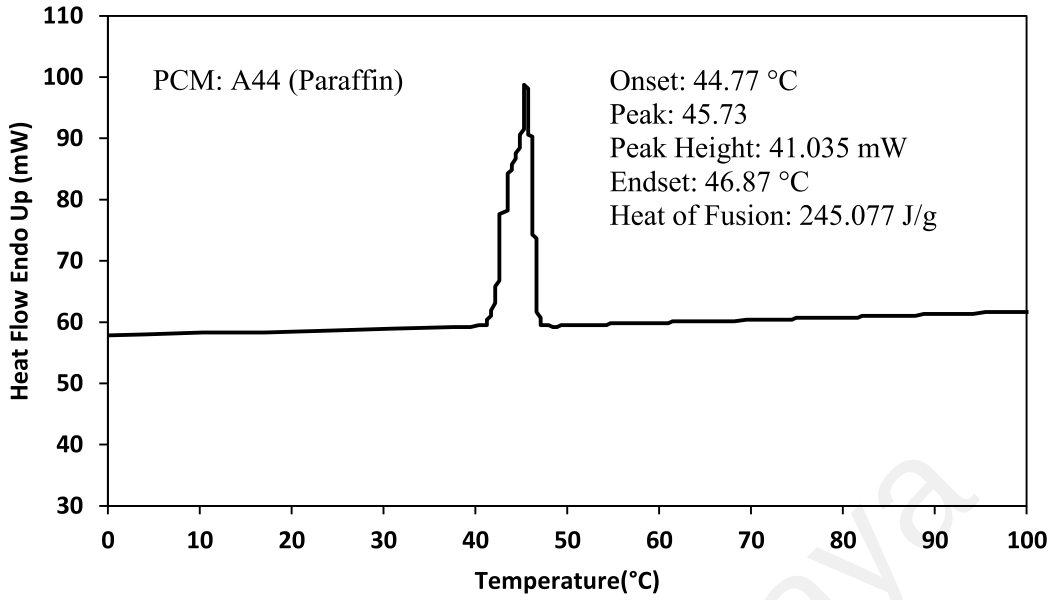

Figure 3.4: Results of differential scanning calorimetry of Paraffin A44

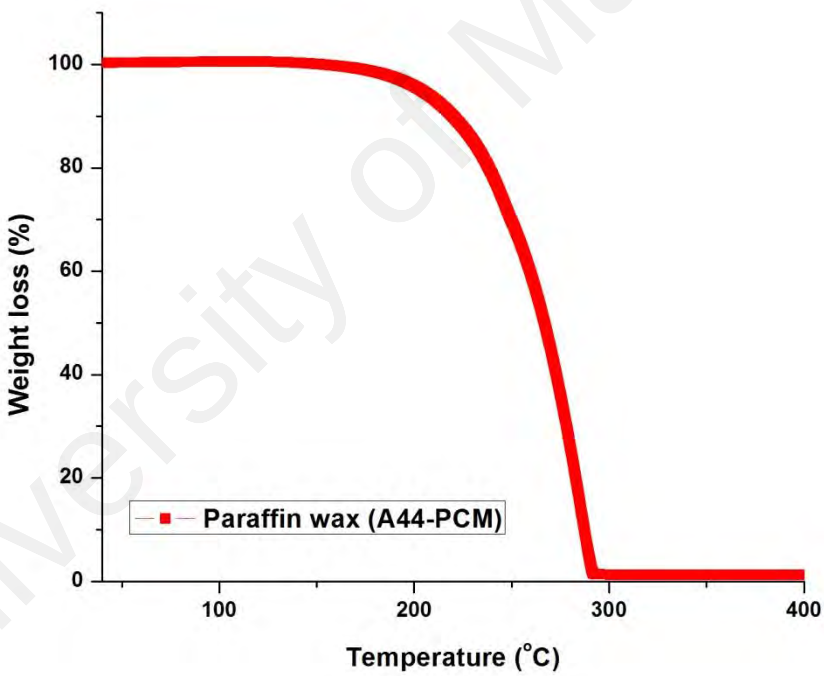

Figure 3.5: TGA pattern of paraffin wax

TGA tests show the stability of weight in the safe working range of temperatures. Therefore, this PCM is proved to be stable and feasible for the current study.

3.3 Photovoltaic Thermal System with Nanofluids as Working Fluid.

The set of governing equations of PVT in case of nanofluid as working fluid are presented below; (Nasrin and Alim, 2014; Sardarabadi and Passandideh-Fard, 2016):

$$-\left(\frac{k}{\rho C_p}\right)\left(\frac{\partial^2 T}{\partial x^2}+\frac{\partial^2 T}{\partial y^2}+\frac{\partial^2 T}{\partial z^2}\right)=0 \tag{3.29}$$

$$\frac{\partial u}{\partial x}+\frac{\partial v}{\partial y}+\frac{\partial w}{\partial z}=0 \tag{3.30}$$

$$\rho_{nf}\left(u\frac{\partial u_i}{\partial x}+v\frac{\partial u_i}{\partial y}+w\frac{\partial u_i}{\partial z}\right)=-\frac{\partial p}{\partial x}+\mu_{nf}\left(\frac{\partial^2 u_i}{\partial x^2}+\frac{\partial^2 u_i}{\partial y^2}+\frac{\partial^2 u_i}{\partial z^2}\right) \tag{3.31}$$

$$\left(\rho C_p\right)_{nf}\left(u\frac{\partial T_{nf}}{\partial x}+v\frac{\partial T_{nf}}{\partial y}+w\frac{\partial T_{nf}}{\partial z}\right)=k_{nf}\left(\frac{\partial^2 T_{nf}}{\partial x^2}+\frac{\partial^2 T_{nf}}{\partial y^2}+\frac{\partial^2 T_{nf}}{\partial z^2}\right) \tag{3.32}$$

where i = 1, 2, 3 represents u, v and w component of the velocity vector of fluid, $\alpha_{nf}=k_{nf}/\left(\rho C_p\right)_{nf}$, $\rho_{nf}=(1-\phi)\rho_f+\phi\rho_s$, $\left(\rho C_p\right)_{nf}=(1-\phi)\left(\rho C_p\right)_f+\phi\left(\rho C_p\right)_s$,

$C_{pnf}=\dfrac{(1-\phi)\left(\rho C_p\right)_f+\phi\left(\rho C_p\right)_s}{(1-\phi)\rho_f+\phi\rho_s}$, $\mu_{nf}=\dfrac{\mu_f}{(1-\phi)^{2.5}}$ and $k_{nf}=k_f\dfrac{k_s+2k_f-2\phi\left(k_f-k_s\right)}{k_s+2k_f+\phi\left(k_f-k_s\right)}$

as in Maxwell Garnett model (Garnett, 1906) and viscosity of Brinkman model (Brinkman, 1952) of nanofluid.

Boundary conditions can be approached at (Fayaz et al., 2018; Nasrin et al., 2018b), and (Luna-Rubio et al., 2012)

The non-dimensional form of heat transfer;

$$\overline{Nu}=-\frac{k_{nf}}{k_f}\sqrt{\left(\frac{\partial\theta}{\partial X}\right)^2+\left(\frac{\partial\theta}{\partial Y}\right)^2+\left(\frac{\partial\theta}{\partial Z}\right)^2} \tag{3.33}$$

$$Nu=\frac{\iint_S \overline{Nu}\,ds}{\iint_s dS}=-\frac{1}{\pi DL}\frac{k_{nf}}{k_f}\iint_S\sqrt{\frac{\partial^2\theta}{\partial X^2}+\frac{\partial^2\theta}{\partial Y^2}+\frac{\partial^2\theta}{\partial Z^2}}\,ds \tag{3.34}$$

where, L, q, D are the height, heat flux and the diameter of the flow pipe.

Multi-walled carbon nanotubes (MWCNT) nanoparticle properties are taken from (Kamyar et al., 2012; Nasrin and Alim, 2014) and shown in Table 3.3. MWCNT nanoparticle length and diameter are and 5 μm 12 nm respectively.

Table 3.3: Properties of MWCNT and water (Luna-Rubio et al., 2012)

Properties	Water	MWCNT	Unit
ρ	997.1	1600	kg/m^3
C_p	4179	796	J/kgK
k	0.613	3000	W/mK

3.4 Mathematical Model Development

It is necessary to have a complete understanding of the basic characteristics of the mass and heat transfer in the integrated system after the development of the physical structure of the system. There are many opportunities still available for researchers to improve the model of heat and mass transfer process in the whole system as indicated by the available literature. Following components of the comprehensive model are required to investigate theoretically such as energy balance equations for PCM melting and solidification, a heat transfer model for conduction and convection and the momentum equations. There should be modelling of PCMs heat extraction for the Building Heat Services and other techniques of the modelling, for example, non-linear transient 2D or 3D numerical models, and finite difference model may be utilised to opt for appropriate one. If possible, the developed numerical model should be approved by experimental tests and analytical solution (Ma et al., 2015).

Simulation software mostly allows one-dimensional analysis or very costly with incomprehensible functionality. Suitable multipurpose simulation software for physics researchers field is very important to achieve numerical analysis motives by saving the time from going practical with extra cost and difficulties. FEM-based simulation software, COMSOL Multiphysics® is made to solve engineering and physics issues such as Multiphysics and attached phenomena. It is best-featured software than ABAQUS, ANSYS, NASTRAN and can act well by the MATLAB® and MATLAB®

syntax also. It focuses on Multiphysics by attaching various physics phenomena according to the problem conditions. This software has an important feature of higher dimensional modelling including the capacity of coupling related physics when required. Further, it is easy and very user-friendly to program according to user-defined differential equations when not employed already. Additionally, this time-dependent solver software has the capacity to predict the performance and long-run reliability of the device. COMSOL Multiphysics® is a multi-physics problem solver and includes many distinguishable features. Moreover, it has professional predefined modelling interfaces and allows the employment of CAD models. Furthermore, it is easy to use the user-defined partial differential equations.

3.5 Experimental Investigation

The investigation of proposed systems is conducted for their performance at controlled indoor and free outdoor working environments of University of Malaya, Kuala Lumpur, Malaysia for the validation of the numerical results. A new thermal collector design is used for increased output temperature and overall electrical performance. All three systems are simultaneously tested under similar conditions for better understanding and strong comparison of the electrical and thermal performances.

3.5.1 Experimental Setup

There are two experimental setups; indoor and outdoor are carried out for the investigation. The details of the indoor and outdoor experimental setups are given in following subsections separately.

3.5.1.1 Indoor experimental setup

The indoor experiment is set up UMPEDAC laboratory, Wisma R&D, University of Malaya for the investigation of the effects of various parameters on the systems' efficiency under controlled conditions. Indoor schematic experimental setup is shown in Figure 3.6 and Figure 3.7.

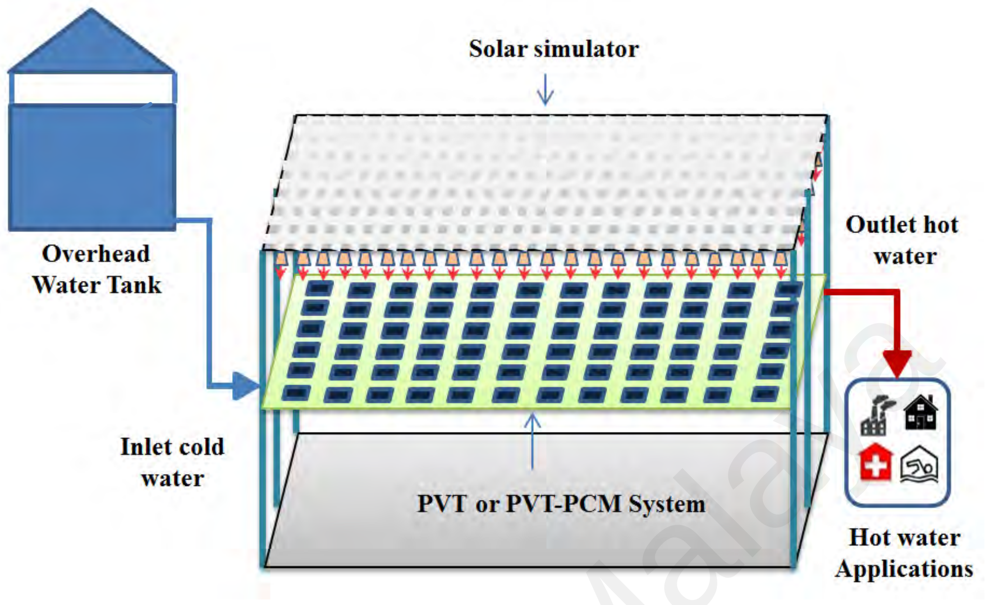

Figure 3.6: Schematic indoor experimental setup of the PVT system

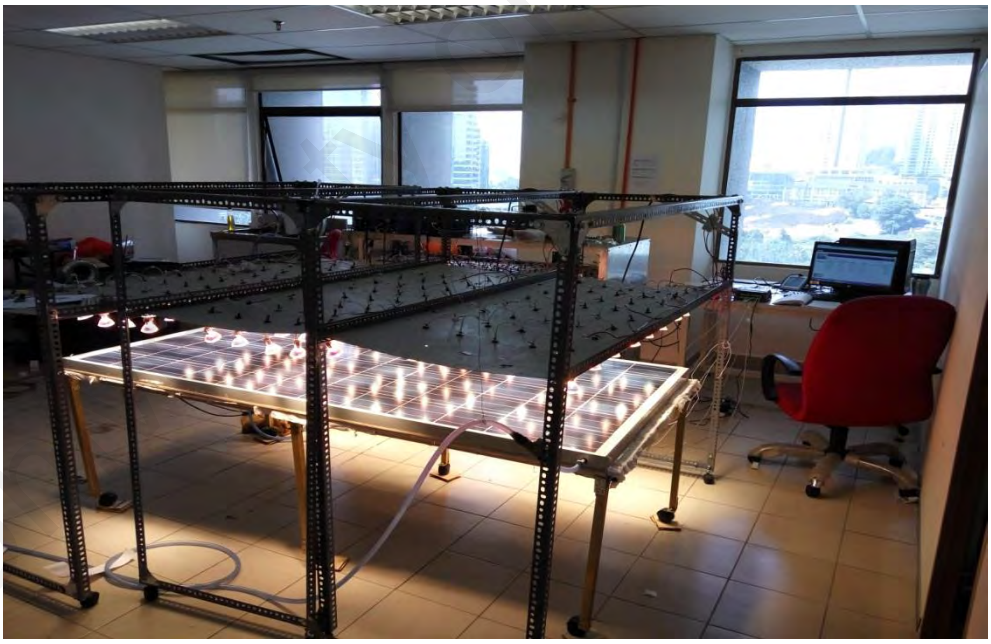

Figure 3.7: Indoor experimental setup of PVT system

For providing required irradiations to solar systems, a solar simulator comprising 120 OSRAM halogen bulbs each with 90 W, 12 V and 7.5 A, is used at full capacity powered by three variable control AC-power-supply transformers each with a capacity of 3 kVA. The total capacity of the emulator is 10800W.

3.5.1.2 Outdoor experimental setup

Outdoor experimental setup is carried out with an overhead tank scheme for water inlet and natural environmental conditions for solar irradiation, ambient temperature and other working conditions according to varying weather. The experiment was carried out wat University of Malaya, Kuala Lumpur, Malaysia. The systems were simultaneously installed to take data for accuracy and proper comparison within the same set of real-time weather conditions. Figures 3.8 and 3.9 show the schematic and installed outdoor experimental setups.

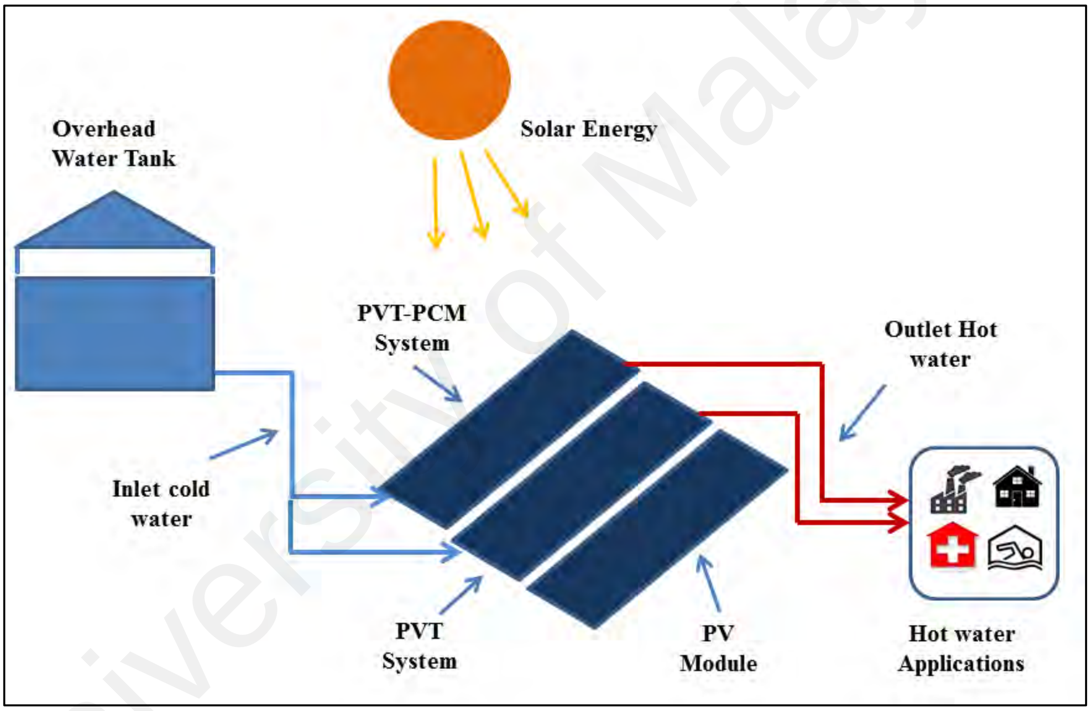

Figure 3.8: Outdoor schematic diagram of the experimental setup

Figure 3.9: Outdoor experimental setup of the PV, PVT and PVT-PCM systems

3.5.2 Photovoltaic Module and Thermal Collector

The PV module used in this study is depicted in the Table 3.4. PV module has size of 2 m^2 with model No.E310P(S)-011 of EPV brand. Further details can be achieved at (Fayaz et al., 2018; Fayaz et al., 2019; Nasrin et al., 2018b). Table 3.5 shows the fabricated PVT systems with all parts properties in details.

Table 3.4: Specifications of the PV module (Nahar et al., 2017)

Item	Specification
Materials	Polycrystalline silicon
Area of a cell	0.02433 m^2
Tolerance	0~+3%
Operating temperature	-40°C to ±85°C
Voltage at P_{max}. (V_{mpp})	30.6V
Current at $P_{max.}$ (I_{mpp})	8.17A
Maximum power	305W
STC	1000 W/m^2, AM 1.5, 25°C

Table 3.5: PV/T collector materials and thermal properties

Layer	Materials	Thickness (mm)	Density [kg/m^3]	Thermal Conductivity [W/(m.K)]	Heat capacity at constant pressure [J/(kg.K)]
Top cover	Glass	3	2450	2	500
Encapsulant	EVA	0.8	950	0.311	2090
Solar cell	Silicon	0.1	2329	148	700
Bottom cover	Tedlar	0.05	1200	0.15	1250
Conductive medium	Thermal paste	0.2	2500	1.42	650
Thermal collector	Aluminium	1	237	204	2700
Working fluid	Water	-	0.68	0.65	998

A new design of thermal collector for cooling the PV module and collecting heat for hot water is shown in Figure 3.10. The thermal collector is attached to the back of PV module with thermal conductive adhesive and thermal conductive paste is applied to increase the thermal contact between the PV and thermal collector for improved heat transfer. In this scheme of PV module and thermal collector combination, absorber plate is not included. Hence, thermal collector is directly attached to bottom (Tedlar) of PV for enhanced heat transfer and reduce the system weight. The dimensions of the thermal collector are set in a way that it can fit inside the PV module easily and keep the clearance of the electrical output box of the PV module. However, the design set to fit in the maximum area of the PV module to enhance heat transfer. Therefore, the length and width of the thermal collector is set as 1650mm X 850mm. The diameter size of the pipe is selected after numerical optimization. Initially, three sizes were selected as 3.5, 7.5 and 15mm for numerical analysis. In the analysis, 7.5mm diameter is selected for the current design as discussed in results and discussion.

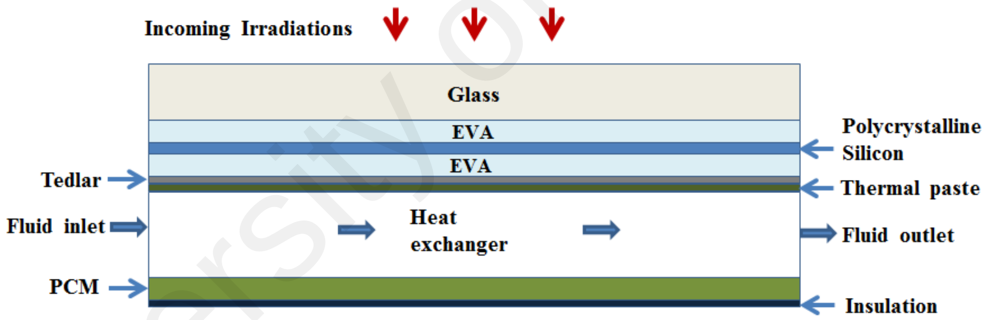

(a)

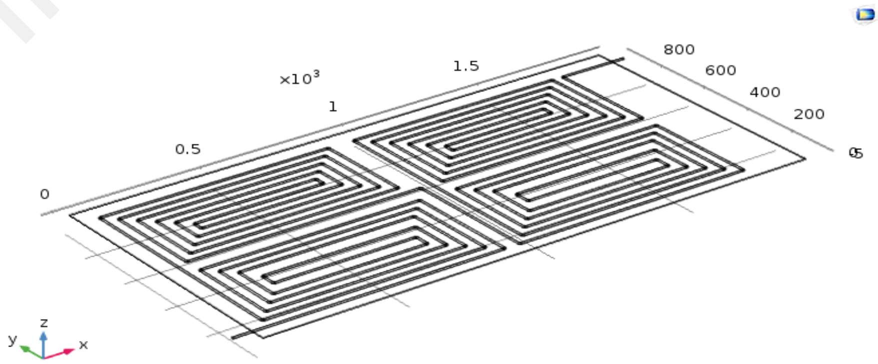

(b)

Figure 3.10: Cross sectional view of PVT-PCM system and 3D COMSOL Multiphysics drawing of the heat exchanger

3.5.3 Experimental Instruments and Equipment

For the collection of necessary data, different instruments are used to measure and collect the data from the experiments conducted. There are different conditions set for the experiments to extract the maximum data to understand the systems from different perspectives. Independent variables are controlled for each set of data by fixing and varying their values for the expected output of dependent variables. Following instruments and equipment are used to conduct the experiments.

3.5.3.1 Data logger

For the data acquisition, DT80 Data Taker is used in the experiments. The data is taken at the interval of 1 minute for the desired periods of experimentation. This device provides reliability and ease of work to collect the data from the experiments. It is connected with the computer for controlled and live data monitoring and it can be used without any computer with its built-in control and monitoring system. Figure 3.11 shows the DT80 Data Taker.

Figure 3.11: Data logger used in the experiments

3.5.3.2 *I-V* tracer

Multifunction IV tracer is used in this experiment developed at UMPEDAC, University of Malaya. This device can be used to measure the electrical data from five PV modules simultaneously. Figures 3.12 shows the IV tracer used in this investigation.

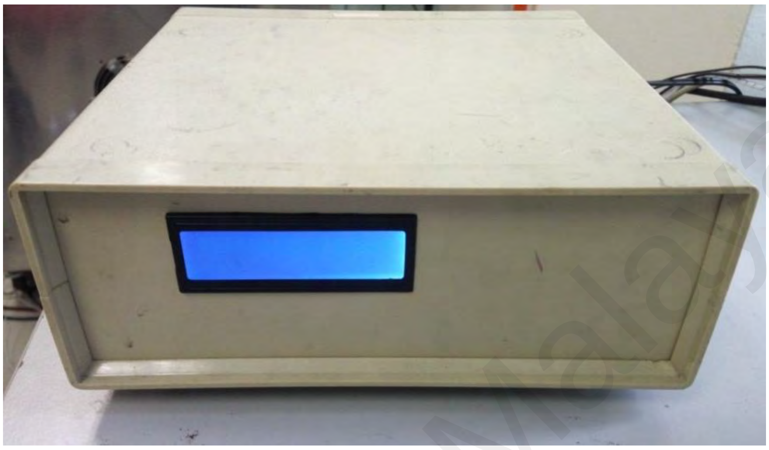

Figure 3.12: *I-V* tracer used in the experiments

3.5.3.3 Mass flow meter

A mass flow meter or liquid rotameter is a variable area meter used to measure mass flow rates of working fluids. Mass flow meter used in this experiment is LZM-15 models flow ranging from 0.5 LPM to 18 LPM. Flow is controlled by regulating the knob manually at the bottom of the meter to ensure the required flow of mass of the working fluid. Figure 3.13 shows the mass flow meter used in this experiment.

Figure 3.13: Mass flow meter used in the experiments

3.5.3.4 Pyranometer

For the measurement of solar irradiation, a solar sensor or pyranometer with model Pyra 300V is used. It can measure the sum of direct and diffuse solar irradiation as global irradiance. It uses the silicon photodiode as a transducer to convert the solar irradiation into electrical current. It can sense the irradiation wavelength from 400 nm to 1100 nm and irradiance levels from 0-1800 W/m^2. Figure 3.14 shows the pyranometer used in the experiment.

Figure 3.14: Pyranometer used in the experiments

3.5.3.5 Thermocouple

In this investigation, K-Type thermocouple of US-SA-AJD-17294 model is used as seen in figure 3.15. K-Type thermocouples are reliable, accurate and inexpensive and are widely used than the other types of thermocouples as it can sense a wide range of temperatures. Its welded sensing tip is made of nickel/chromium material. All thermocouples were checked for their accuracy and compared with each other for the uniformity of temperature data.

Figure 3.15: Themocouple (k-type) used in the experiments

3.5.4 Experimental Procedure

The novel design of thermal collector attached with PV module with and without PCM is investigated for its thermal performance. To understand the performance behaviour of PV, PVT and PVT-PCM, the experimental procedures are carried out indoor with controlled working conditions and environment and outdoor with natural environmental conditions of Malaysian weather. Both indoor and outdoor procedures are presented in the following subsections.

3.5.4.1 Indoor experimental procedure

The indoor experiments are conducted at the controlled environment of 27 ºC ambient and water inlet temperature. Module's top surface centre (glass) and bottom surface centre (Tedlar) for PV and glass, Tedlar, water inlet and outlet temperature for PVT and PVT-PCM are taken with k-type thermocouples. Solar irradiations, electrical data and temperatures of Tedlar, glass, inlet and outlet temperatures are collected through data logger. Ambient temperature, mass flow rate and irradiations are controlled according to the required experimental data set scheme. Controlled power supplies were used to regulate the irradiation levels. Collected data are analyzed for the investigation of the effect of reduced PV temperature with a proposed change in mass flow rates and solar irradiations on PVT and PVT-PCM. Figure 3.16 and Figure 3.17 show the schematic and real indoor experimental setups of the systems.

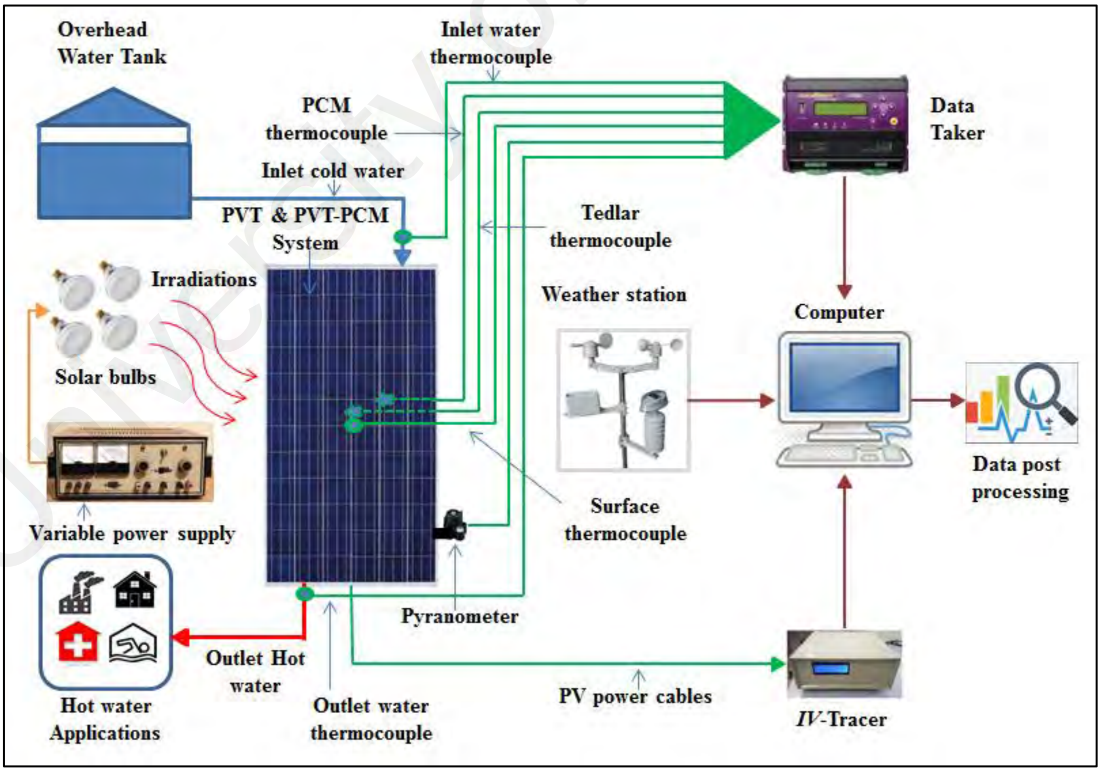

Figure 3. 16: Schematic diagram of indoor experimental setup with components details.

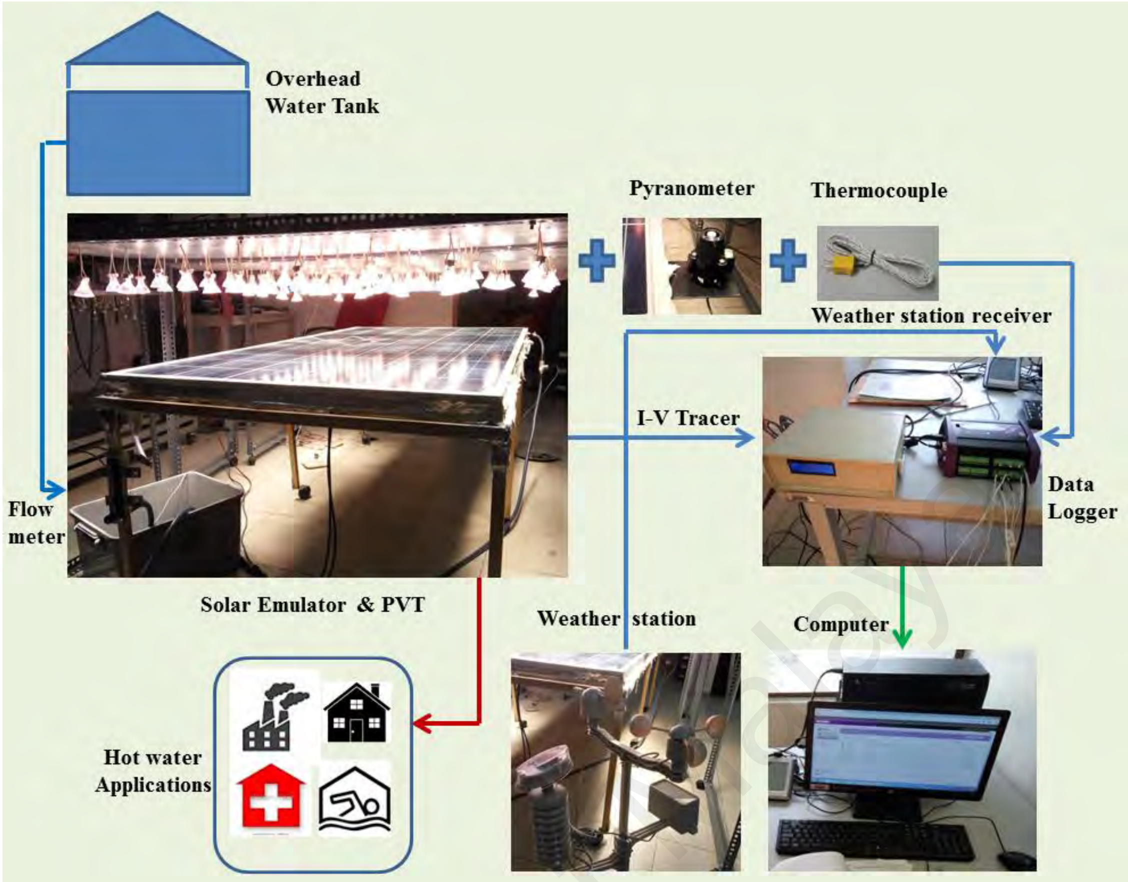

Figure 3.17: Indoor experimental setup

3.5.4.2 Outdoor experimental procedure

Outdoor experiments are carried out at the solar garden of UMPEDAC, University of Malaya. The systems are set at a tilt angle of 0-15° to face the Sun directly to make irradiation incidence angle of 90° to planes of PV modules to achieve maximum solar irradiations. Whole day data is achieved from May to August 2017 with the minimum and maximum solar irradiations values ranging from 50 W/m^2 to 1100 W/m^2. The data was achieved for few months to avoid errors and uncertainty of the weather. The schematic and real setup of the outdoor experiment is shown in Figure 3.18 and Figure 3.19.

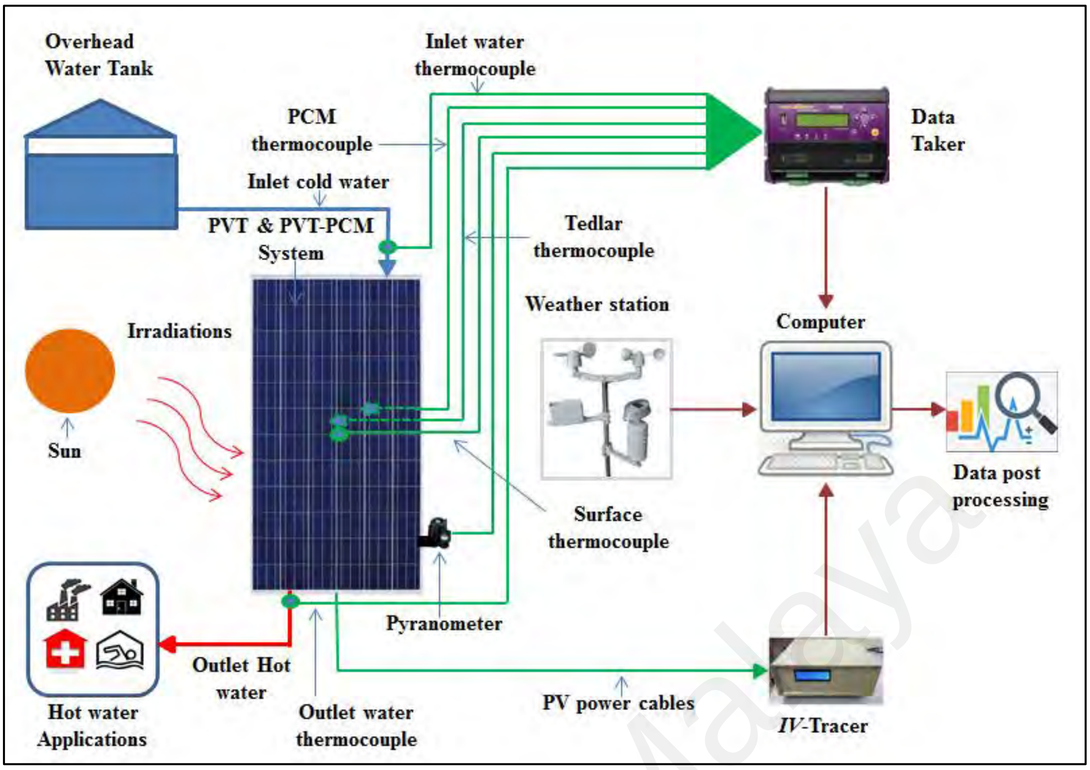

Figure 3. 18: Schematic outdoor experimental setup with details of components

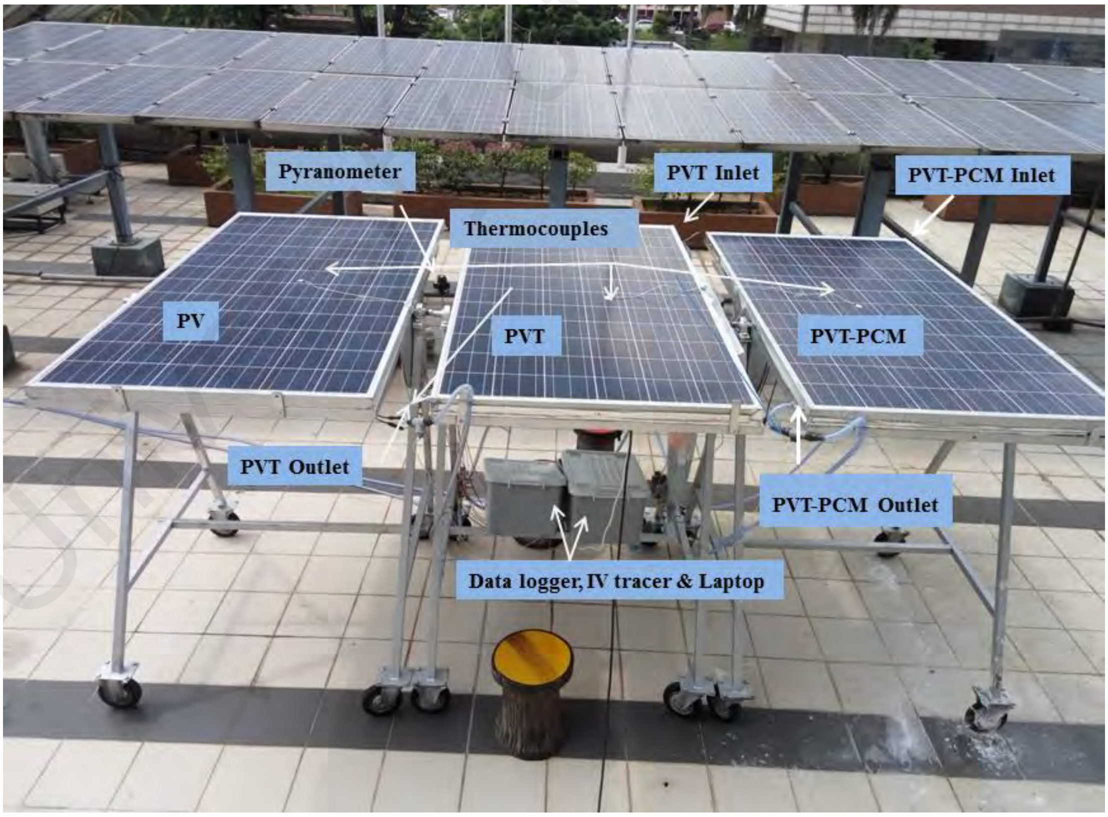

Figure 3.19: Outdoor experimental setup

3.6 Uncertainty and Sensitivity Analysis

The uncertainty and sensitivity analysis is carried out in this investigation. The necessary equations are provided. Details can also be found in (Fayaz et al., 2019). The sensitivity analysis for numerical results is shown in Figure 3.17.

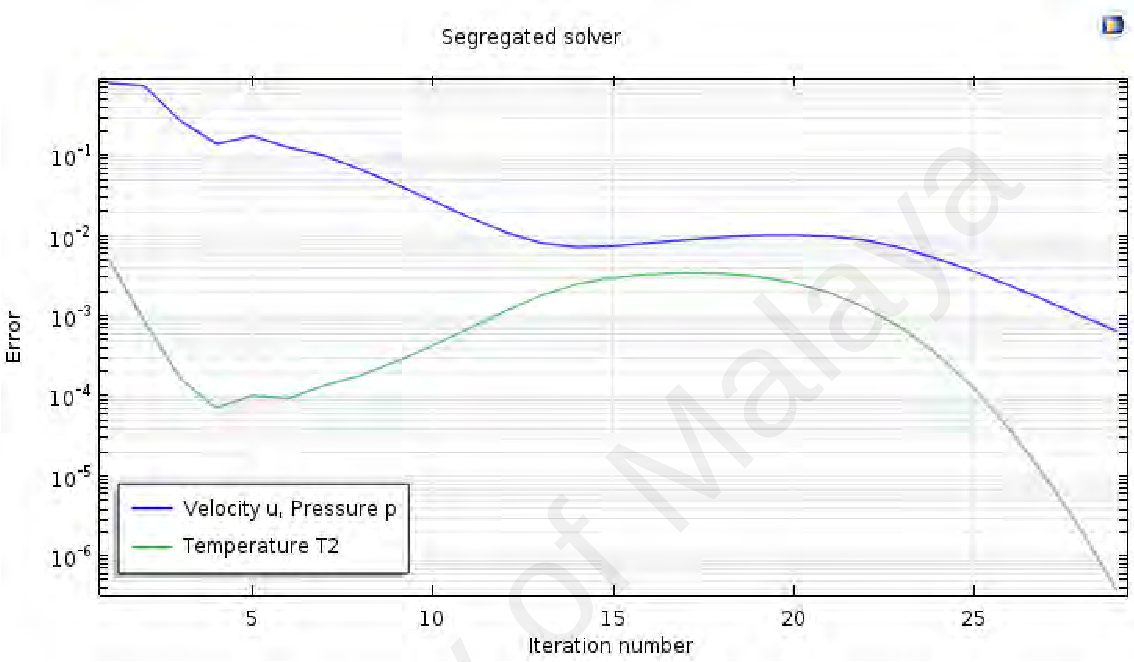

Figure 3. 20: Convergence achieved by COMSOL Multiphysics software

It can be seen that numerical results produced were at minimum possible error and the best results were achieved at 30 iterations in segregated solver. The convergence was achieved in the best minimum error and solutions were obtained very to the actual solutions. Following are used for the uncertainty analysis and details can be found at (Fayaz et al., 2019).

$$U_x = \sqrt{B^2 + \left(t_{\lambda,95\%} \times R\right)} \tag{3.35}$$

$$\lambda = N - 1 \tag{3.36}$$

$$R_x = \frac{S_F}{N^{1/2}} \tag{3.37}$$

$$S_F = \sqrt{\frac{1}{N}\sum_{i=1}^{N}(X_i - \bar{X})^2} \tag{3.38}$$

$$;X' = \bar{X} \pm U(95\%) \tag{3.39}$$

3.7 Conclusion

For the analysis PV, PVT and PVT-PCM systems, the numerical and experimental investigation has been done using COCMSOL Multiphysics® and indoor and outdoor experimental setup. In the numerical standard procedure, the new design of thermal collector coupled with PV module in PVT and with PCM in PVT-PCM is prepared for meshing and execution of models with required physical laws and governing equations. Experimental validation of numerical results is carried out by setting up experimental setups in indoor and outdoor environments. PVT and PVT-PCM systems are separately assembled for achieving electrical and thermal data from all systems simultaneously with higher comparison accuracy. All the necessary instrumentation and data acquisition processes are achieved to get experimental results in the desired parameters with minimum errors.

CHAPTER 4: RESULTS AND DISCUSSION

4.1 Introduction

The numerical and experimental investigation is carried out on the poposed systems. Numerical modelling is done on newly designed thermal collector for heat retention efficiency of the PV module to enhance its electrical performance. Also, thermal energy is carried out in the working fluid for hot water usage. To understand the heat flow phenomenon and effect of heat removal on the PV module, the numerical model is set up and executed in COMSOL Multiphysics. However, to validate the obtained data from the numerical model, experiments are carried out. The systems performance is investigated from the data achieved and is elaborated in detail with discussions. The results achieved are in good agreement between numerical and experimental data. Detailed results and discussion on each set of data from the numerical and experimental procedures are presented in following sections.

4.2 Justification for Diameter and Material Selection for Thermal Collector

Numerical analysis of material and different sizes of diameters of the proposed thermal collector has been done. It is very necessary to select the proper diameter of the thermal collector before further heat transfer analysis of the whole PVT system as diameter plays an important role on the efficiency, economy and other physical factors of the system. Furthermore, copper and aluminium materials are analysed numerically for their efficiency influence in heat transfer of PVT as well as an economic factor for their selection for the PVT system.

4.2.1 Justification for Diameter Selection

The justification of diamter selection is carriout out for the proper size and design of the pipe for maximum possible heat transfer efficiency as shown in Table 4.1. Three sizes were examined in numerically analysis such as 15, 7.5 and 3.5 mm.

Table 4.1: Numerical results comparison for different diameter design of thermal collector made of aluminium material

Diameter (mm)	Mass flow rate (LPM)	Output temperature (°C)	Thermal efficiency (%)
15	0.5 LPM	58.45	62.8
7.5	0.5 LPM	61.11	69.1
3.5	0.5 LPM	63.92	75.7

The criterion of analysis was based on the thermal efficneicy achievemnt. Different factors were considered before the selection of diamater. Finally, the diamter of 7.5 mm was selected for its feasibility in the current application (Fayaz et al., 2019; Joshi and Khandwawala, 2014).

4.2.2 Justification for the Material Selection

The justification of material selection is carriout out for the suitalbe materials of the pipe for maximum possible heat transfer efficiency as shown in Table 4.2. Two materials such as copper and aluminium were examined in numerically analysis.

Table 4.2: Numerical results comparison between copper and aluminium of thermal collector design for 7.5mm diameter

Material	Mass flow rate (LPM)	Output temperature (°C)	Thermal efficiency (%)
Aluminum	0.5 LPM	61.11	69.1
Copper	0.5 LPM	62	71.24

It is well assessed and defined that copper as compared to aluminum is high in thermal conductivity and let heat flow with better heat transfer efficiency (Fayaz et al., 2018; Hust and Lankford, 1984). It can be seen in the Table 4.2 that there is not big difference in the thermal performance in between these two materials. In addition, high cost and demand of the copper makes is less feasible for the use in the solar cooling applications.

4.3 Indoor Performance Investigation of Proposed Systems

Investigation of the systems is carried out under indoor controlled weather conditions using a solar emulator. Temperatures of PV, PVT and PVT-PCM collectors systems are analyzed with COMSOL Multiphysics® numerical analysis in sections 4.2.1 to 4.2.3. Furthermore, the electrical and thermal performance of the collectors is also investigated in detail. Numerical analysis done on the photovoltaic module in COMSOL Multiphysics® FEM based software on different solar radiation in 3D model gives valuable detailed information as compared to 1D and 2D numerical models. The simulation parameter for solar radiation values is set from 200 W/m^2 minimum to 1000 W/m^2 with the interval of every 200 W/m^2 solar radiations value at indoor experimental setup.

4.3.1 Analysis of Surface Temperature Distribution of Photovoltaic Module

As shown in Figure 4.1, the photovoltaic module temperature varies significantly at different solar radiations intensities. It is obvious from the figures that the photovoltaic module achieves maximum temperature gain of 82.4°C approximately without any cooling medium. But, with controlled parameters, the heat transfer to the environment is allowed with natural free convections at the ambient temperature of 27°C and with no wind speed. Whereas, the minimum surface temperature of the photovoltaic module is noted as 38°C approximately at 200 W/m^2 solar radiations at the same conditions. In addition, the temperatures on the module are not uniformly distributed. It is because the heat flows easily to the environment from the edges of the module as compared to the middle part of the module. Three-dimensional heat transfer allows the edges of the module be at a lower temperature than the middle part which only radiates back to the environment from glass and Tedlar only.

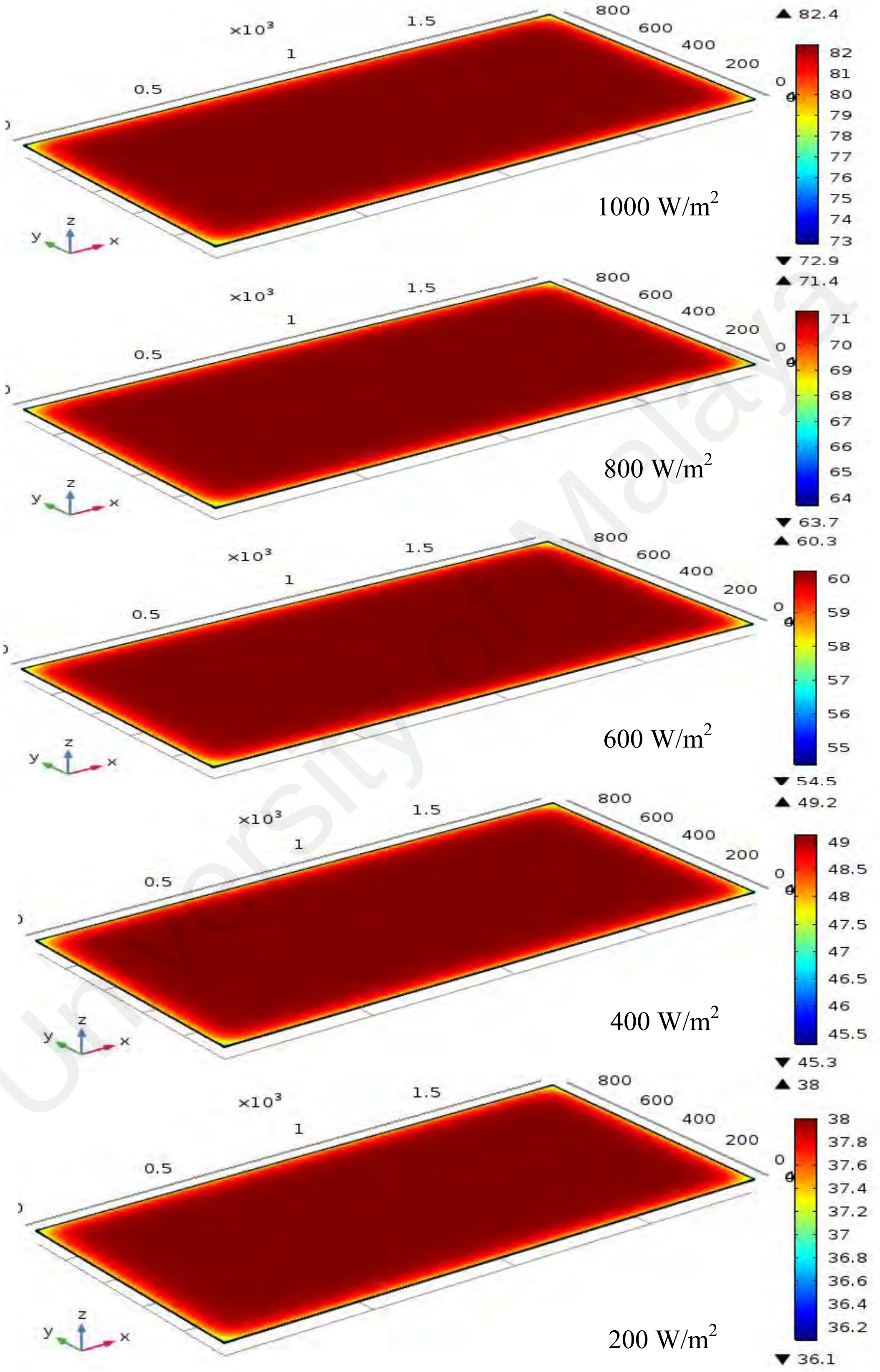

Figure 4.1: Surface temperature plot of the PV for the effect of irradiation from 200 W/m^2 to 1000 W/m^2

4.3.2 Analysis of Temperature Behaviour of PVT System

The temperate surface profile for the photovoltaic thermal system at different solar radiations at the intervals of 200 W/m^2 is shown in Figure 4.2 at a fixed mass flow rate of 0.5 LPM. Whereas, Figure 4.3 depicts the results for thermal collector temperature distribution from the inlet of water flow to the outlet of the collector. Hence, as seen in the figure 4.2 temperatures vary significantly at different solar radiations intensities. It is clear from the figures that the photovoltaic module achieves maximum temperature of 70 to 78.6°C approximately at 1000 W/m^2 with the cooling effect of water flow in the thermal collector. Glass temperature is near to 70°C because of the thermal collector contact with the PV module which extracts the heat from the surface whereas, 78.6°C that is higher as shown in the temperature bar is due to edges of the panel because at the edges thermal collector is not in direct contact, and only free convection to the environment occurs but at the rest area of panels two type of convections occur due to free convection to the and forced convectino in the pipe. The minimum surface temperature of the photovoltaic-thermal module is noted as 30 to 39°C approximately at 200 W/m^2 solar radiations at same conditions. Streamline effect of solar radiations on the thermal collector is depicted in Figure 4.3. The highest temperature the thermal collector is noted as 60°C approximately, and the lowest is shown as 37.6°C approximately. In this case, the inlet temperature is set at 27°C. As water flows through its course or the length of the pipe, its temperature increases gradually and reaches the maximum value as mentioned above.

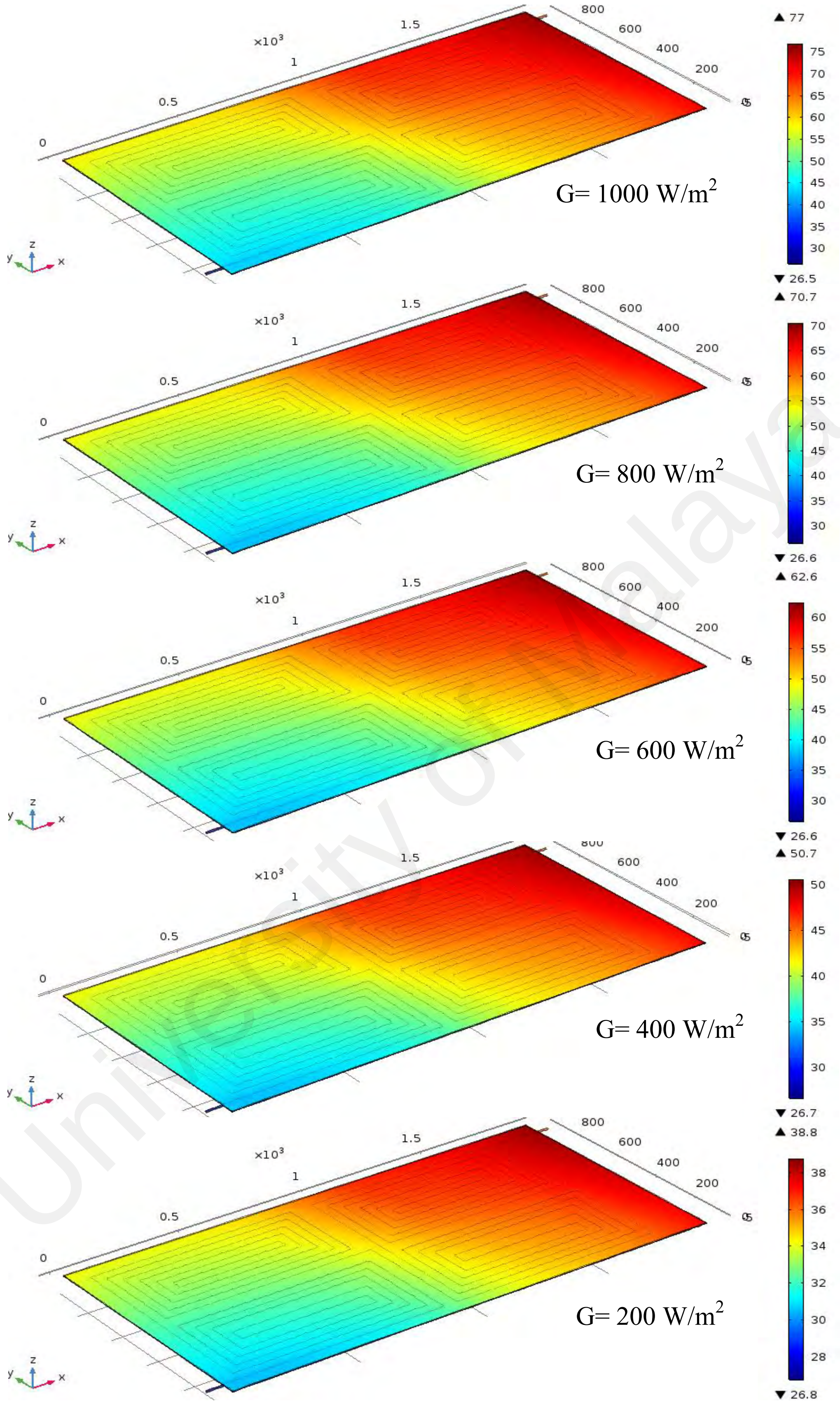

Figure 4.2: Surface temperature plot of the PVT for the effect of irradiation from 200 W/m^2 to 1000 W/m^2

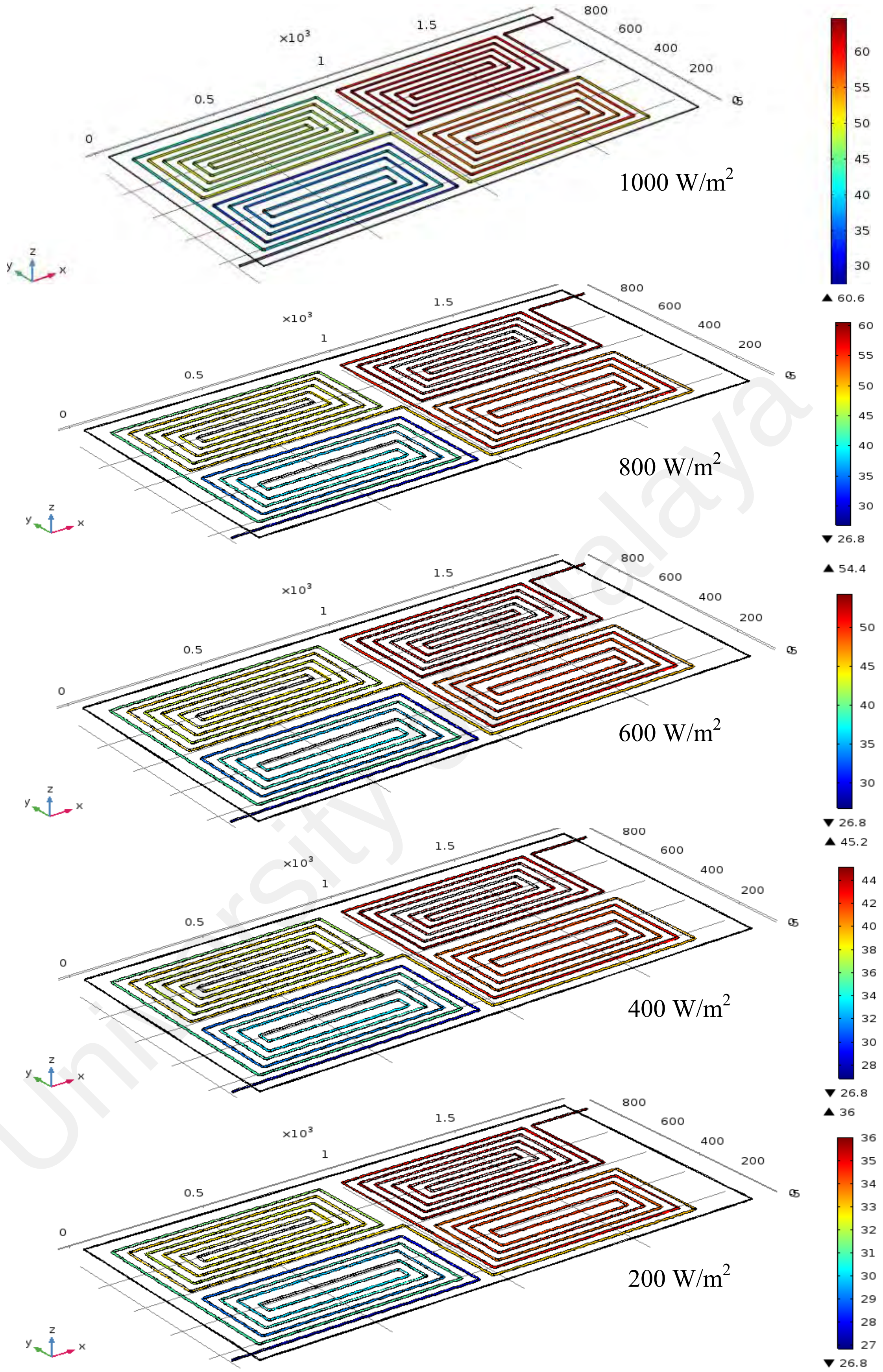

Figure 4.3: Streamlines plot of the PVT for the effect of solar radiation from 200 W/m^2 to 1000 W/m^2

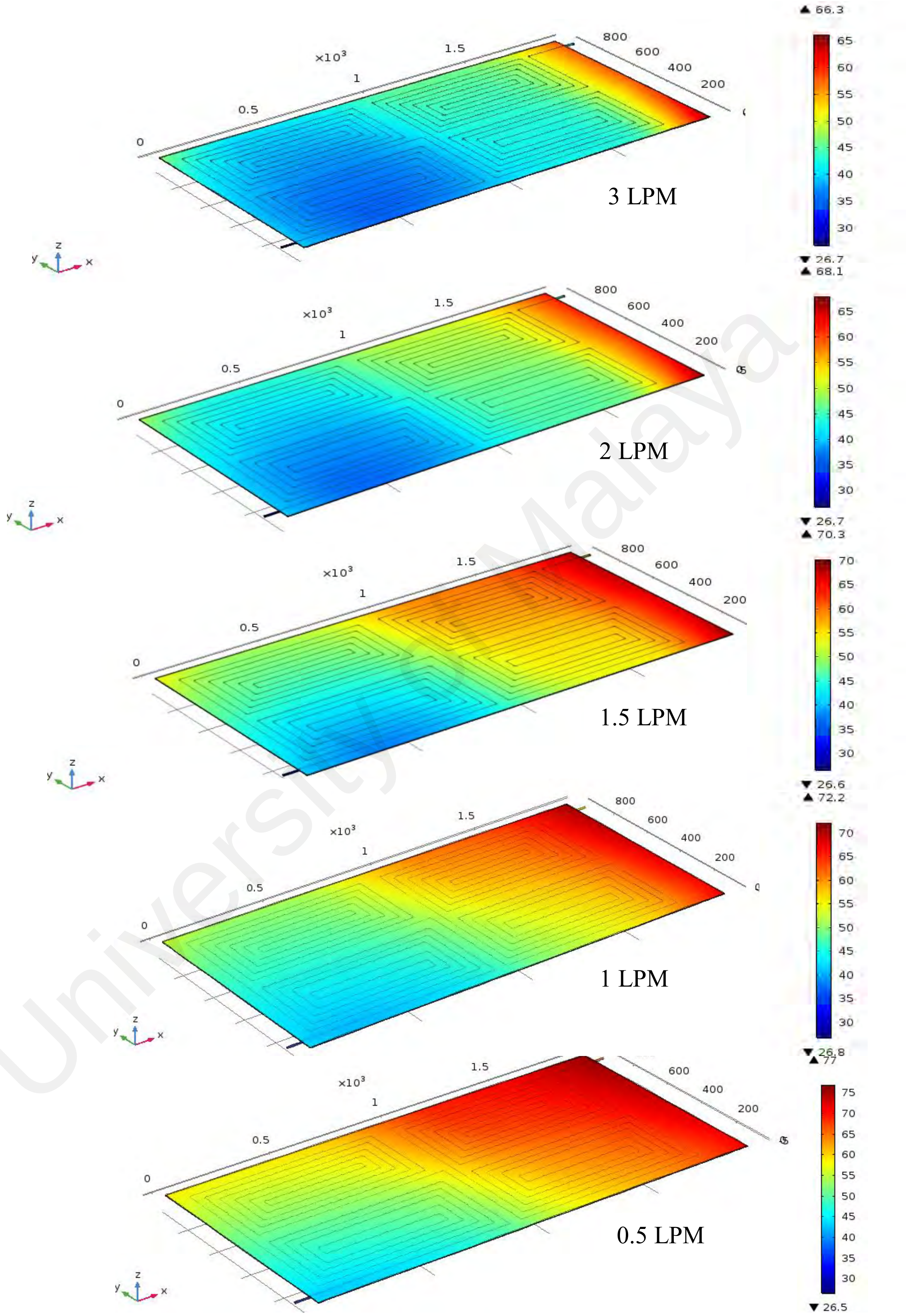

Figure 4.4: Surface temperature plot of the PVT for the effect of mass flow rate From 0.5 LPM to 3 LPM at 1000 W/m^2

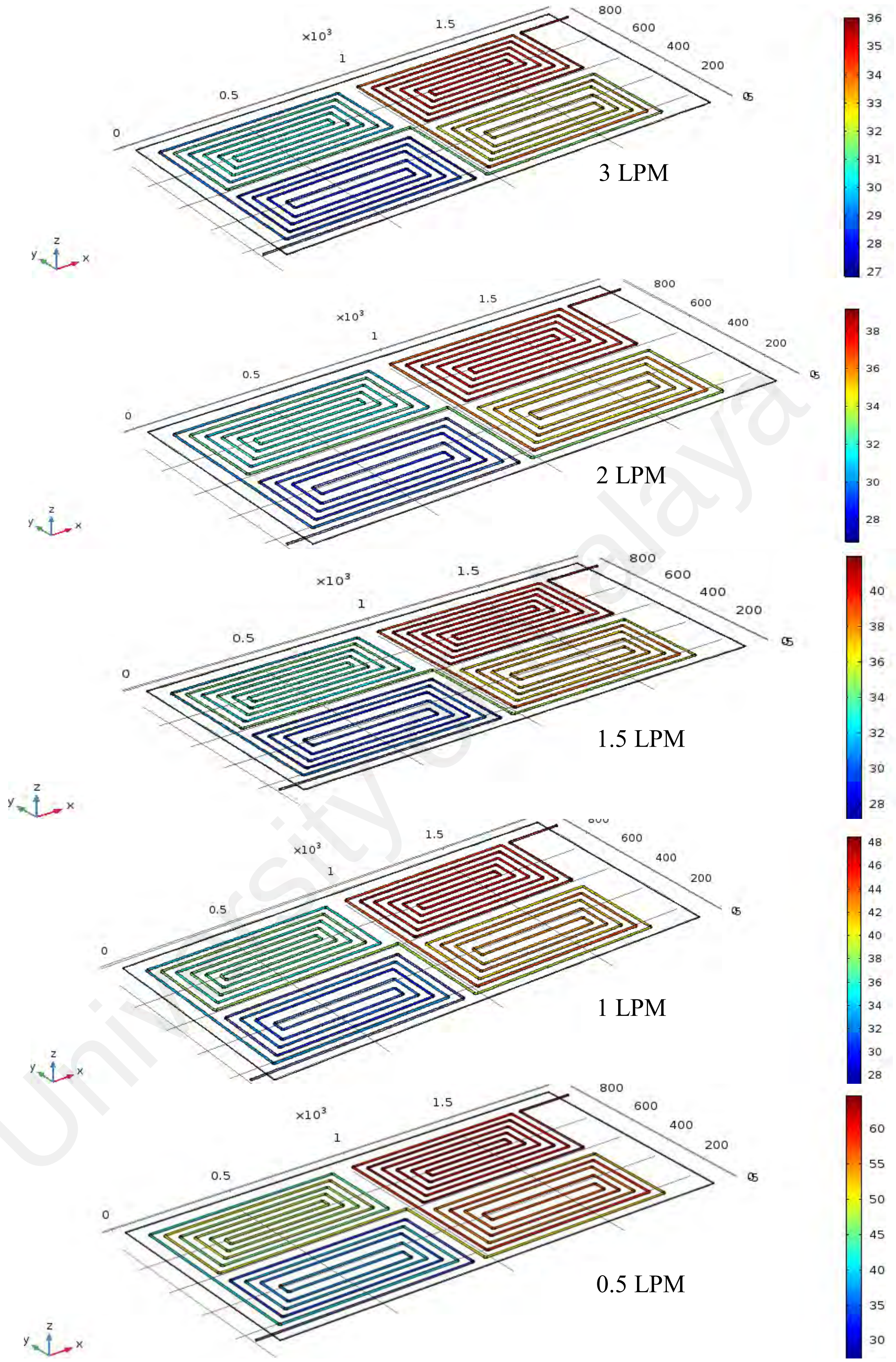

Figure 4.5: Streamlines plot of the PVT for the effect of mass flow rate from 0.5 LPM to 3 LPM at 1000 W/m^2

Effect of the mass flow rate of water is shown in Figure 4.4 for the surface temperature of the photovoltaic module and Figure 4.5 for streamline temperature of the thermal collector at fixed 1000 W/m^2. The surface temperature profile for the photovoltaic thermal system at different mass flow rates ranging from 0.5 LPM to 3 LPM is shown. As seen in Figure 4.4, the temperature varies significantly at different mass flow rates. It is clear from the figures that the photovoltaic module achieves a maximum temperature of 78.6°C approximately at 0.5 LPM, which is due to slower cooling effect of water flow in the thermal collector. Glass temperature is near to 78.6°C because of the thermal collector contact with the PV module which extracts the heat from the surface. However, this value of temperetuer is higher as shown in the temperature bar is due to edges of the panel. This is because of the reason that at the edges the thermal collector is not in direct contact, and there is only free convection due to environment . Conversely, at the rest area of panel, two type of convections occur due to free convection to the environment and forced convection in the pipe. The minimum surface temperature of the photovoltaic-thermal module is noted as 60 to 67°C approximately at 3 LPM of the mass flow rate at the same conditions. Streamline effect of mass flow rates on the thermal collector is depicted in Figure 4.3. The highest temperature is noted as 63°C approximately at 0.5 LPM, and the lowest is shown as 37°C approximately at 3 LPM.

4.3.3 Analysis of Temperature Behaviour of PVT-PCM

Phase change materials play a very important role in regulating photovoltaic modules cell temperatures. Figure 4.6 shows the effect of phase change material which is paraffin used here with melting or phase change temperature of 44°C with irradiation. This analysis is carried out when irradiation are at the peak incident on the system. The complete temperature behaviour is studied in these simulations. The temperate surface profile for the photovoltaic thermal system with PCM at different timings at the 1000 W/m2 and mass flow rate of 0.5 LPM is shown in Figures 4.6 and 4.7. Whereas, Figures 4.8 and 4.9 depict the results for thermal collector temperature distribution from the inlet of water flow to the outlet of the collector with and without irradiations. Similar to surface temperature, thermal collector temperatures profile is also studied in these conditions. Almost reverse phenomenon of the temperature gain and drain of the system is observed when irradiations are introduced and stopped. Temperature gain occurs when irradiations are introduced and temperature is drain and vanished completely after some time when suddenly irradiations are stopped from the incidence on the system. Hence, as seen in the figure 4.7 temperatures vary significantly at different timings. It is clear from the figures that the photovoltaic module achieves maximum temperature of 70 to 78.6°C approximately at 1000 W/m2 with the cooling effect of water flow in the thermal collector.

Photovoltaic thermal analysis with phase change materials is done with time-dependent simulations because phase change takes places with time as it gains heat from the panel and stabilizes after some time with the minor change in the temperature further. At the first 100 seconds, the temperature is increased to about 38.2°C from an initial temperature of 27°C. It gradually increases as times goes on till 3600 seconds and reaches to a maximum of 70.3°C. The important matter to note is that temperature varies fast at intervals of 600 seconds to 1200 seconds which is about 65°C and 68°C respectively. Conversely, the temperature increased with the very low value after a time interval of 1200 seconds and finally stabilizes with no significant change in temperature at about 3600 seconds. The reason behind is that heat is stored by the phase change material latently after the 44°C. Consequently, the PV module temperature remains lower as compared to the photovoltaic-thermal module without PCM. Figure 4.8 shows the streamline of thermal collector temperature distributions across the length of the pipe or flow path. Similarly, as the surface temperature of PV module, the water in thermal collector receives the maximum temperature very fast at the intervals of 600 seconds and 1200 seconds but temperature changes decrease significantly after 1200 seconds until 3600 seconds. At first 100 seconds temperature is noted as 32°C whereas, at 3600 seconds it reaches to approximately 63°C.

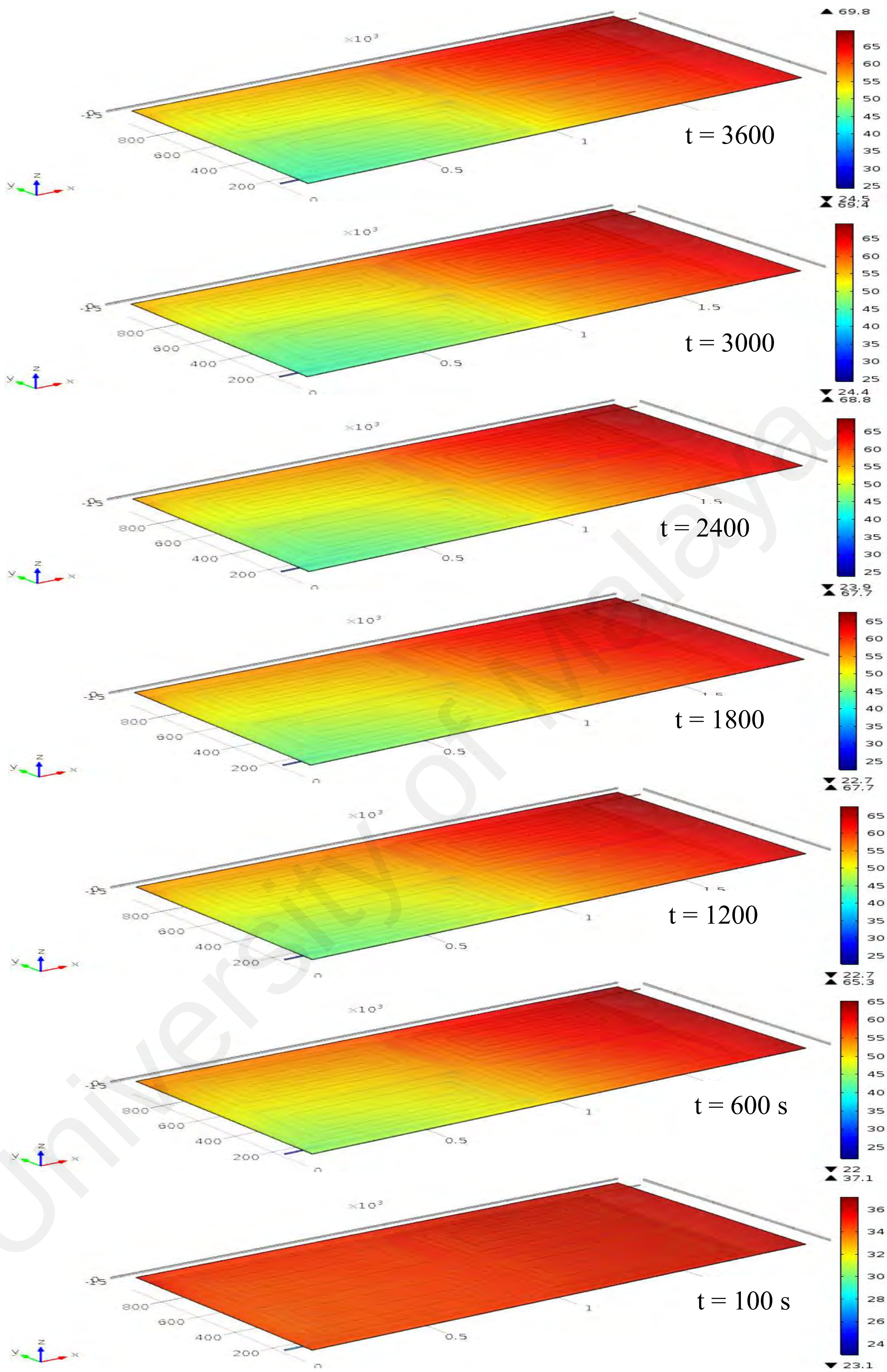

Figure 4.6: Surface temperature plot of the PVT-PCM for time variation at 1000 W/m^2 irradiation and flow rate 0.5 LPM

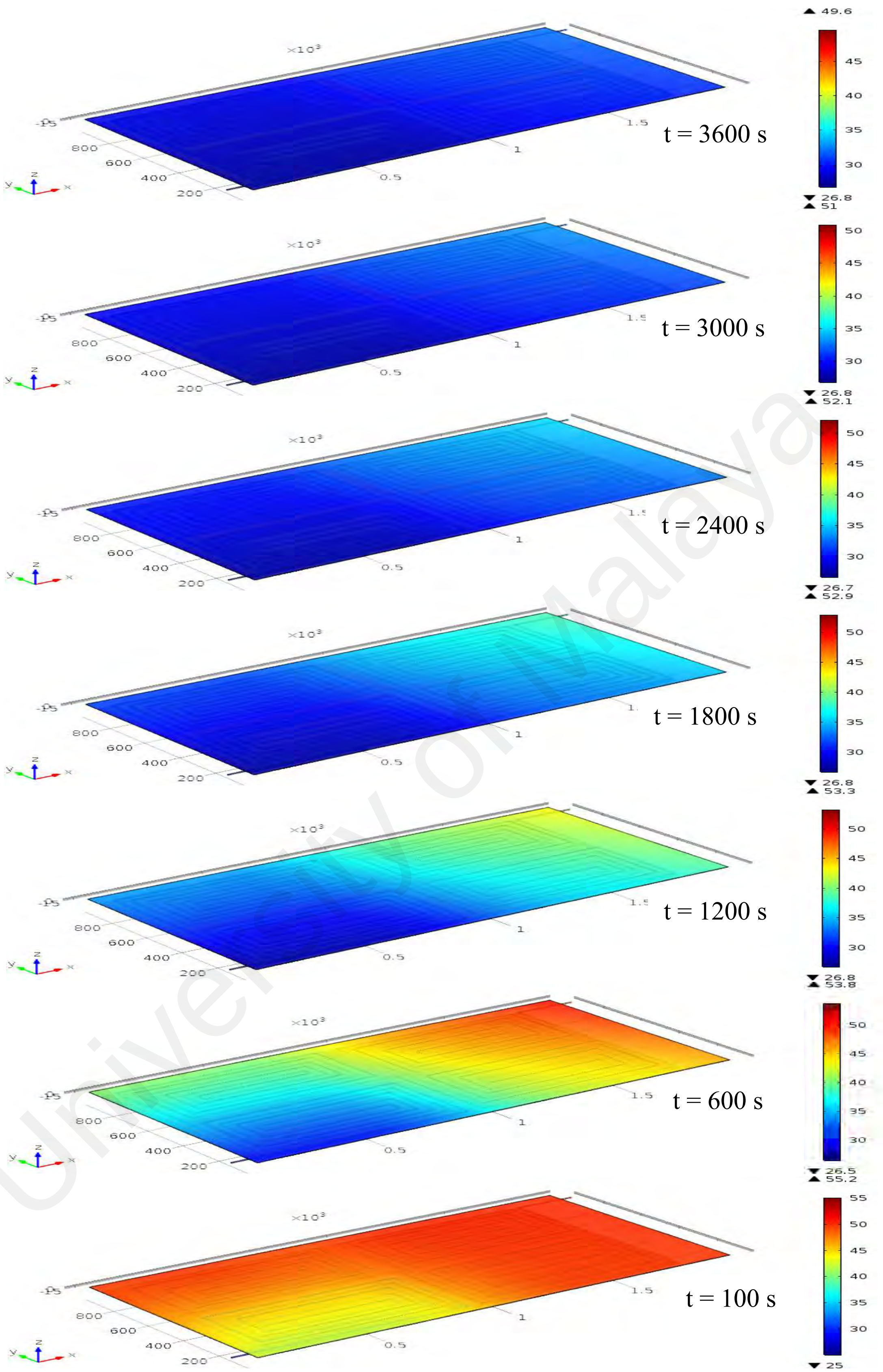

Figure 4.7: Surface temperature plot of the PVT-PCM for time variation at flow rate 0.5 LPM without irradiation

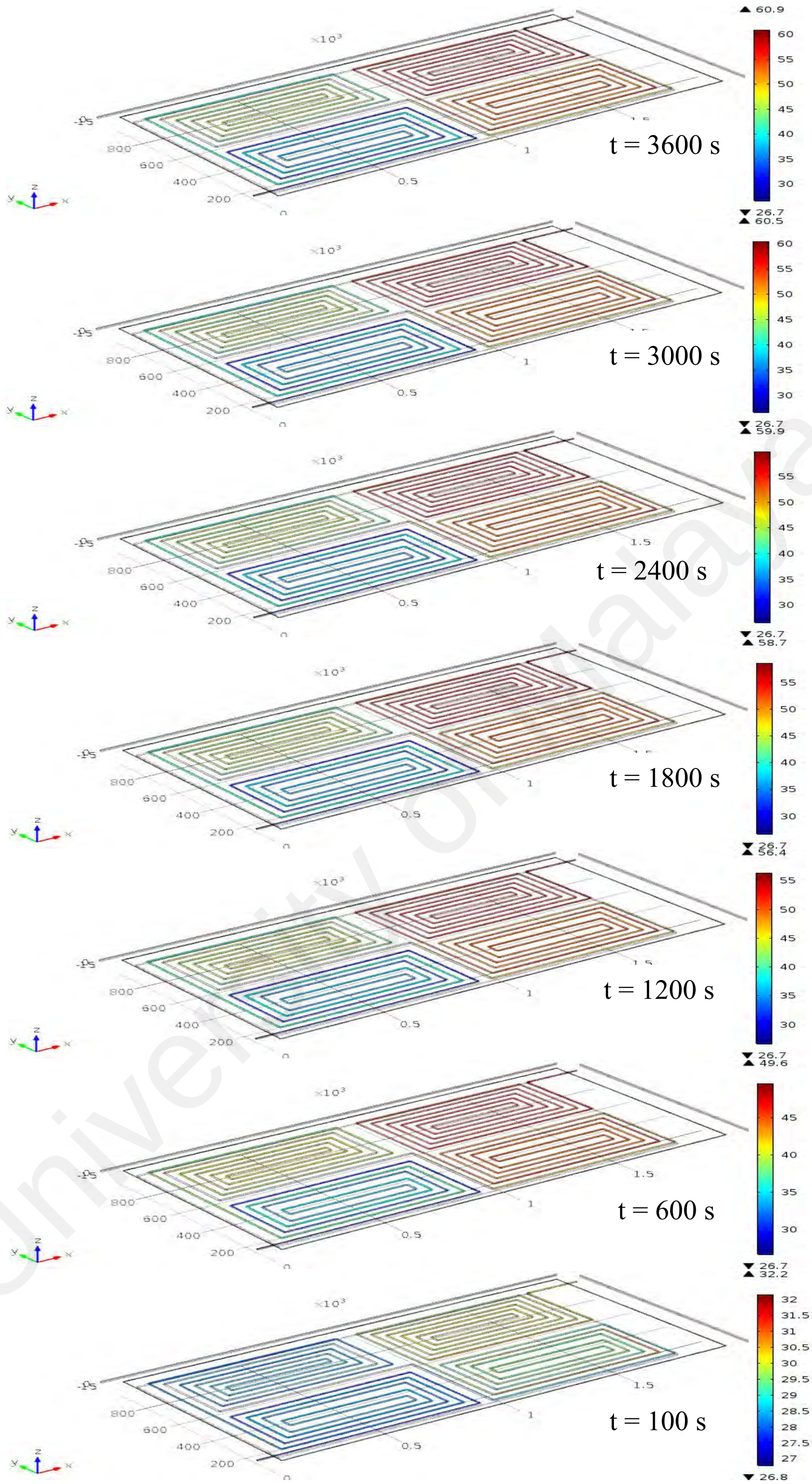

Figure 4.8: Streamlines of the PVT-PCM for time variation at 1000 W/m^2 irradiation and flow rate 0.5 LPM

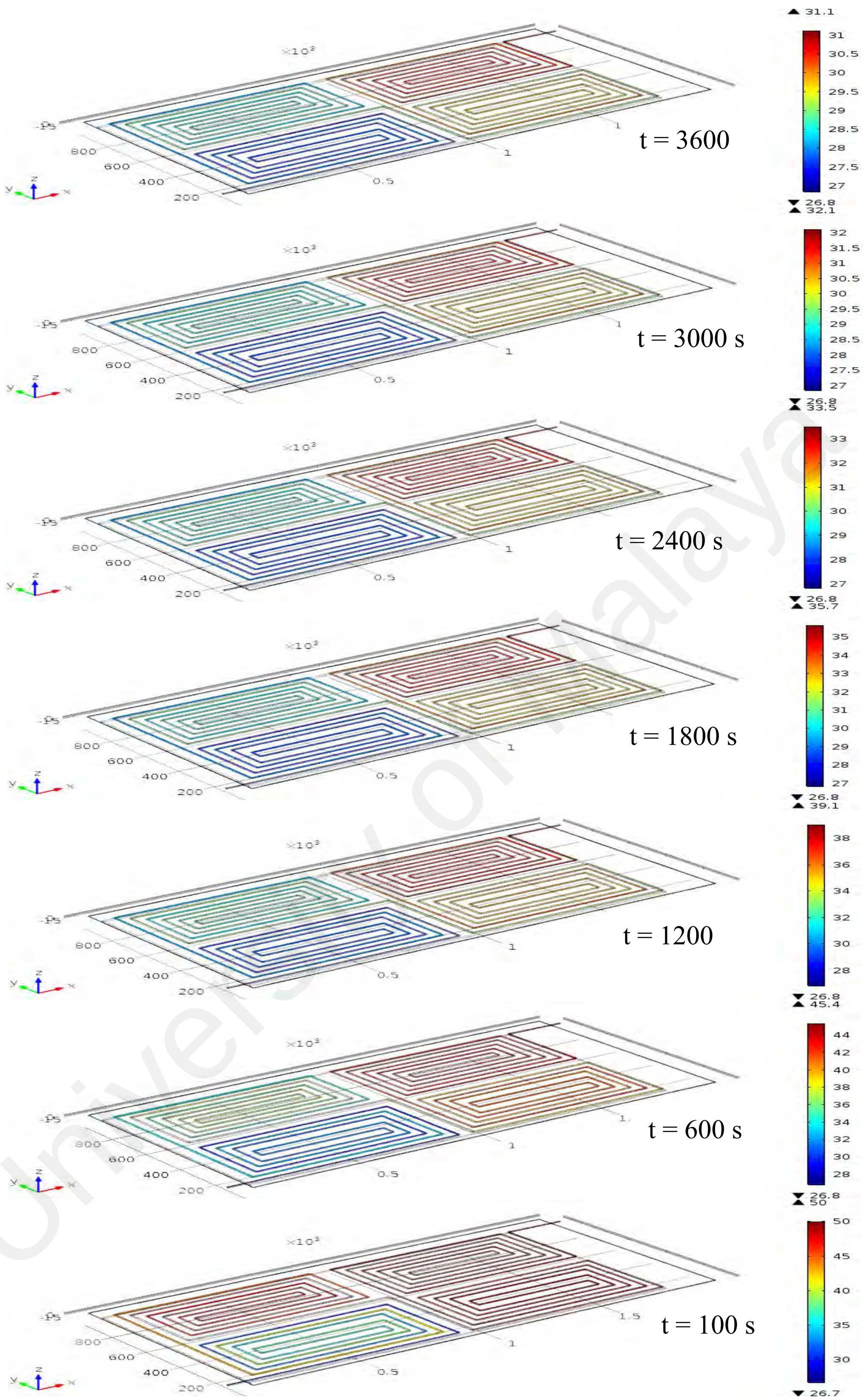

Figure 4.9: Streamlines of the PVT-PCM for time variation at flow rate 0.5 LPM without irradiation

Figure 4.7 shows the effect of phase change material when it already has gained temperature, and suddenly no irradiation is available. The initial conditions are set as 10 W/m^2 solar irradiation and mass flow rate of 0.5 LPM. This phenomenon will give the information about how temperature is dissipated if mass flow continues under no sunlight or irradiation in case of clouds, sunset or shadow of buildings etc. on the photovoltaic panels. In the first 100 seconds, the temperature falls to approximately 55°C from an initial temperature of about 70.5°C. It shows that temperatures fall very fast at first 100 seconds then gradually decreases as times goes on till 3600 seconds and reaches to a minimum surface temperature of about 50.5°C. In this case, the important matter to note is that temperature varies fast at first 100 seconds only then temperatures occurs slower and stable for the rest of the time, which is almost 15°C. Conversely, temperature decreased with the very low value after a time interval of 55°C. It is due to the reason that temperature is released by PCM rapidly at a higher value as extra energy more than its latent heat of capacity is given off and is taken by flowing water mass. Water receives the energy both from PCM and glass which results in a rapid decrease in glass temperature. Figure 4.9 shows the streamline of thermal collector temperature distributions across the length of the pipe or flow path. Unlike the surface temperature of the PV module, the water in the thermal collector receives the heat from PCM back steadily. At first 100 seconds temperature is noted as 51.5°C whereas, at 3600 seconds it reaches to approximately 33°C.

4.3.4 Irradiation Effect on the Systems

4.3.4.1 Irradiation effect on PV and PVT electrical performance

Figure 4.10 depicts the irradiation effect on cell temperatures of the PV and PVT. The figure shows the clear relationship between the irradiations and cell temperature as the irradiation increase the cell temperature also increases. However, this proportional relationship is not perfectly direct. At the higher irradiation levels, cell temperatures curves decline as compared to the radiations levels of 200 W/m^2 and 400 W/m^2. There is increase observed in the cell temperature due to the reason that higher irradiations have more energy to put into the PV and PVT but the declining behaviour of cell temperature at is due to the temperature gradient. The more the temperature gradient occurs the more heat flow from a hot body to the cold body (Nordmann and Clavadetscher, 2003). Some difference in results of experimental and numerical analysis is observed because of the uncertainty and error percentage of the sensors and equipment.

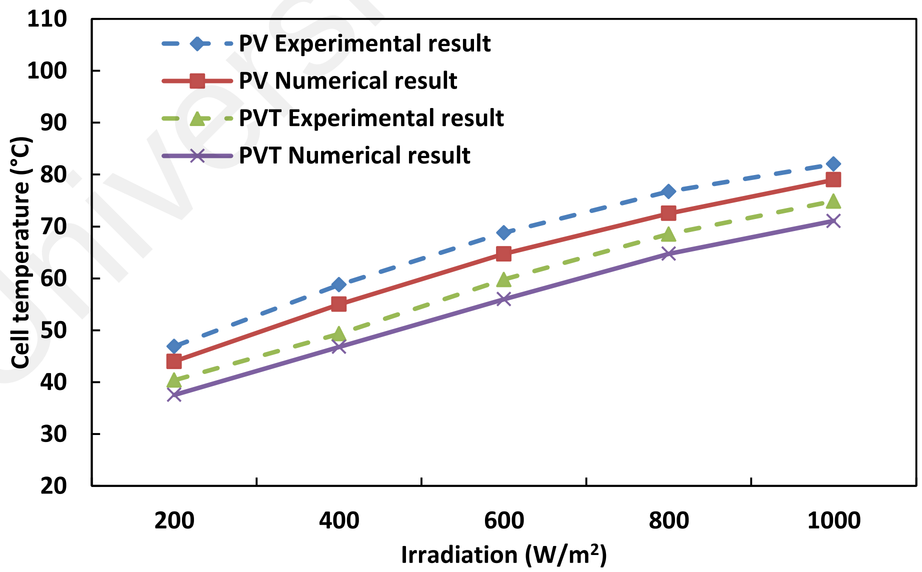

Figure 4.10: Irradiation effect on PV and PVT cell temperature

Figure 4.11 shows the cell temperature is achieved for PV at 82°C and 79°C experimentally and numerically respectively. For PVT, it is 74.89°C and 71.05°C experimentally and numerically respectively, which much lower than PV module.

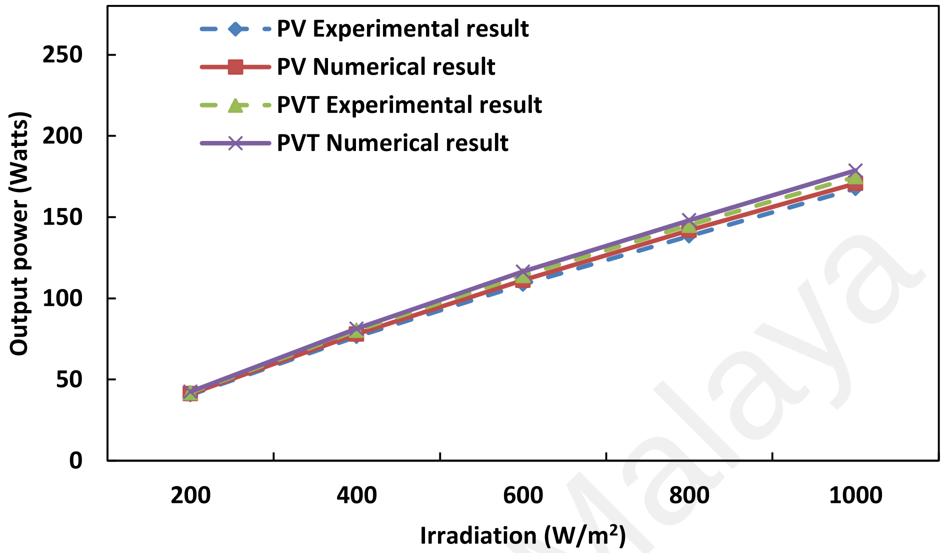

Figure 4.11: Irradiation effect on output power of PV and PVT

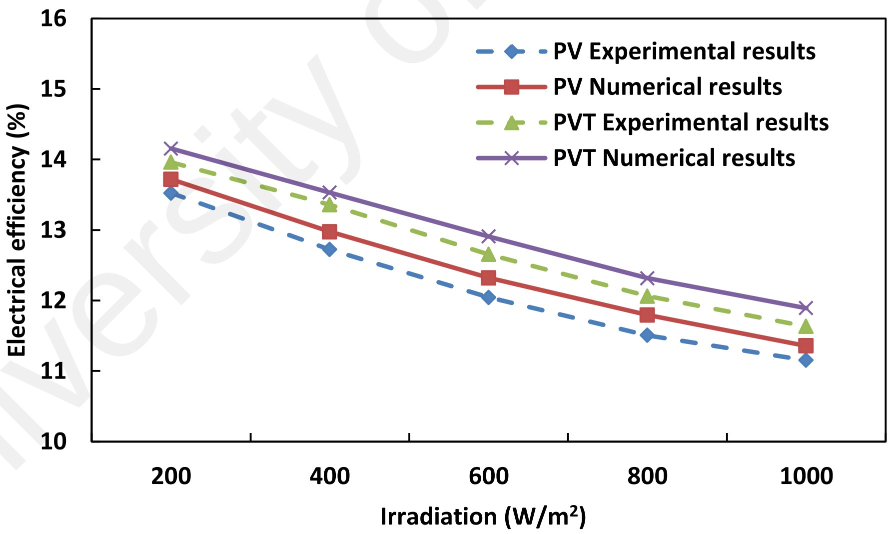

Figure 4.12: Irradiation effect on the electrical efficiency

Power and electrical efficiency are shown in the figures 4.11 and 4.12. This relationship shows that the irradiations have a proportional effect on the power as it increases the power also increases but not fully linearly. Power increases because the current and voltage increase with an increase in irradiations but the current increases higher than the voltage (Başoğlu and Çakır, 2016; Radziemska, 2003). Due to cooling effect in PVT, the power is higher in value as compared PV module. Some experimental deviations are observed at high irradiation intensity. The maximum output power of PVT is obtained as 178.77W and 174.87W numerically and experimentally respectively. Whereas, the minimum output power is derived as 42.55W and 41.97W in numerical and experimental results respectively.

Conversely, electrical efficiency is observed to be decreased due to rise in cell temperature as shown in Figure 4.12. Effect of delta T/G on electrical and thermal efficiency is also shown by (Tripanagnostopoulos et al., 2002) under constant working conditions. Polycrystalline PV electrical efficiency was achieved as 12.4% for PVT with water as working fluid, and 58% of thermal energy is achieved.

4.3.4.2 Varying irradiation effect on PVT thermal performance

The water outlet a temperature is increased due to increase in irradiations as observed in the Figures 4.13. The reason behind this increase in output temperature is the high energy input due to high intensity of irradiations incident on the system (Rohsenow et al., 1998). The heat transfer phenomenon changes its pattern after the 600 W/m^2 and some of the heat starts to flow to the environment due to higher temperature difference in between PVT and environment (Kreith and Black, 1980). In Figure 4.14, the effect of irradiation on the thermal energy is shown. Irradiation at higher levels put more energy into the systems and in result water circulating into thermal collector absorbs more energy. Therefore, the thermal gain in water is higher at high values of irradiations. Furthermore, declining trend in the thermal energy is seen which is because at high irradiations the temperature is higher at the system, therefore, some energy is lost into the environment before it gets transferred into the water. This is similar to the output hot water temperature described in Figure 4.13.

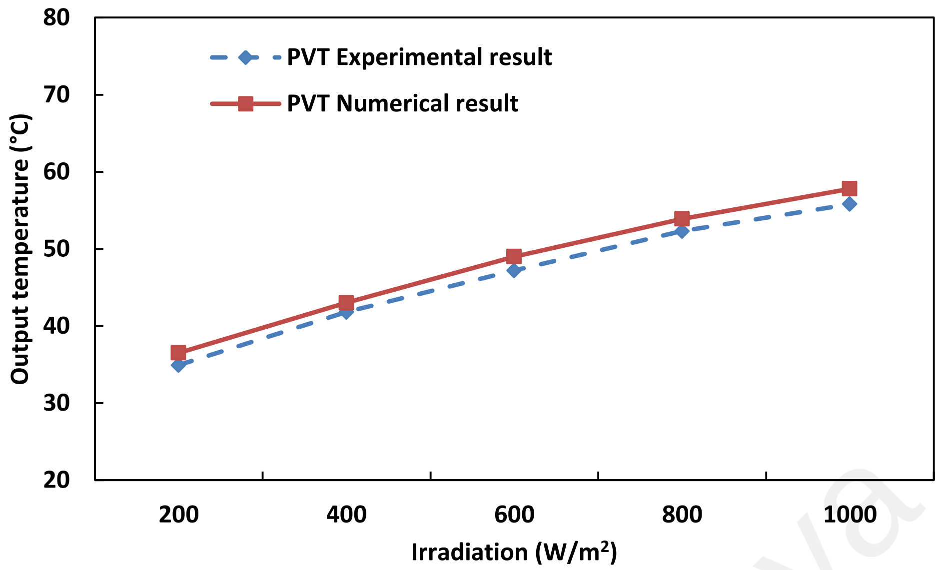

Figure 4.13: Impact of irradiation on PVT output temperature at 0.5 LPM

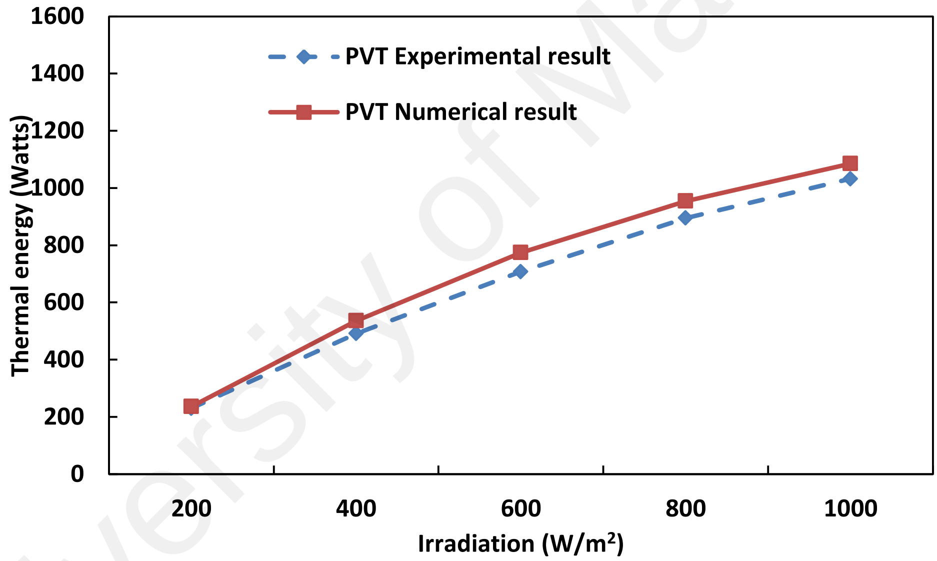

Figure 4.14: Irradiation effect on thermal energy

In figure 4.15, the irradiation effect is shown on the thermal efficiency of the PVT system. The thermal efficiency is taken from the thermal energy obtained. It is observed that thermal efficiency reduces at higher irradiation levels especially after 600 W/m^2. This is due the reason that total of the energy is not efficiently converted into useful energy as some the energy is lost into the environment at higher temperatures due to a high temperature gradient. However, at low irradiation the losses are at a minimum as the maximum of the energy is transferred to flowing water but still, some energy is lost in this case.

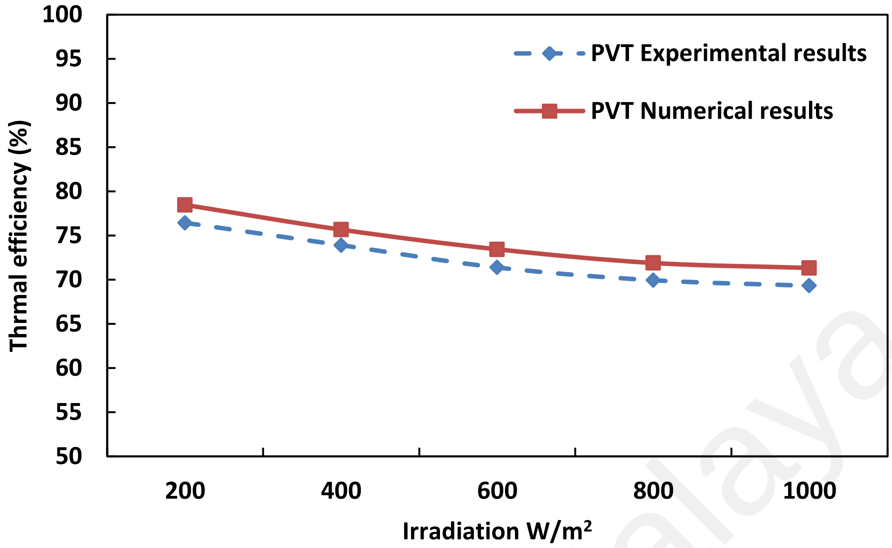

Figure 4.15: Irradiation effect on thermal efficiency

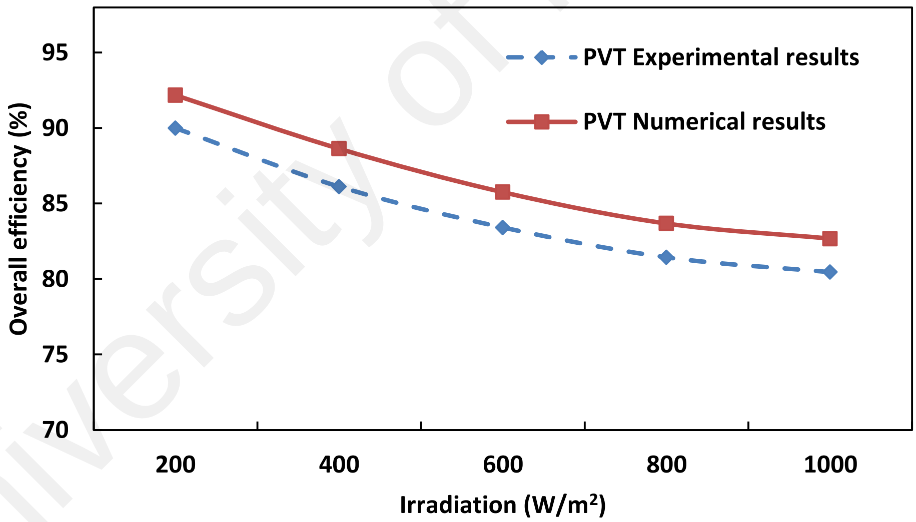

Figure 4.16: Solar irradiation effect on overall efficiency

Overall efficiency also decreases with increasing irradiation levels due to the effect of losses of energy back into the environment. It is the similar effect explained Figures 4.12 and 4.15. Overall efficiency achieved at 200 W/m^2 is better than 1000 W/m^2 irradiations. The values of 92.17% and 89.94% are achieved for highest overall efficiency at 200 W/m^2 and 82.67% and 80.45% are obtained for minimum overall efficiency at 1000 W/m^2 numerical and experimental results respectively.

4.3.4.3 PVT-PCM electrical performance at varying irradiation

Figure 4.17 depicts the irradiation effect on cell temperatures of the PV and PVTPCM. The figure shows the clear relationship between the irradiations and cell temperature as the irradiation increase the cell temperature also increases. PCM (A44) plays role to absorb and store heat latently to further cool the PV module(Browne et al., 2016). However, this proportional relationship is not perfectly direct. At the higher irradiation levels, cell temperatures curves decline as compared to the radiations levels of 200 W/m^2 and 400 W/m^2. There is increase observed in the cell temperature due to the reason that higher irradiations have more energy to put into the PV and PVT-PCM but the declining behaviour of cell temperature at higher temperatures is because of the temperature gradient. The more the temperature gradient occurs the more heat flow from a hot body to the cold body.

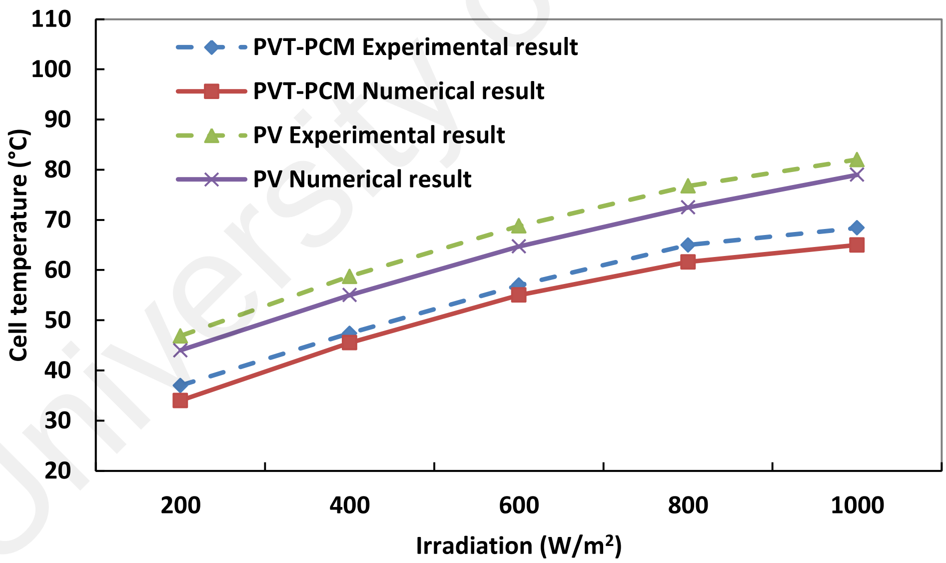

Figure 4.17: PVT-PCM cell temperature at different irradiations

Effect of incident irradiation on power and electrical efficiency are shown in the Figures 4.18 and 4.19. This relationship shows that the irradiations have a proportional effect on the power as it increases the power also increases but not fully linearly. Power increment is due to an increase in irradiations but the current increases higher than voltage.

PVT-PCM system acquires higher values of power as compared to PV module because PVT-PCM system has cooling of PV through two ways of circulating water and PCM heat storage. Hence, it can also be concluded that this cooling is more effective than the PVT system as PVT doesn't have PCM, which is responsible for excessive heat absorption. Figure 4.19 shows that electrical efficiency relationship with cell temperature, where, it decreases with increase of cell temperature. More loss of electrical energy is observed in the case of PV as compared to PVT-PCM.

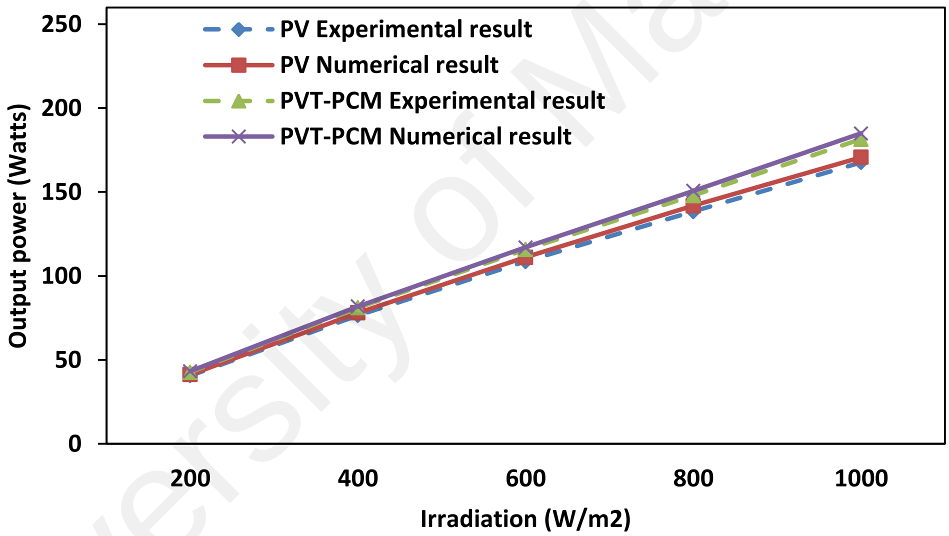

Figure 4.18: PVT-PCM output power at different irradiations

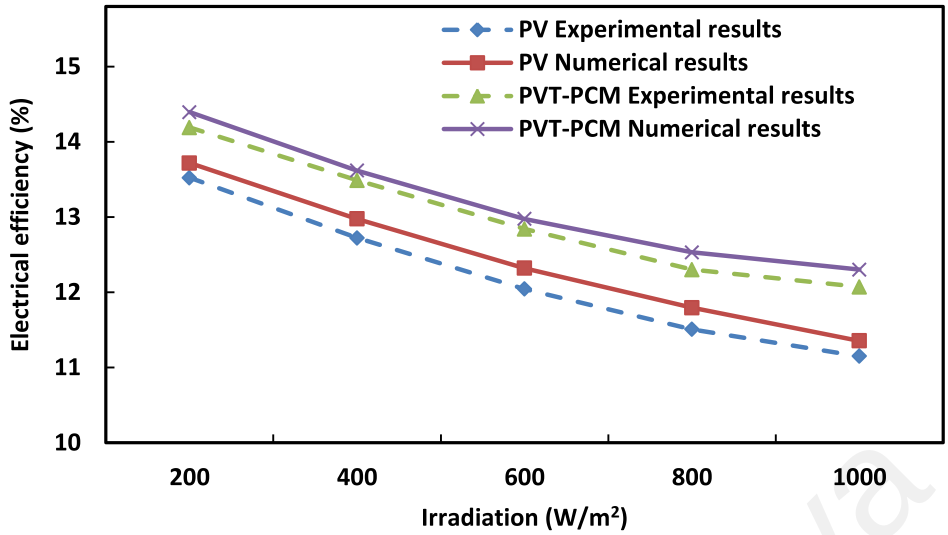

Figure 4.19: PVT-PCM electrcial efficiency at different irradiations

4.3.4.4 PVT-PCM system thermal performance at varying irradiations

The water outlet a temperature is increased due to increase in irradiations as observed in the Figures 4.20. The reason behind this increase in output temperature is the high energy input due to high intensity of irradiations incident on the system. The heat transfer phenomenon changes its pattern after the 600 W/m^2 and some of the heat starts to flow to the environment due to higher temperature difference in between PVT-PCM and environment (Browne, M.C. et al., 2015; Rohsenow et al., 1998).

Thus, the heat taken by the PVT-PCM is divided into heat carried by flowing water and the rest is stored in the PCM other than heat loss. Therefore, heat carried by water is lower in the PVT-PCM system as compared to only a PVT system (Gaur et al., 2017). In Figure 4.21, the effect of irradiation on the on the thermal energy is shown. Irradiation at higher levels put more energy into the systems and in result water circulating into thermal collector absorbs more energy. Therefore, the thermal gain in water is higher at high values of irradiations. Furthermore, declining trend in the thermal energy is seen which is because at high irradiations the temperature is higher at the system, therefore, some of the thermal energy is lost into the environment before it gets transferred into the water. This is similar to the output hot water temperature described in Figure 4.20 the effect of the temperature gradient. However, thermal energy obtained for PVT-PCM is lower than PVT case due to the reasons described in Figure 4.18.

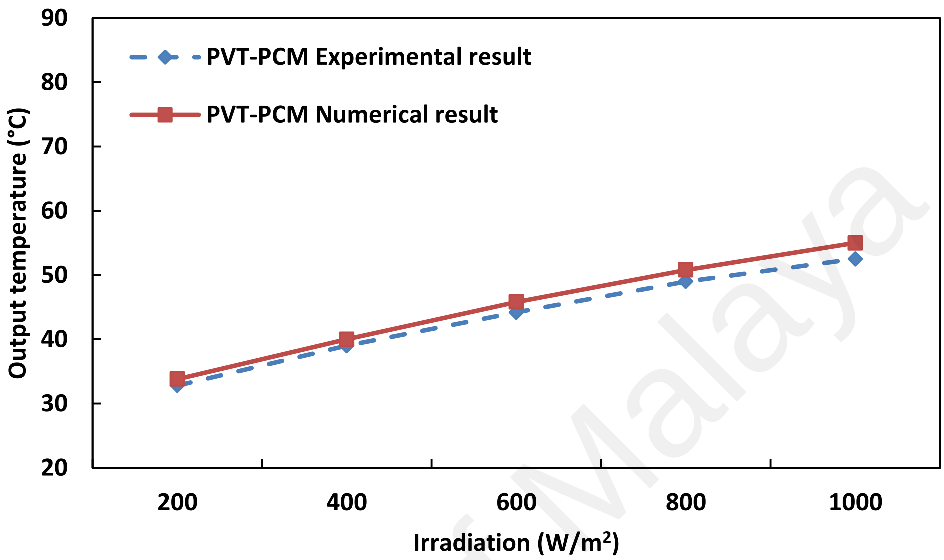

Figure 4.20: PVT-PCM output temperature at different irradiations

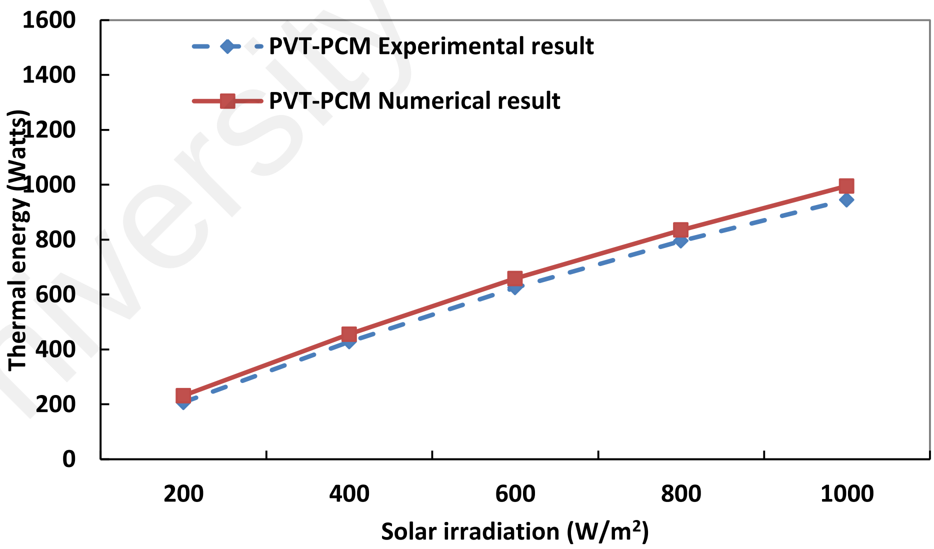

Figure 4.21: PVT-PCM thermal energy at different irradiations

In Figure 4.22, the irradiation effect is shown on the PVT-PCM system thermal efficiency. The thermal efficiency is taken from the thermal energy obtained. It is observed that thermal efficiency reduces at higher irradiation levels especially after 600

W/m^2. This is due the reason that total of the energy is not efficiently converted into useful energy as some of the energy is lost into the environment at higher temperatures due to a high-temperature gradient. However, at low irradiation the losses are at a minimum as most of the energy is transferred to flowing water but still, some energy is lost in that case.

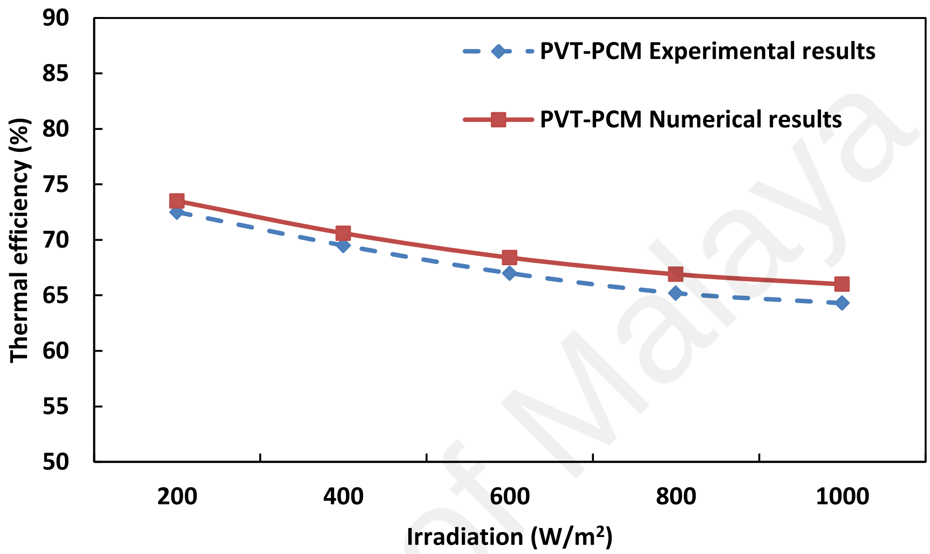

Figure 4.22: Thermal efficiency of the PVT-PCM system at different irradiations

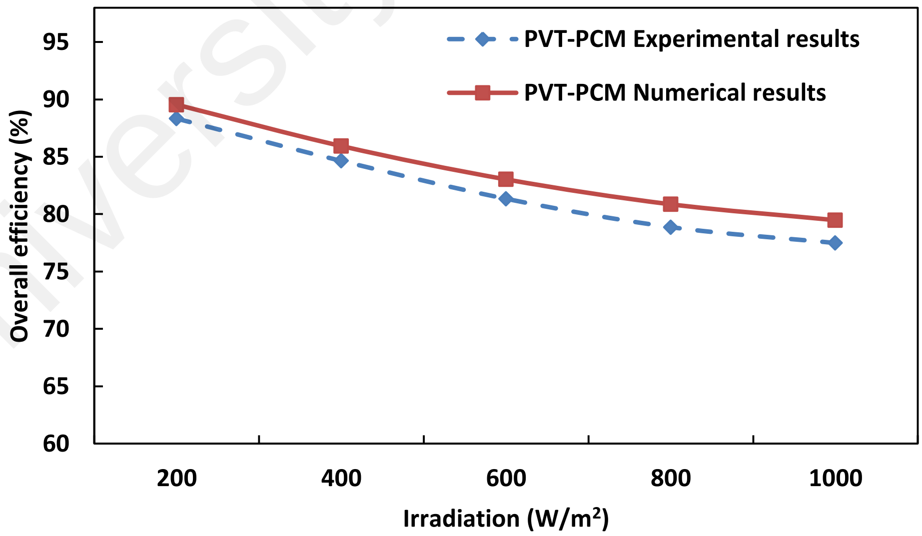

Figure 4.23: PVT-PCM system overall efficiency at different irradiations

The overall efficiency decreases with increasing irradiation levels due to the effect of losses of energy back into the environment as seen in Figure 4.23. It is the similar effect explained in the Figures 4.19 and 4.22. Overall efficiency achieved at 200 W/m^2 is better than 1000 W/m^2 irradiations. The values of 89.54% and 88.32% are achieved for highest overall efficiency at 200 W/m^2 and 79.47% and 77.4% are obtained for minimum overall efficiency at 1000 W/m^2 numerical and experimental results respectively.

4.3.5 Mass Flow Rate Effect on PVT and PVT-PCM Performance

4.3.5.1 Mass flow rate effect on PVT electrical performance

Mass flow rates of working fluids have prominent effects on the heat removal phenomenon in the system. It is observed in Figure 4.24 that the cell temperature of the PVT system reduces as the mass flow rate of water increases from 0.5 LPM to 3 LPM. As the inlet mass flow rate is increased the excessive heat is transferred to water from the module by convection phenomenon resulting in the reduction of cell temperature. There is a huge reduction in cell temperature at 0.5 LPM to 1 LPM but this trend reduces after 1 LPM (Wu et al., 2011). It is because of the reason that cell temperature is higher and the inlet mass flow rate is at a lower temperature, therefore, maximum heat is removed due to a higher temperature gradient. It is noted that numerical trend line is quite stable after 1 LPM but the experimental line is fluctuating through the course because of the reason of indoor some out of controlled operating conditions or instrumental basic error percentage. However, experimental and numerical values are almost similar overall.

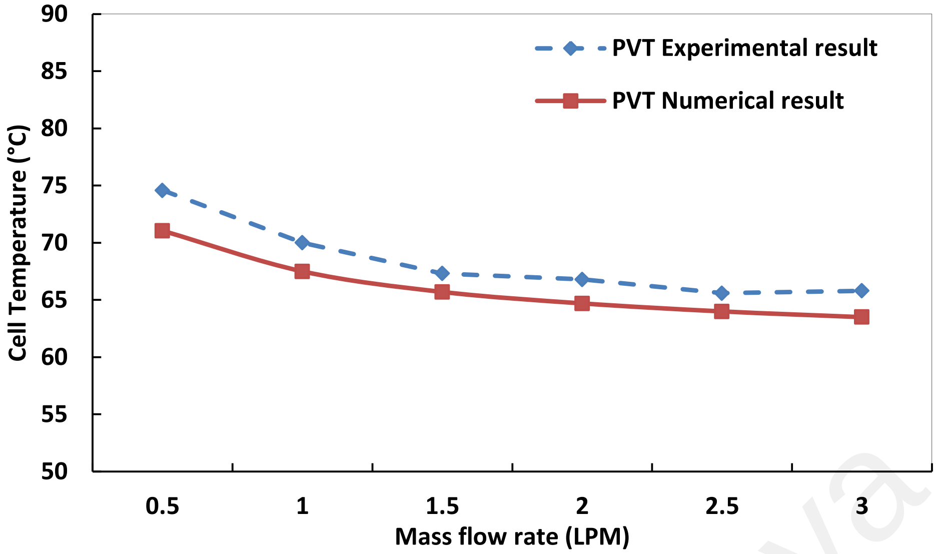

Figure 4.24: Mass flow rate effect on cell temperature

Mass flow rate effect on electrical efficiency and power is depicted in figures 4.25 and 4.26. The power and electrical efficiency increase with the cell temperature drop prominently due to the increase in mass flow rate, which transfers heat from the PV module. Consequently, PVT voltage increases noticeably while current reduces to some level, resulting in electrical efficiency and a power increase of the PVT. The highest values for the power are achieved as 186.43W and 184.71W numerically and experimentally respectively. Whereas, the minimum output power is obtained as 178.77W and 174.87W numerically and experimentally respectively. Furthermore, on average output power increment is obtained as 1.25W and 1.58W per 0.5 LPM.

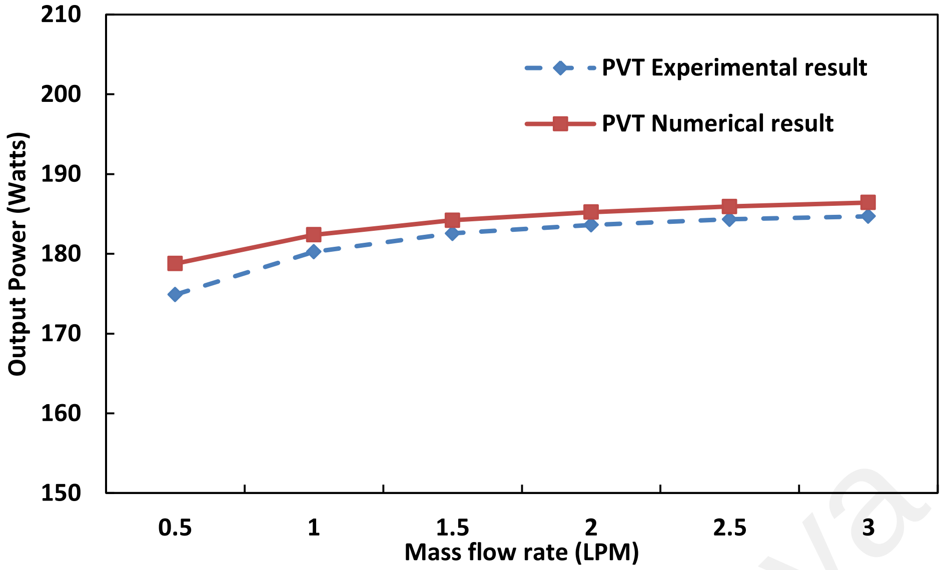

Figure 4.25: Mass flow rate effect on output power

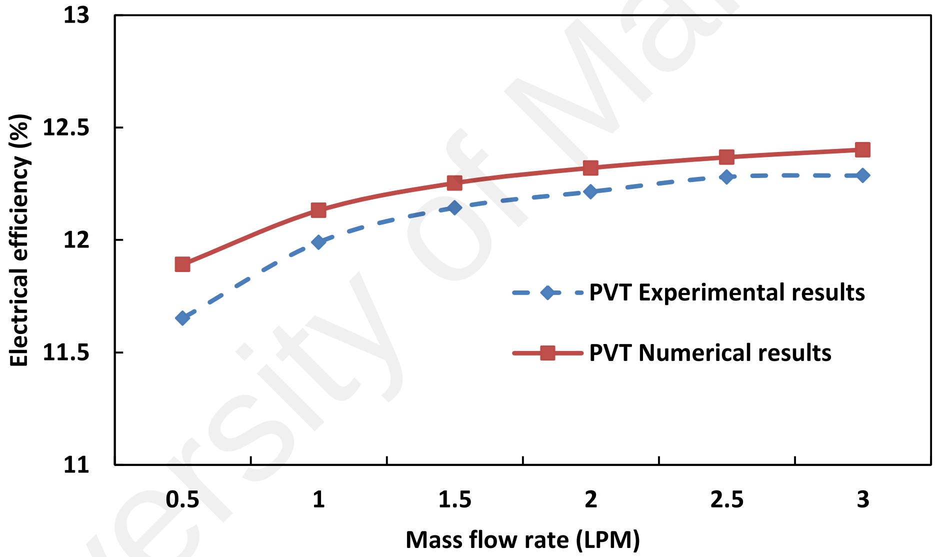

Figure 4.26: Mass flow rate effect on electrical efficiency

The maximum values for electrical efficiency are obtained as 12.4% and 12.28% numerically and experimentally respectively. Further, the electrical efficiency with the minimum values is obtained as 11.89% and 11.62% for numerically and experimentally respectively. Additionally, electrical efficiency increment per 0.5 LPM is observed as 0.08% and 0.10% for numerical and experimental results respectively. It is found that numerical values are higher to some value than the experimental values. These differences are due to the weather conditions, which are not fully in control and may deviate from stable position. There is no ideal control of working parameters especially the ambient temperature in the experimental setup but 27°C ambient temperature is set for experimental and numerical investigation.

4.3.5.2 Mass flow rate effect on thermal performance of PVT

Figures 4.27 and 4.28 show the impact of mass flow rate on the output temperature and thermal energy of the PVT system. There is a decrease in water outlet temperature with increase in inlet mass flow rate as seen in Figure 4.27. At lower mass flow rates more heat is occupied in the small mass of water, therefore, results in higher output temperature of water. Thus, the reduction in output temperature with an increase in the mass flow rates determines that a huge mass of water accumulates higher heat but with less temperature. This is attributed to reason that a certain amount of heat absorbed by low mass have a higher temperature than the same amount of heat absorbed by huge mass. However, at higher mass flow rates more heat is transferred even though the output temperature is low as compared to 0.5 LPM of mass flow rate. Therefore, the amount of heat removed is increased with the increase in mass flow rate with lesser time.

Figure 4.27 also shows that the satisfactory agreement in results is achieved numerically and experimentally with small deviations in experimental data, which shows the validation of the numerical model confidently. Maximum output temperatures are observed as 57.4°C and 56°C numerically and experimentally respectively. Whereas, minimum output temperatures are 33.1°C and 32.43°C for numerically and experimentally respectively. Furthermore, on average 4.05°C and 3.92°C increment is achieved per 0.5 LPM numerically and experimentally respectively.

Achieved thermal energy versus mass flow rate shown in Figure. 4.28 increases with increasing mass flow rate through the flow channel. Convective heat transfer rate increases at mass flow rate increases. However, it is observed that after 0.5 LPM it is slowed down as compared to an initial situation, which is due the reason discussed in the case of Figure 4.27, indicating the same trend for heat transfer rate for both Figures. Therefore, excessive heat is transferred under the similar conditions at higher mass flow rates.

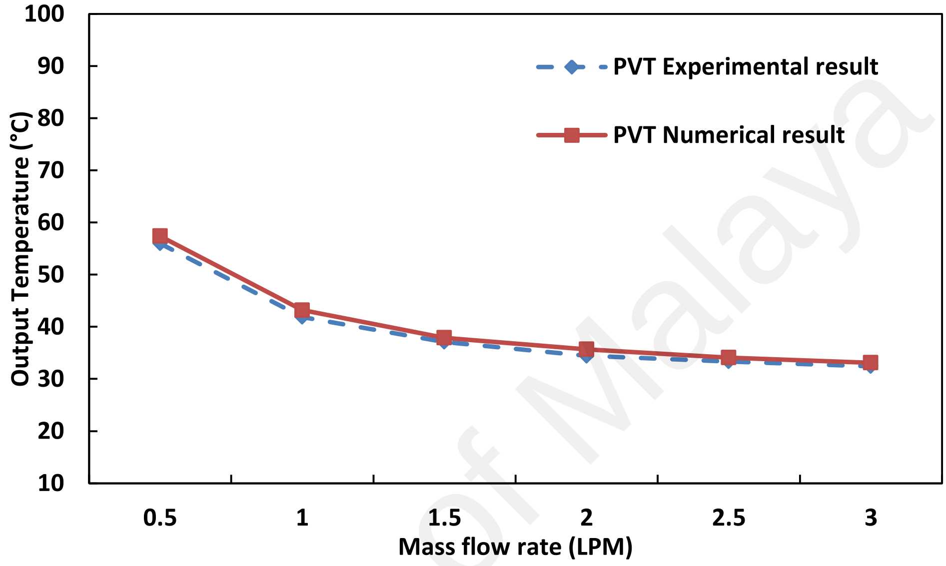

Figure 4.27: Effect of mass flow rate on output temperature

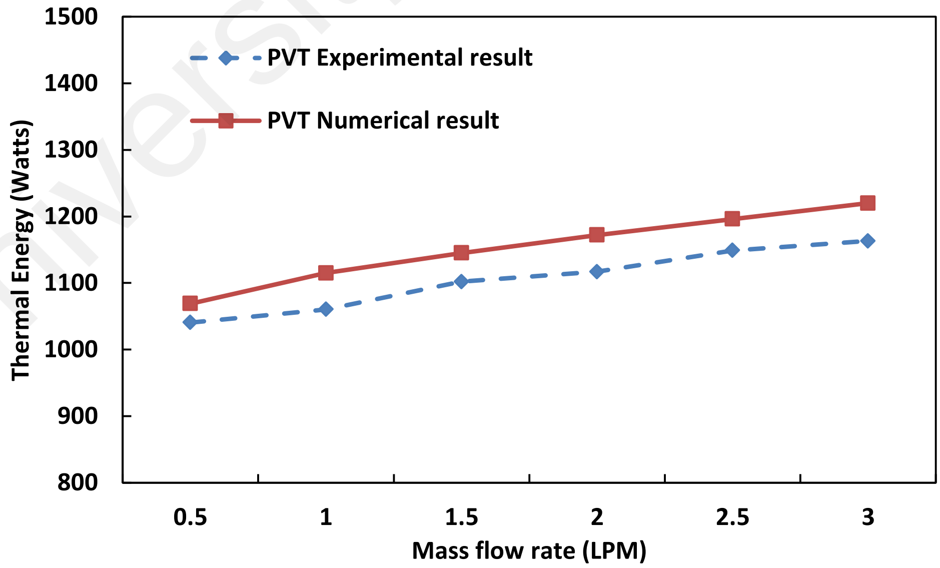

Figure 4.28: Effect of mass flow rate on thermal energy

Figures 4.29 shows that thermal efficiency increases with increasing water mass flow rate through the system. Increase in mass flow rate enhances the heat transfer through convection between water and thermal collector, which causes in excessive heat transfer at higher mass flow rates, resulting in enhancing the thermal efficiency. The highest values achieved for thermal efficiency are 81% and 77.36% numerically and experimentally respectively. Additionally, the lowest values are obtained as 71% and 69% for numerical and experimental cases. Furthermore, the rate of thermal efficiency increment is obtained as 1.67% and 1.39% per 0.5 LPM for numerically and experimentally respectively. The overall efficiency of the system is shown in Figure 4.30. The thermal efficiency increases simultaneously with the increment in mass flow rates with the similar trend noted in the electrical and thermal efficiency of the system. Values for the overall efficiency of PVT are achieved as 93.4% and 82.89% at highest numerically and experimentally respectively. Lowest values of the overall thermal efficiency are obtained as 82.89% and 80.65% numerically and experimentally respectively. Furthermore, the rate of efficiency increment is found as 1.75% and 1.5% for each mass flow rate of 0.5 LPM.

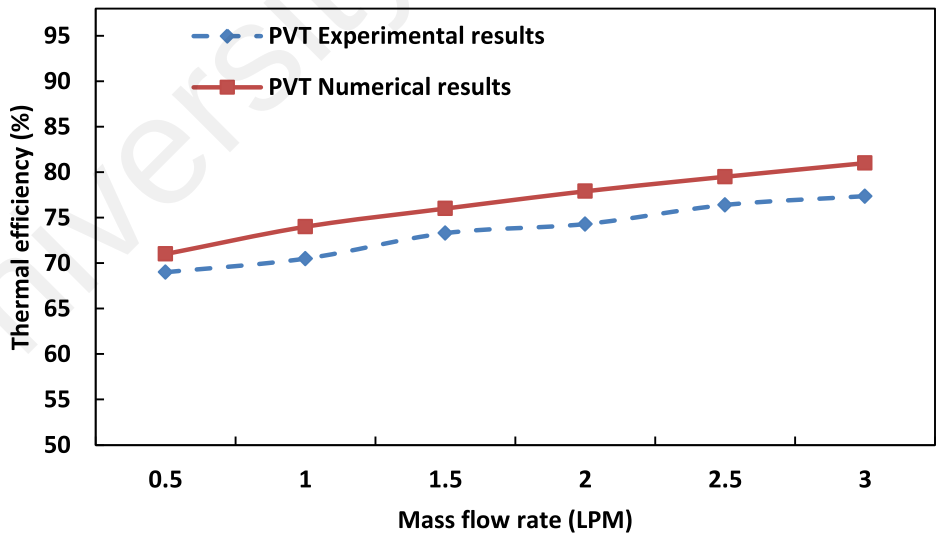

Figure 4.29: Mass flow rate effect on thermal efficiency

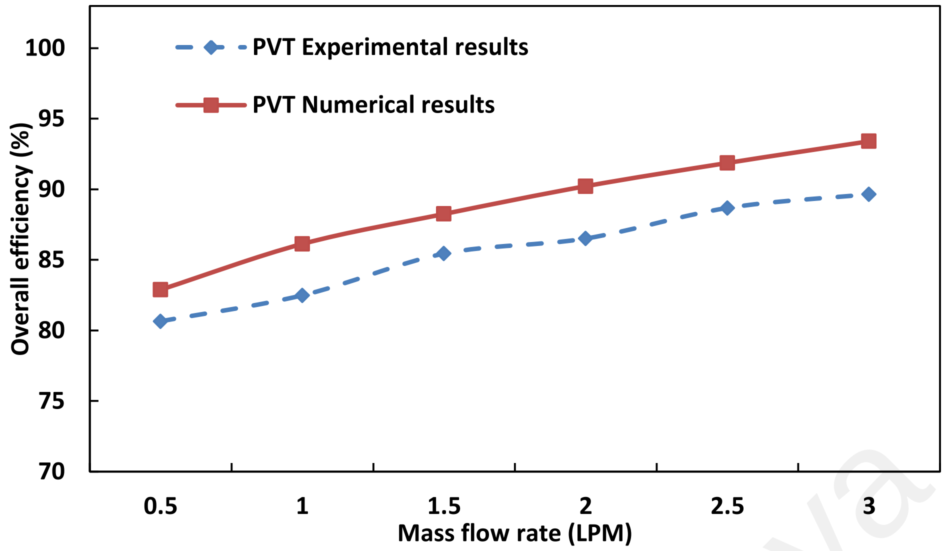

Figure 4.30: Mass flow rate effect on overall efficiency

4.3.5.3 Mass flow rate effect on PVT-PCM electrical performance

The influence of flow rate on the PVT-PCM cell temperature is depicted in Figure 4.31. It is observed that the cell temperature of the PVT system reduces as the mass flow rate of water increases from 0.5 LPM to 3 LPM. As the inlet mass flow rate is increased the excessive heat is transferred to water from the module by convection phenomenon resulting in the reduction of cell temperature. There is a huge reduction in cell temperature at 0.5 LPM to 1 LPM but this trend reduces after 1 LPM (Wu et al., 2011). It is because of the reason that cell temperature is higher and the inlet mass flow rate is at a lower temperature at first as well as PCM absorbs heat from cell simultaneously, therefore, maximum heat is removed due to a higher temperature gradient. From Figure 4.31, it can be observed that numerical trend line is quite stable after 1 LPM but the experimental line is fluctuating through the course because of the reason of indoor some out of controlled operating conditions or instrumental basic error percentage. However, experimental and numerical values are almost the similar overall.

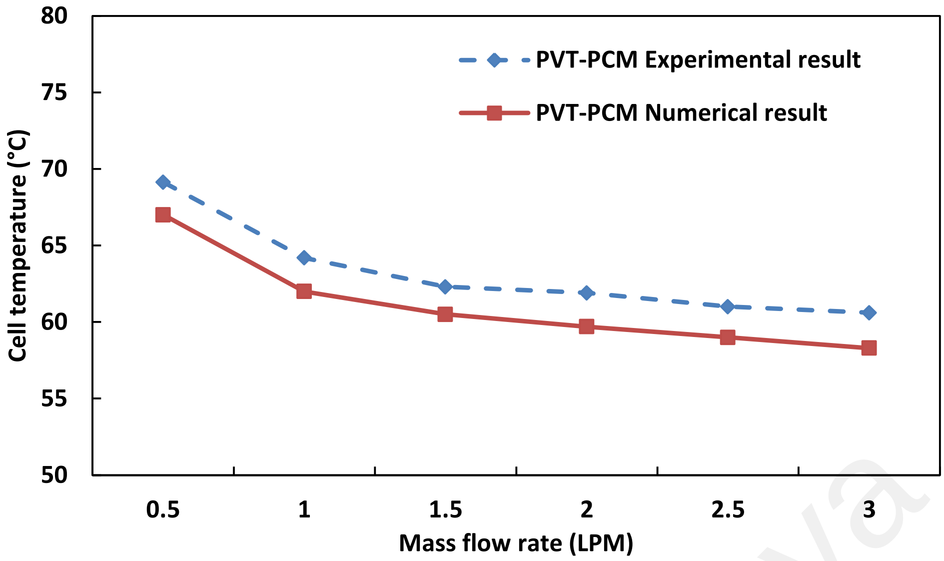

Figure 4.31: Effect of mass flow rate on cell temperature of the PVT-PCM system

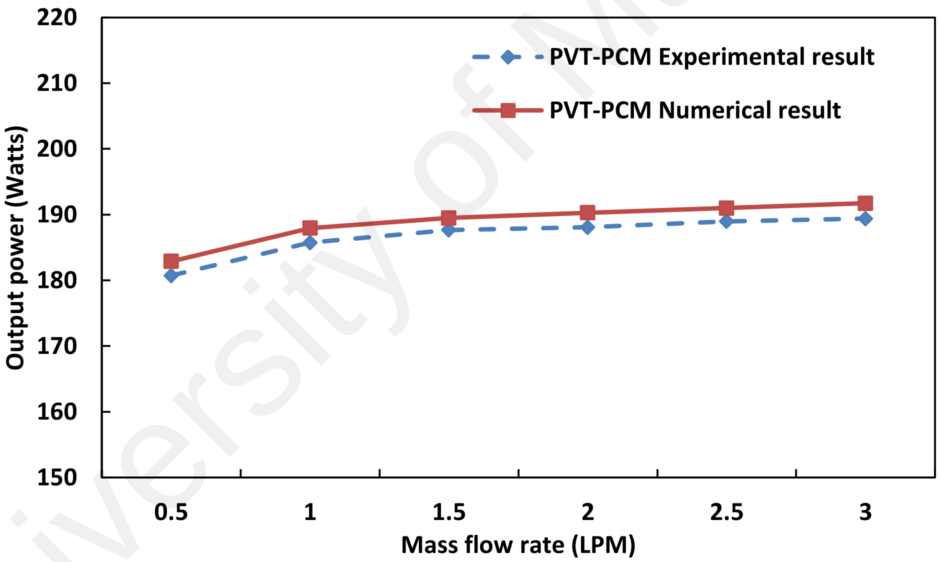

Figure 4.32: Mass flow rate effect on the output power of the PVT-PCM system

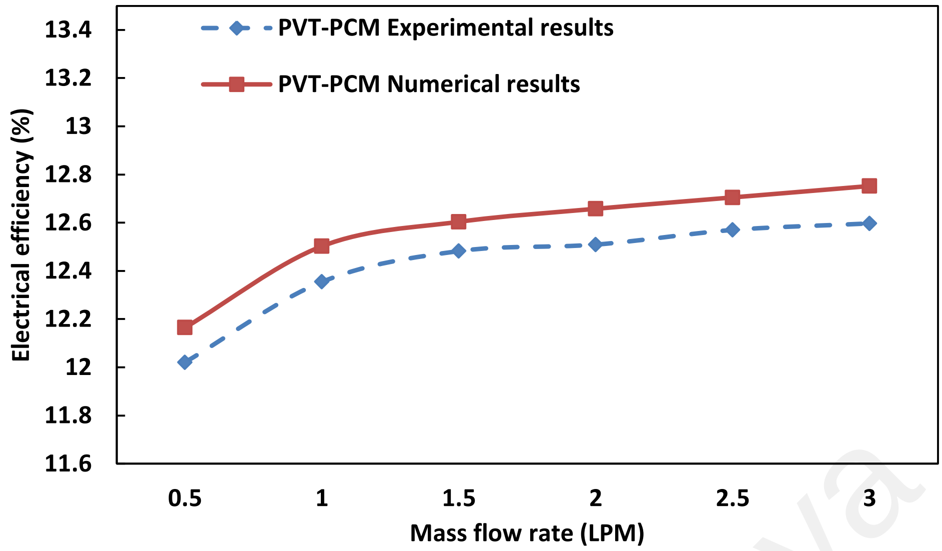

Figure 4.33: Mass flow rate effect on the electrical efficiency of the PVT-PCM system

Mass flow rate influence on electrical efficiency and power is depicted in Figures 4.32 and 4.33. The power and electrical efficiency increase as the cell temperature drops prominently due to the increase in mass flow rate, which transfers heat from the PV module. Consequently, PVT voltage increases noticeably while current reduces to some level, resulting in electrical efficiency and output power increase of the PVT. The highest values for the output power of PVT-PCM are achieved as 191.71W and 189.37W numerically and experimentally respectively. Whereas, the minimum output power is obtained as 182.88W and 180.72W numerically and experimentally respectively. Furthermore, on average output power increment is obtained as 1.43 and 1.44W per 0.5 LPM. Identically, the maximum values for electrical efficiency are obtained as 12.75% and 12.59% numerically and experimentally respectively. Whereas, the minimum electrical efficiency is achieved at about 12.16% and 12.02% numerically and experimentally respectively. It is found that numerical values are higher to some value than the experimental values. These differences are due to the weather conditions, which are not fully in control and may deviate from a stable position. There is no ideal control of working parameters especially the ambient temperature in the experimental setup but 27°C ambient temperature is set for experimental and numerical investigation.

4.3.5.4 Mass flow effect on thermal performance of PVT-PCM

Figures 4.34 and 4.35 show the impact of mass flow rate on the output temperature and thermal energy of the PVT-PCM system. The decrease in outlet temperature with increase in inlet mass flow rate is seen in Figure 4.35. At lower mass flow rates more heat is occupied in the small mass of water, therefore, results in higher output temperature of water, however, this value is smaller as compared to PVT because of the incorporation of PCM some heat is absorbed in it. Thus, the drop in output temperature with the rise in the mass flow rates determines that a huge mass of water accumulates higher heat but with lower temperature. This is attributed to the reason of a certain amount of heat absorbed by low mass have a higher temperature than the same amount of heat absorbed by huge mass and some amount absorbed by PCM as well. However, at higher mass flow rates more heat is transferred even though the output temperature is low as compared to 0.5 LPM of mass flow rate. Therefore, the amount of heat removed is increased with the increase in mass flow rate with lesser time. Figure 4.34 also shows that the satisfactory agreement in results is achieved numerically and experimentally with small deviations in experimental data, which shows the validation of the numerical model confidently. Maximum output temperatures are observed as 57.58°C and 53°C numerically and experimentally respectively. Whereas, minimum output temperatures are 33°C and 32°C for numerical and experimental cases respectively. Thermal energy obtained versus mass flow rate shown in Figure. 4.35 increases with increasing mass flow rate through the flow channel. Convective heat transfer rate increases at mass flow rate increases. However, it is noted that after 0.5 LPM it is slowed down as compared to an initial situation which is due the reason discussed in the case of Figure 4.34, indicating the same trend for heat transfer rate for both Figures of PVT-PCM. Therefore, excessive heat is transferred under the similar conditions at higher mass flow rates.

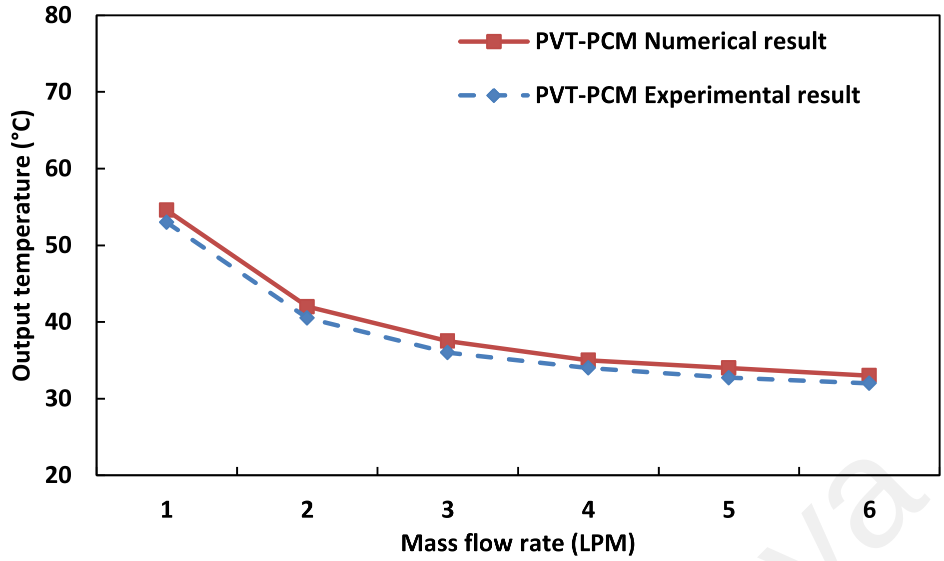

Figure 4.34: Mass flow rate effect on the output temperature of the PVT-PCM system

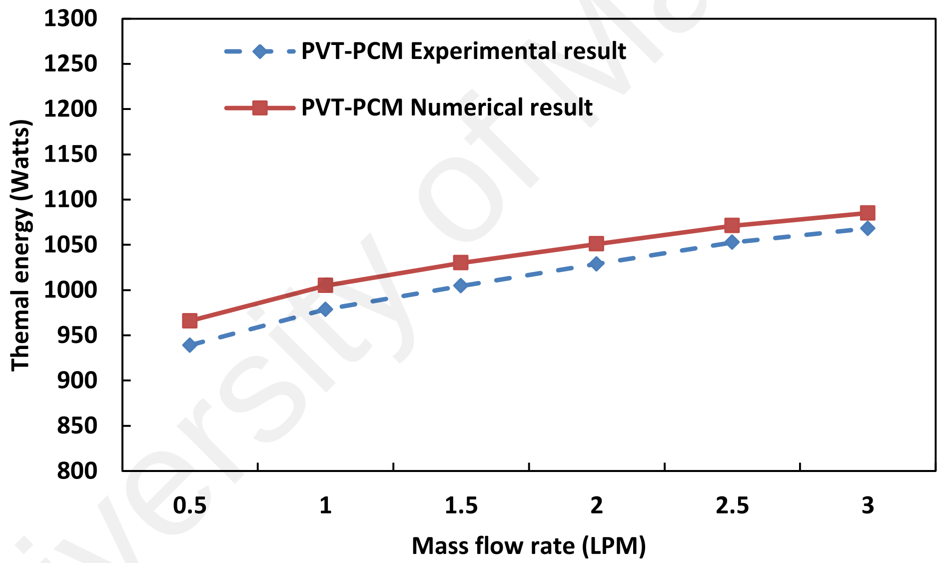

Figure 4.35: Mass flow rate effect on the thermal energy of the PVT-PCM system

Figures 4.36 shows that thermal efficiency increases with increasing water mass flow rate through the system. Increase in mass flow rate enhances the heat transfer through convection between water and thermal collector as well as it gets less time for PCM to get heat form fast flowing water. It causes in excessive heat transfer at higher mass flow rates, resulting in enhancing the thermal efficiency. Thus, more heat is transferred at higher mass flow rates, resulting in increasing the thermal efficiency. The highest values achieved for thermal efficiency are 72% and 71% numerically and experimentally respectively.

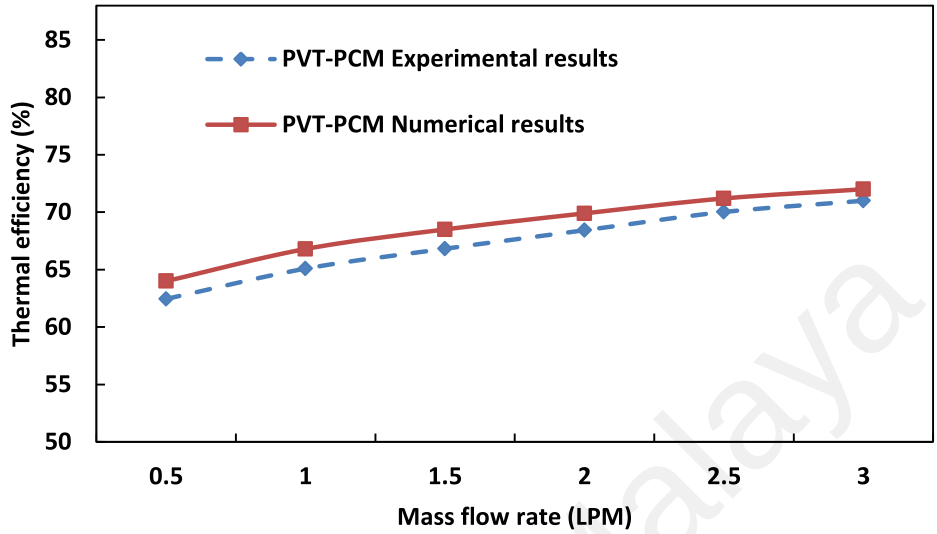

Figure 4.36: Mass flow rate effect on the thermal efficiency of the PVT-PCM system

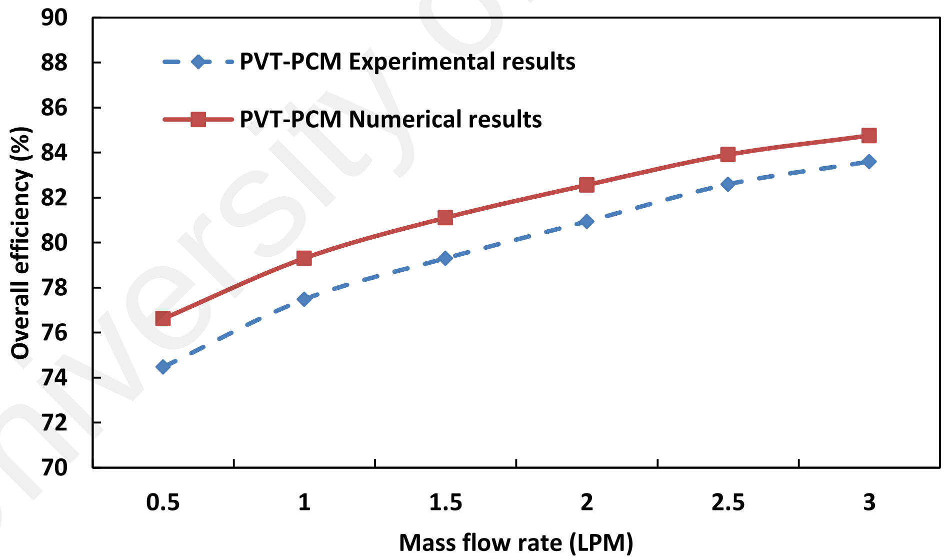

Figure 4.37: Mass flow rate effect on the overall efficiency of the PVT-PCM system

Furthermore, thermal efficiency increment of PVT-PCM is obtained as 1.33% and 1.42% per 0.5 LPM numerically and experimentally respectively. Figure 4.37 depicts the overall efficiency of the PVT-PCM system. The thermal efficiency increases simultaneously with the increment in mass flow rates. The values of PVT-PCM overall efficiency are achieved as 84.75% and 76.16%, numerically and experimentally respectively. Lowest values of the overall thermal efficiency are obtained as 76.16% and 74.47% numerically and experimentally. . Furthermore, the rate of efficiency increment is found as 1.42% and 1.51% for each mass flow rate of 0.5 LPM.

4.4 Outdoor Performance Investigation of PV, PVT, and PVT PCM

4.4.1 Analysis of Surface Temperature Distribution of PV Module

3D Numerical analysis done on the photovoltaic module in COMSOL Multiphysics® FEM based software on different solar radiation gives valuable detailed information as compared to 1D and 2D numerical models. The simulation parameter for solar radiation values is set from 200 W/m^2 minimum to 1000 W/m^2 with the interval of every 200 W/m^2 solar radiations value at outdoor experimental setup. As shown in Figure 4.38, photovoltaic module temperature varies significantly at different solar radiation intensities. It is obvious from the figures that the photovoltaic module achieves maximum temperature gain of 80°C approximately without any cooling medium. But, with controlled parameters, the heat transfer to the environment is allowed with natural free convections at 32°C ambient temperature. Whereas, the minimum surface temperature of the photovoltaic module is noted as 48.2°C approximately at 200 W/m^2 solar radiations at same conditions. In addition, the temperatures on the module are not uniformly distributed. It is because the heat flows easily to the environment from the edges of the module as compared to the middle part of the module. Three-dimensional heat transfer allows the edges of the module be at a lower temperature than the middle part which only radiates back to the environment from glass and Tedlar only.

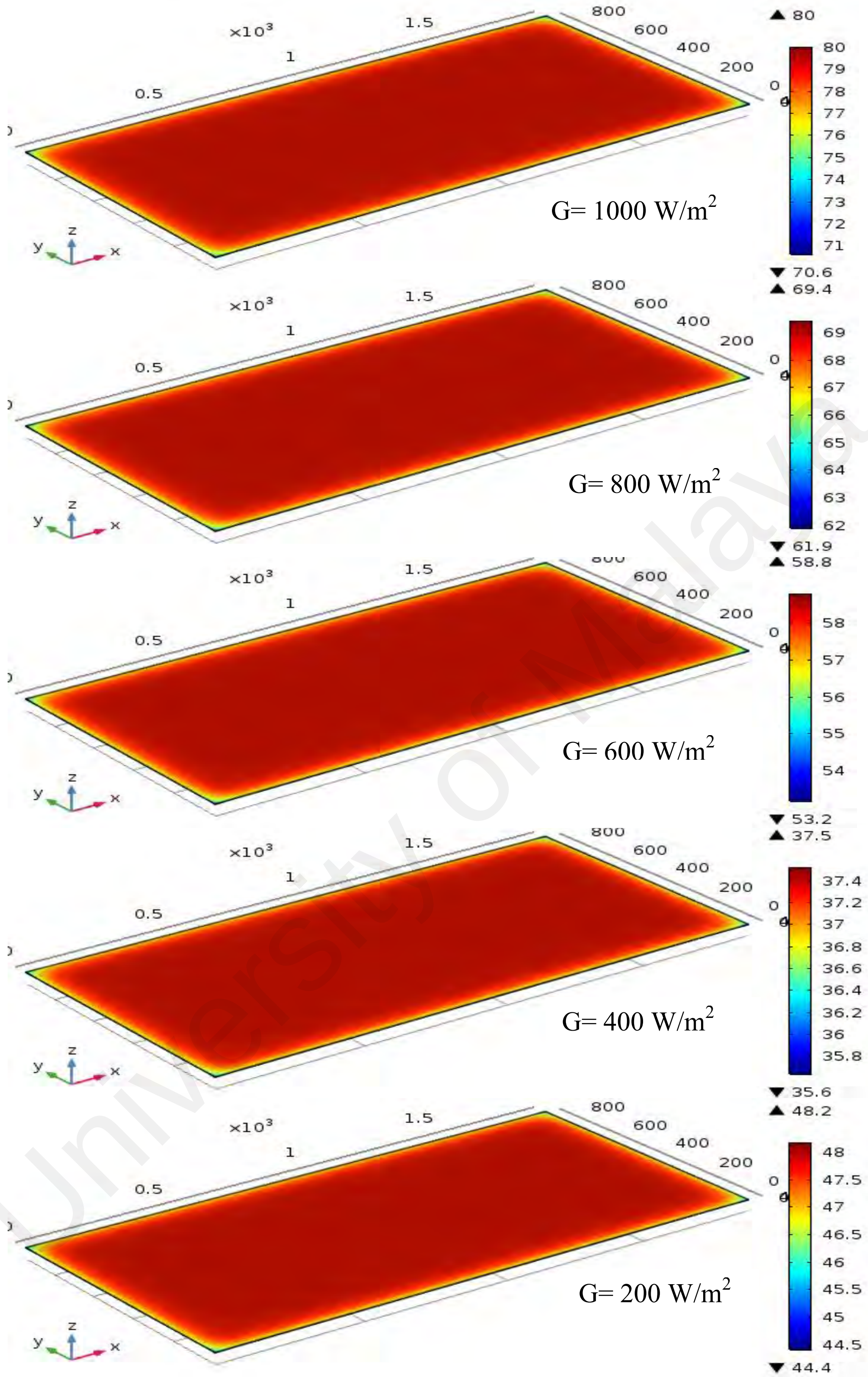

Figure 4.38: Surface temperature plot of the PV for the effect of irradiation from 200 W/m^2 to 1000 W/m^2

4.4.2 Temperature Distribution Analysis of PVT

The surface temperature profile for the photovoltaic thermal system at different solar radiations at the intervals of 200 W/m^2 is shown in Figure 4.39 at a fixed mass flow rate of 0.5 LPM. Whereas, Figure 4.40 depicts the results for thermal collector temperature distribution from the inlet of water flow to the outlet of the collector. Hence, as seen in figure 4.39 temperatures vary significantly at different solar radiations intensities. It is clear from the figures that the photovoltaic module achieves maximum temperature of 77°C approximately at 1000 W/m^2 with Cooling effect of water flow in the thermal collector. Glass temperature is near to 70°C because of the thermal collector contact with the PV module which extracts the heat from the surface. Whereas, 77°C which is higher as shown in the temperature bar is due to edges of the panel because at the edges thermal collector is not in direct contact, and there only free convection due to environment happens. Conversely, at the rest area of panels two type of convections occurs due to free convection of environment and forced convection in the thermal collector pipe. The minimum surface temperature of the photovoltaic-thermal module is noted as 38.8°C approximately at 200 W/m^2 solar radiations at same conditions. Streamline effect of solar radiations on the thermal collector is presented in Figure 4.40. The highest temperature at the outlet of the thermal collector is noted as 64°C approximately, and the lowest is shown as 41°C approximately at the inlet temperature of 32°C. As water flows through its course or length of the pipe, its temperature increases gradually and reaches the maximum value.

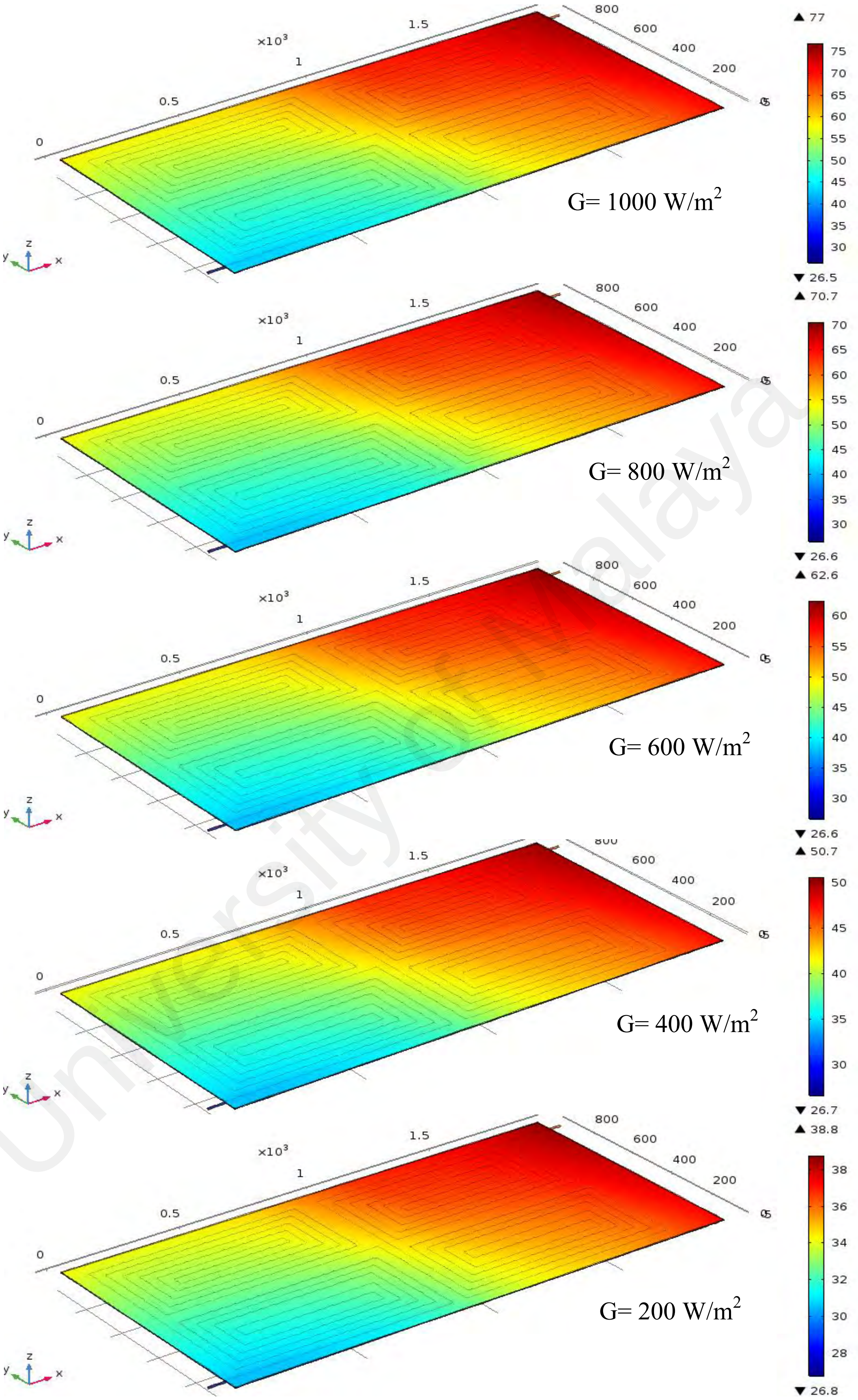

Figure 4.39: Surface temperature plot of the PVT for the effect of irradiation from 200 W/m^2 to 1000 W/m^2

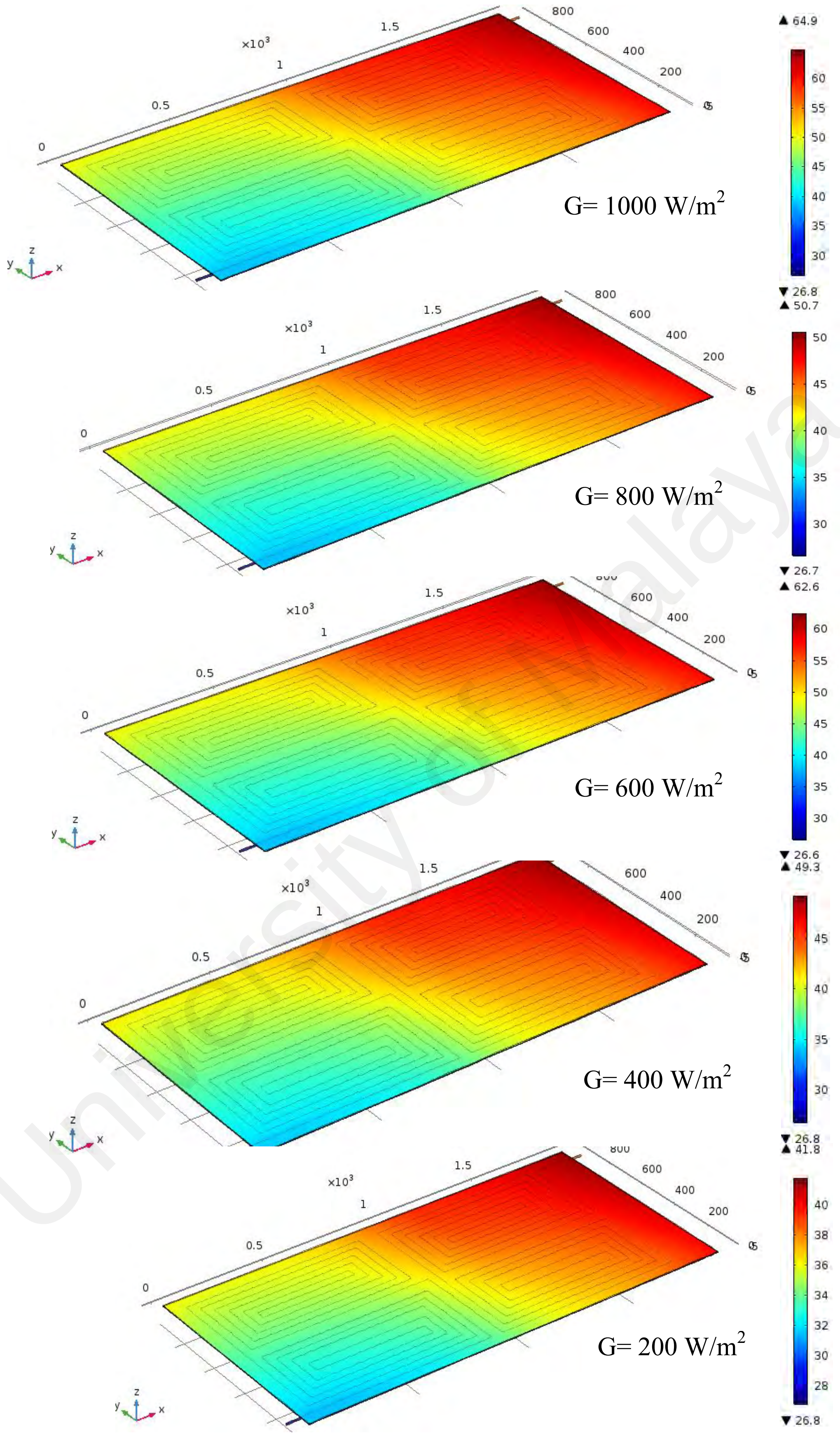

Figure 4.40: Streamlines plot of the PVT for the effect of solar radiation from 200 W/m^2 to 1000 W/m^2

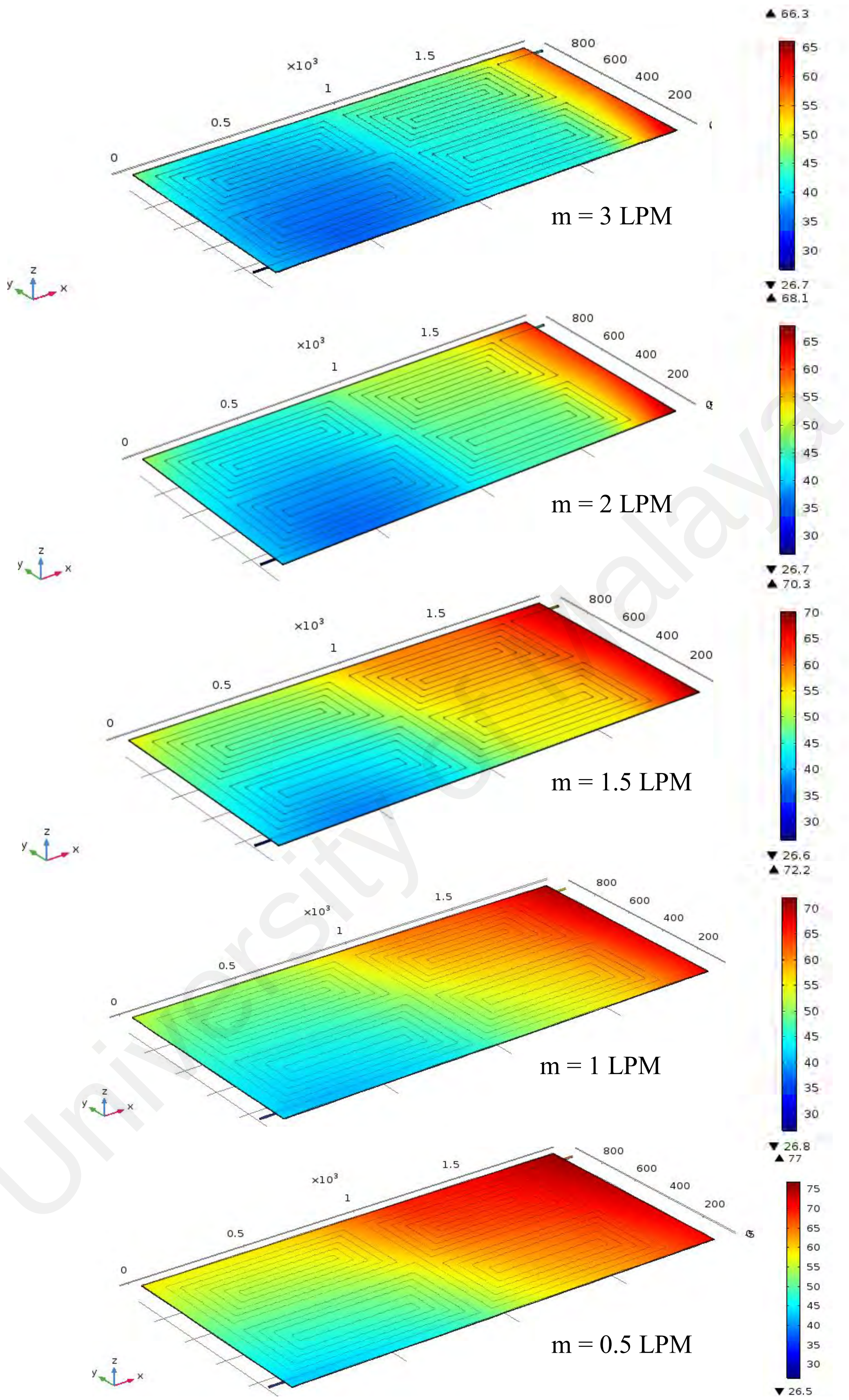

Figure 4.41: Surface temperature plot of the PVT for the effect of mass flow rate from 0.5 LPM to 3 LPM

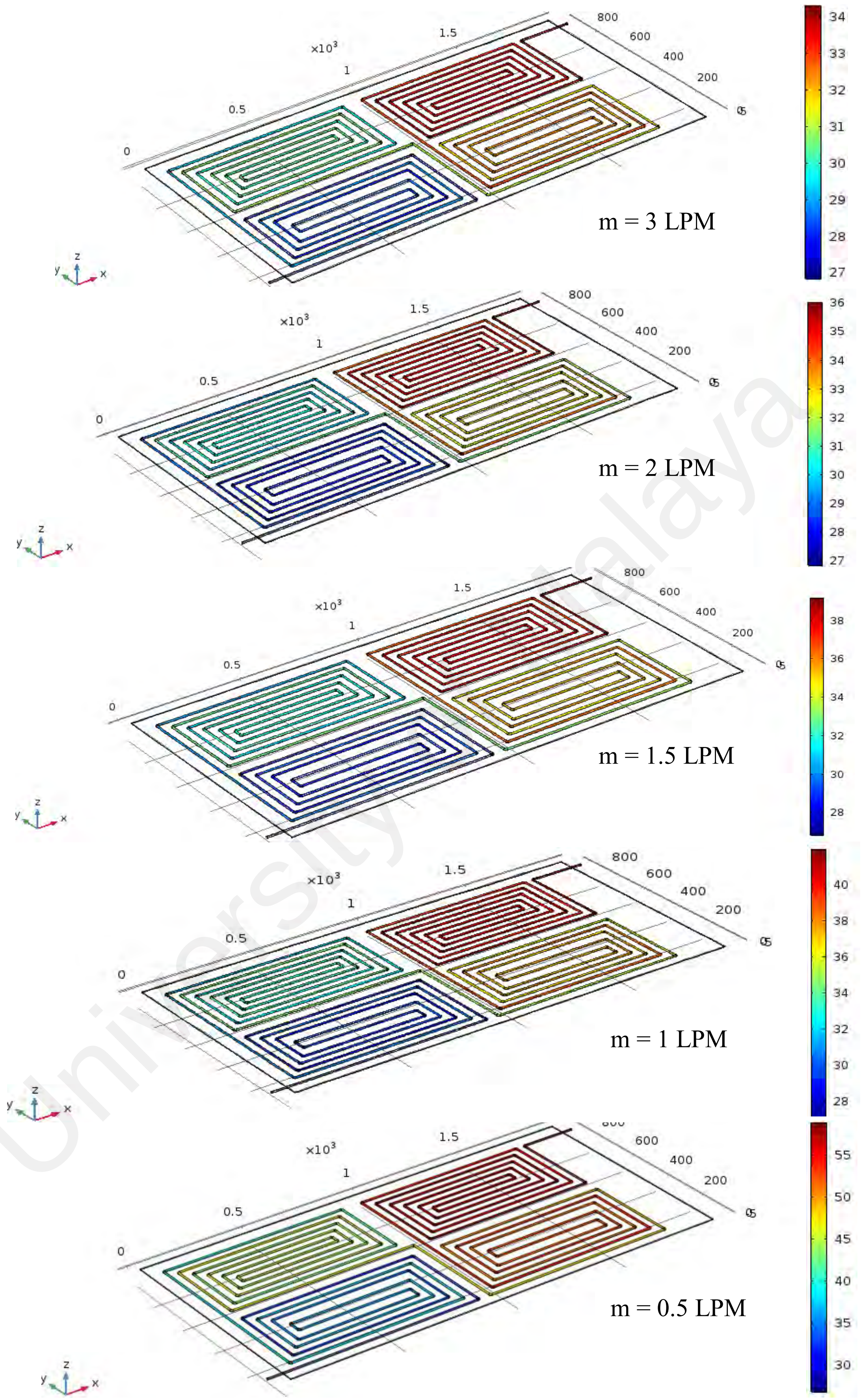

Figure 4.42: Streamlines plot of the PVT for the effect of mass flow rate from 0.5 LPM to 3 LPM

The surface temperature profile for the photovoltaic thermal system at different mass flow rates is presented in Figure 4.41. Effect of the mass flow rate of water is shown for the surface temperature of the photovoltaic module and Figure 4.42 for streamline temperature of the thermal collector. As seen in the Figure 4.41, temperature varies significantly at different mass flow rates. It is obvious from the figures that the photovoltaic module achieves a maximum temperature of 77°C approximately at 0.5 LPM due to the slower cooling effect of water flow in the thermal collector. Glass temperature is near to 77°C because of the thermal collector contact with the PV module which extracts the heat from the surface. Whereas, 77°C which is higher shown in the temperature bar is due to edges of the panel because at the edges thermal collector is not in direct contact and there only free convection due to environment happens. However, at the rest area of module two types of convections occur due to free convection of environment and forced convection in the thermal collector pipe. The minimum surface temperature of the photovoltaic-thermal module is noted as 66.3°C approximately at 3 LPM of the mass flow rate at the same conditions. Streamline effect of mass flow rates on the thermal collector is depicted in Figure 4.42. The highest temperature or temperature at the outlet of the thermal collector is noted as 62°C approximately at a flow rate of 0.5 LPM, and the lowest is shown as approximately 36°C at 3 LPM.

4.4.3 Temperature Distribution Analysis of PVT-PCM

Phase change materials play a very important role in regulating photovoltaic modules cell temperatures. Figure 4.43 shows the effect of phase change material which is paraffin used here with a melting temperature of 44°C. Photovoltaic thermal analysis with phase change materials is done with time-dependent simulations because phase change takes places with time as it gains heat from the panel and stabilizes after some time with the minor change in the temperature further. The complete temperature behaviour is studied in these simulations. The temperate surface profile for the photovoltaic thermal system with PCM at different timings at the 1000 W/m2 and mass flow rate of 0.5 LPM is shown in Figures 4.43 and 4.44. Whereas, Figures 4.45 and 4.46 depict the results for thermal collector temperature distribution from the inlet of water flow to the outlet of the collector with and without irradiations. Similar to surface temperature, thermal collector temperatures profile is also studied in these conditions. Almost reverse phenomenon of the temperature gain and drain of the system is observed when irradiations are introduced and stopped. Temperature gain occurs when irradiations are introduced and temperature is drain and vanished completely after some time when suddenly irradiations are stopped from the incidence on the system. Hence, as seen in the figure 4.43 temperatures vary significantly at different timings. It is clear from the figures that the photovoltaic module achieves maximum temperature of 70 to 78.6°C approximately at 1000 W/m2 with the cooling effect of water flow in the thermal collector.

At the first 100 seconds, the temperature is increased to about 37°C from an initial temperature of 32°C. It gradually increases as times goes on till 3600 seconds and reaches to a maximum of 70°C. The important matter to note is that temperature varies fast at intervals of 600 seconds to 1200 seconds which is about 65°C and 67°C respectively. Conversely, the temperature increased with very low value after a time interval of 1200 seconds and finally stabilizes with no significant change in temperature at about 3600 second. The reason behind is that heat is stored by the phase change material latently after the 44°C. Consequently, the temperature of the photovoltaic module remains lower as compared to the photovoltaic-thermal module without PCM. Figure 4.45 shows the streamline of thermal collector temperature distributions across the length of the pipe or flow path. Similarly as the surface temperature of PV and water receive the maximum temperature very fast at the intervals of 600 seconds and 1200 seconds but temperature changes decrease significantly after 1200 seconds until 3600 seconds. At first 100 seconds temperature is noted as 32°C whereas, at 3600 seconds it reaches to approximately 60°C.

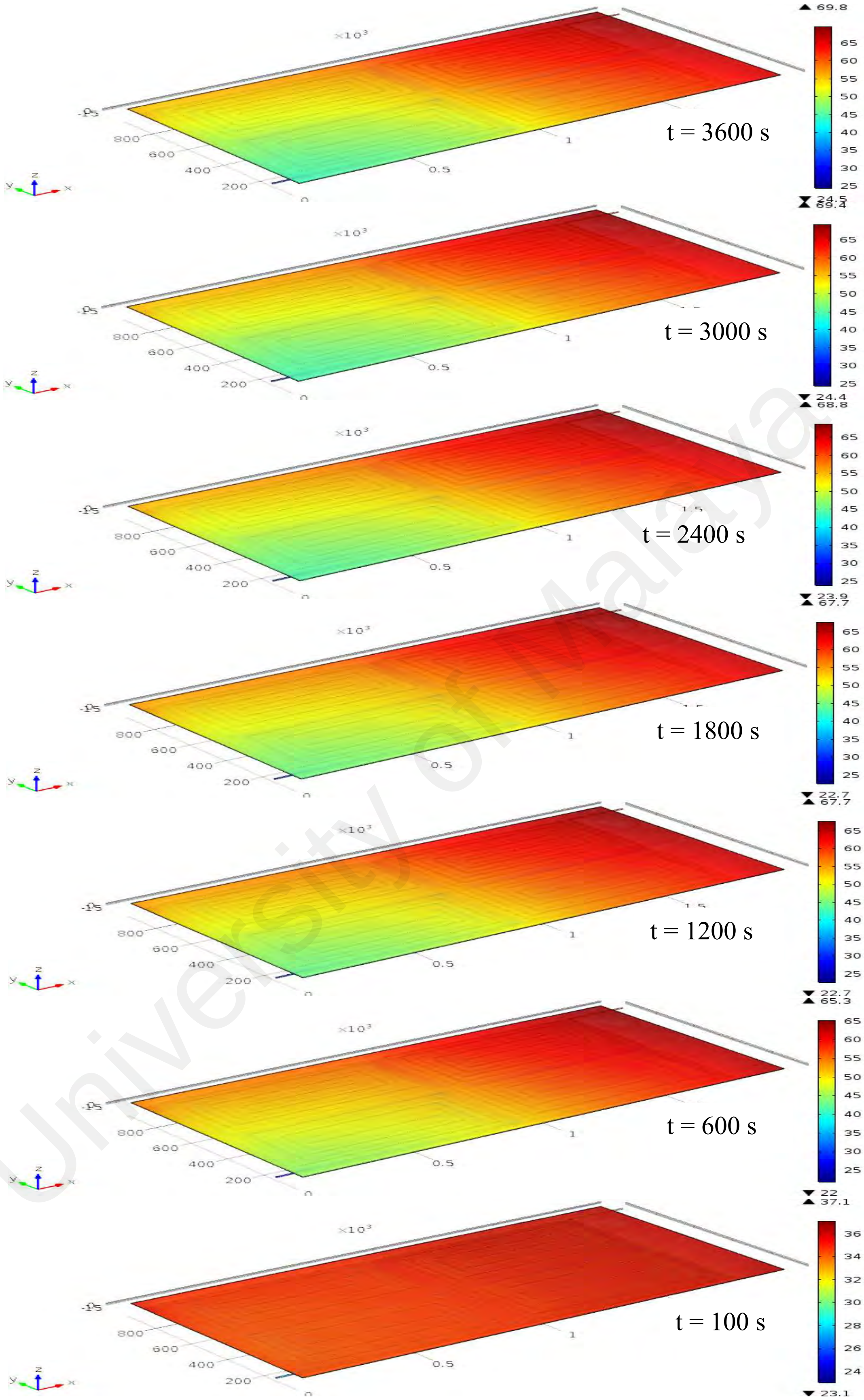

Figure 4.43: Surface temperature plot of the PVT-PCM for time variation at 1000 W/m^2 irradiation and flow rate 0.5 LPM

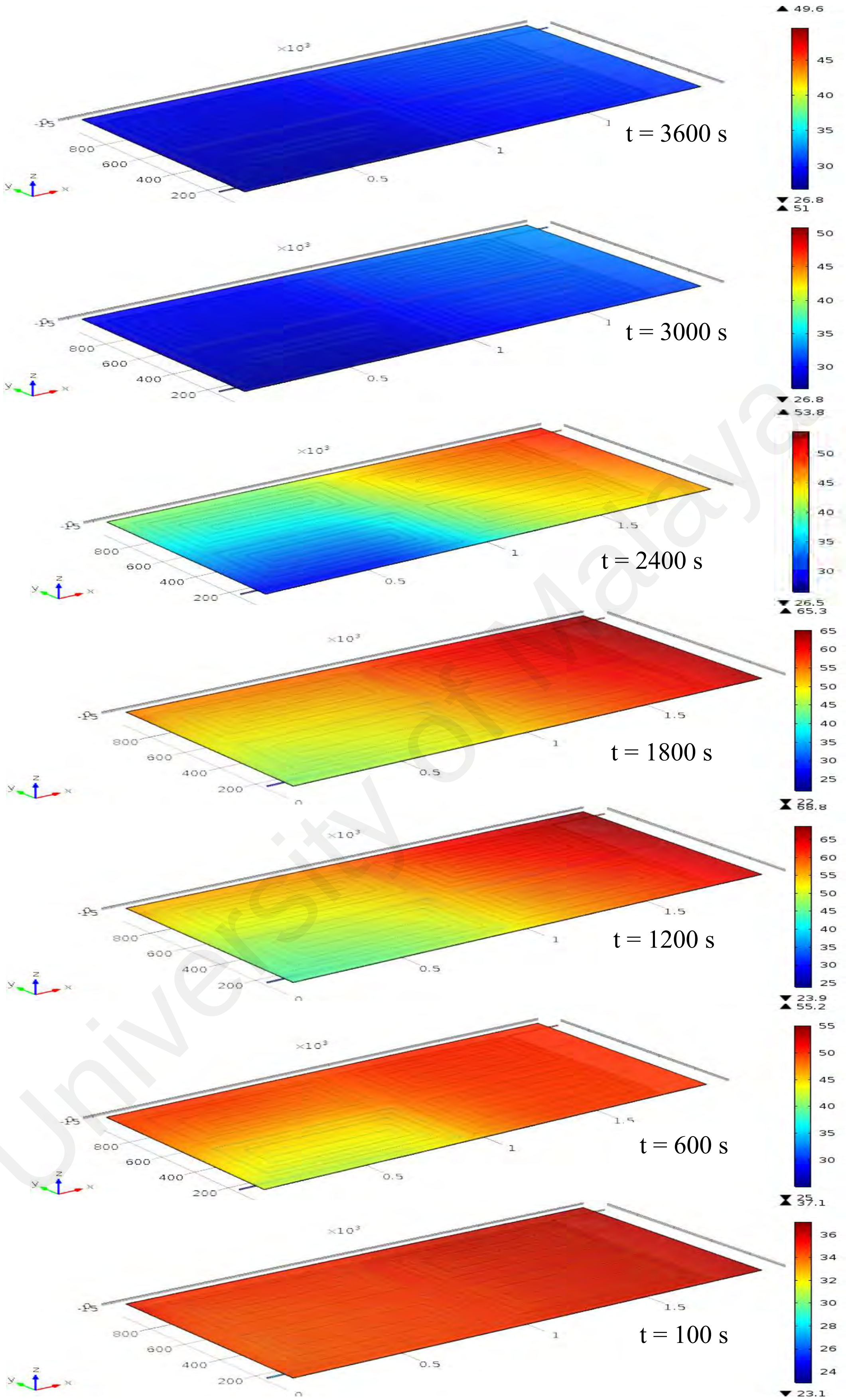

Figure 4.44: Surface temperature plot of the PVT-PCM for time variation at flow rate 0.5 LPM without irradiation

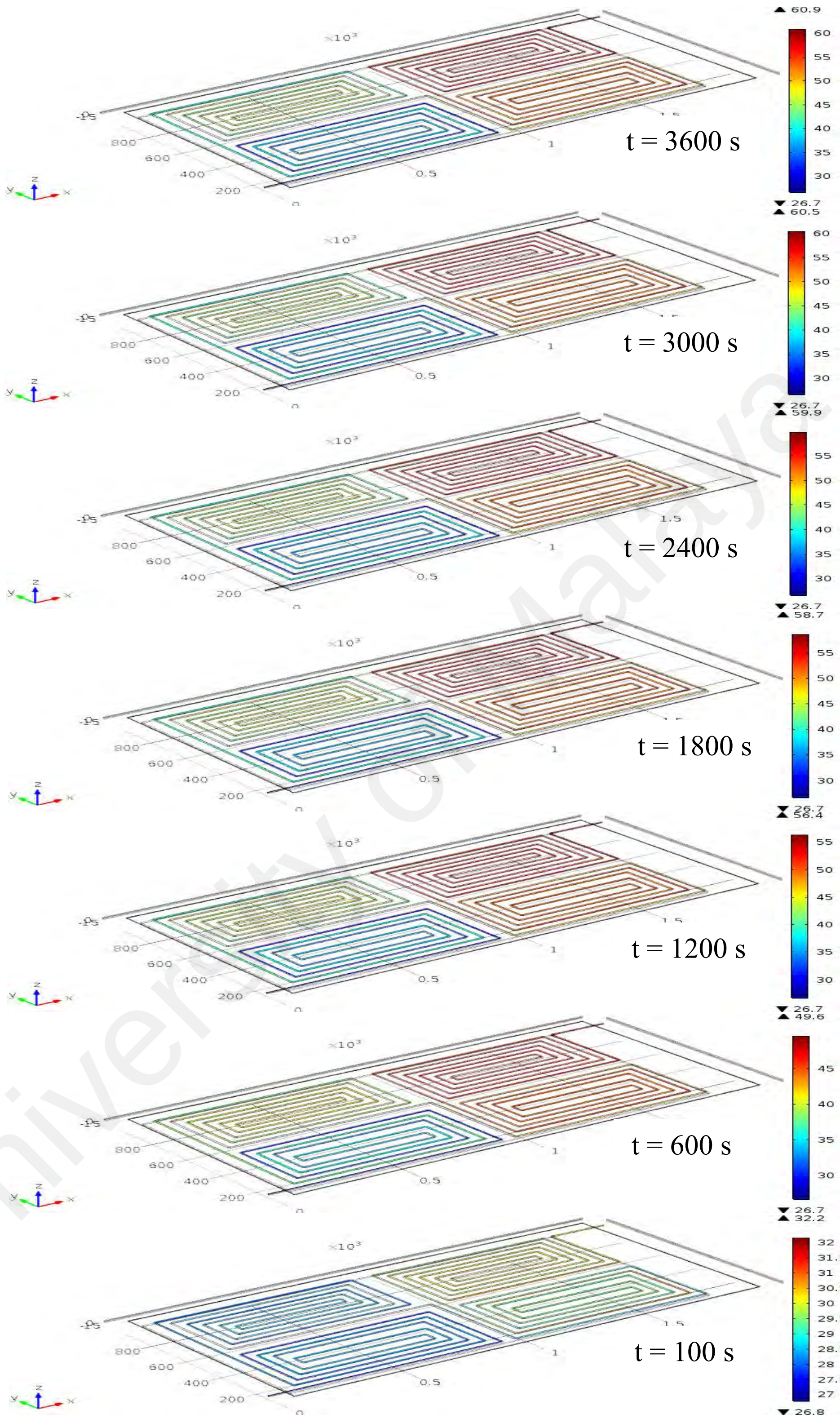

Figure 4.45: Streamlines of the PVT-PCM for time variation at 1000 W/m^2 irradiation and flow rate 0.5 LPM

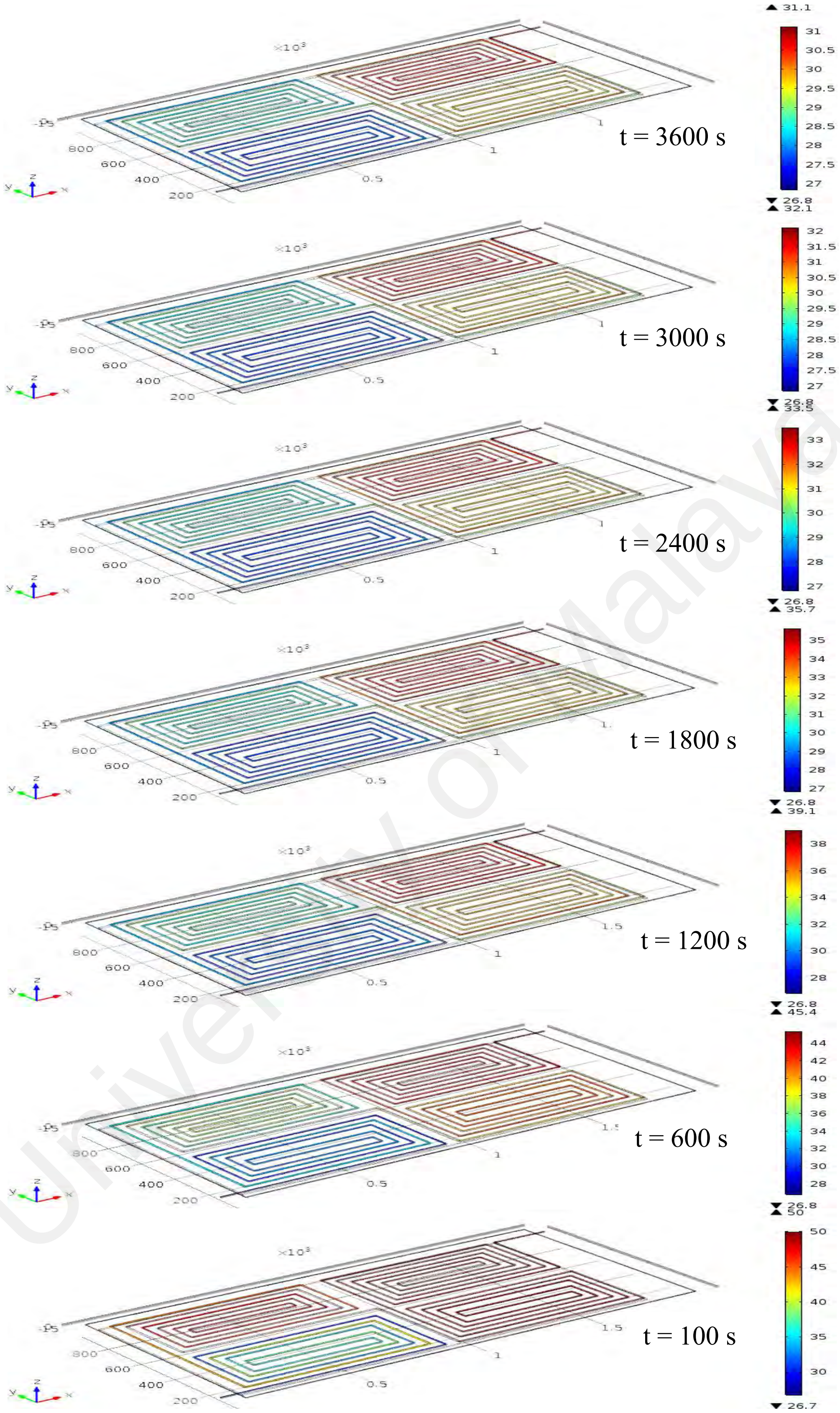

Figure 4.46: Streamlines of PVT-PCM for time variation at flow rate 0.5 LPM without irradiation

Figure 4.44 shows the effect of phase change material when it already has gained temperature and suddenly no irradiation is available. The initial conditions are set as 0 W/m^2 solar irradiation and mass flow rate of 0.5 LPM. This phenomenon will give the information about how temperature is dissipated if mass flow continues under no sunlight or irradiation in case of clouds, sunset or shadow of buildings etc. on the photovoltaic panels. At the first 100 seconds, the temperature falls down to approximately 55°C from an initial temperature of about 69.8°C. It shows that temperature falls very fast at first 100 seconds then gradually decreases as times goes on till 3600 seconds and reaches to a minimum surface temperature of about 49°C. In this case, the important matter to note is that temperature varies fast at first 100 seconds only then temperatures occurs slower and stable for the rest of the time, which is almost 15°C. Conversely, temperature decreased with the very low value after a time interval of 1800 seconds. This is due to the reason that temperature is released by PCM rapidly at a higher value as extra energy more than its latent heat of capacity is given off and is taken by flowing water mass. Water receives the energy both from PCM and glass which results in a rapid drop in the temperature of the glass. Figure 4.46 shows the streamline of thermal collector temperature distributions across the length of the pipe or flow path. Unlikely, the surface temperature of PV and water receives the heat back from PCM steadily for a limited time without irradiations. At first 100 seconds temperature is noted as 50°C whereas, at 3600 seconds it reaches to approximately 31°C.

4.4.4 Solar Irradiation Effect on the Systems

4.4.4.1 Solar irradiation effect on PVT electrical performance

Figure 4.47 depicts the irradiation effect on cell temperatures of the PV and PVT. The figure shows the clear relationship between the irradiations and cell temperature as the irradiation increase the cell temperature also increases. However, this proportional relationship is not perfectly direct. At the higher irradiation levels, cell temperatures curves decline as compared to the radiations levels of 200 W/m^2 and 400 W/m^2. There is increase observed in the cell temperature due to the reason that higher irradiations have more energy to put into the PV and PVT but the declining behaviour of cell temperature at higher temperatures is because of the temperature gradient. The more the temperature gradient occurs the more heat flow from a hot body to the cold body (Nordmann and Clavadetscher, 2003). Some difference in results of experimental and numerical analysis is observed because of the uncertainty and error percentage of the sensors and equipment. Figure 4.47 shows the cell temperature is achieved for PV at 75°C and 77°C experimentally and numerically respectively. For PVT, it is 69.3°C and 67°C experimentally and numerically respectively, which much lower than PV module. Power and electrical efficiency are shown in the figures 4.48 and 4.49. This relationship shows that the irradiations have a proportional effect on the power as it increases the power also increases but not fully linearly. Power increases because the current and voltage increase with an increase in irradiations but the current increases higher than the voltage (Başoğlu and Çakır, 2016; Radziemska, 2003). Due to cooling effect in PVT, the power is higher in value as compared PV module. Some experimental deviations are observed at high irradiation intensity.

The maximum output power of PVT is obtained as 182.88W and 180.54W numerically and experimentally respectively. Whereas, the minimum output power is derived as 41.65W and 41.32W for numerical and experimental results respectively.

Conversely, electrical efficiency is observed to be decreased due to rise in cell temperature as shown in Figure 4.12. Effect of delta T/G on electrical and thermal efficiency is also shown by (Tripanagnostopoulos et al., 2002) under constant working conditions. Polycrystalline PV electrical efficiency was achieved as 12.4% for PVT with water as working fluid, and 58% of thermal energy is achieved.

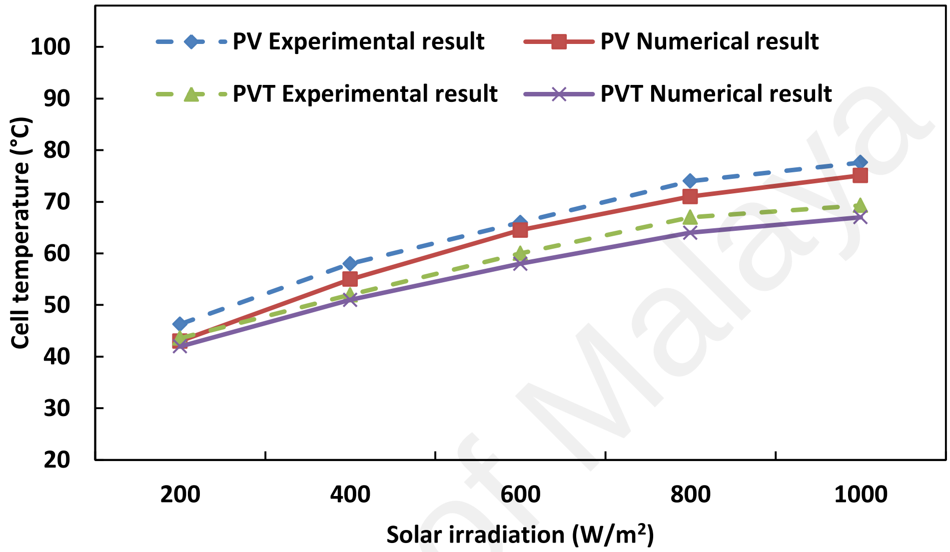

Figure 4.47: Solar irradiation effect on cell temperature

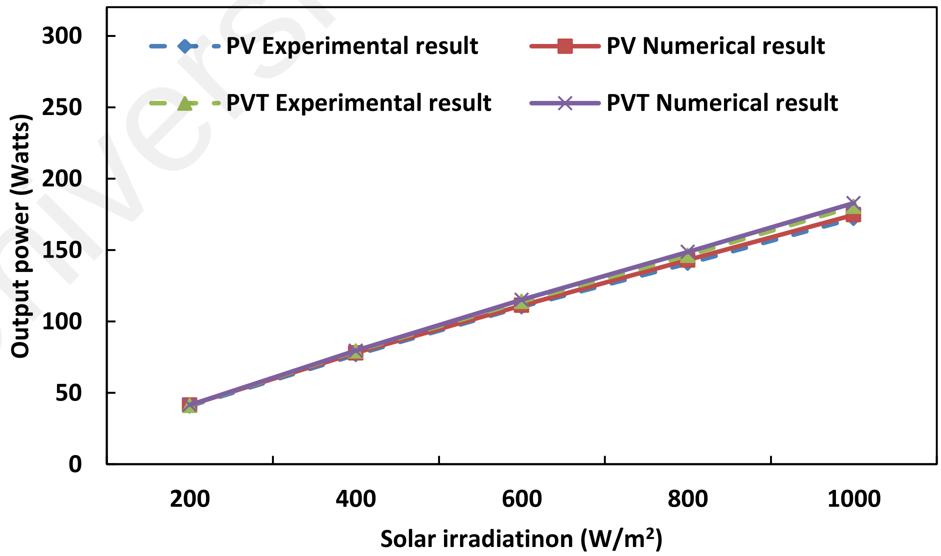

Figure 4.48: Solar irradiation effect on output power

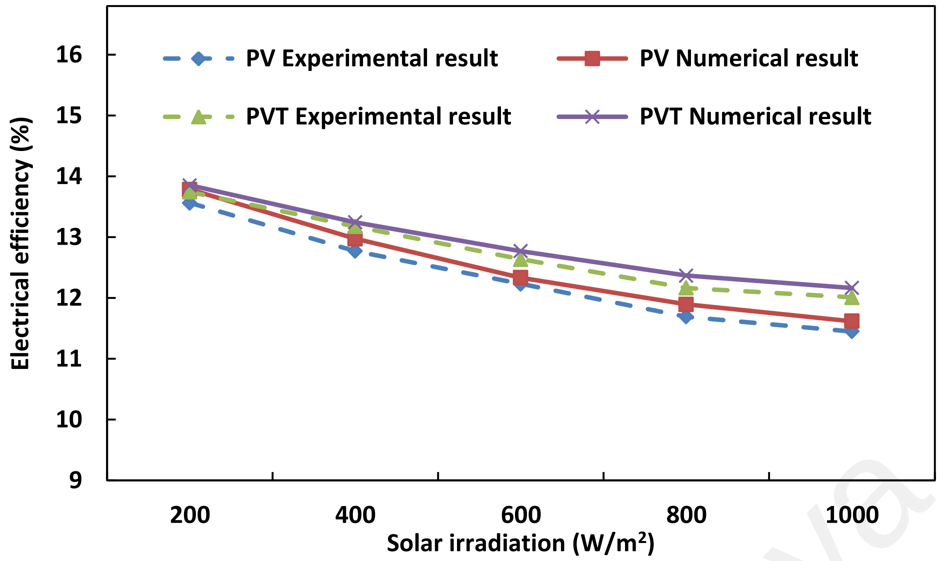

Figure 4.49: Solar irradiation effect on electrical efficiency

4.4.4.2 Irradiation effect on thermal performance of PVT

The water outlet temperature is increased due to increase in irradiations as observed in the Figures 4.50. The reason behind this increase in output temperature is the high energy input due to high intensity of irradiations incident on the system (Rohsenow et al., 1998). The heat transfer phenomenon changes its pattern after the 600 W/m^2 and some of the heat starts to flow to the environment due to higher temperature difference in between PVT and environment (Kreith and Black, 1980). Output temperature is achieved as 61.11°C and 59.89°C at 1000 W/m^2 experimentally and numerically respectively. In Figure 4.51, the effect of irradiation on the thermal energy is shown. Irradiation at higher levels put more energy into the systems and in result water circulating into thermal collector absorbs more energy. Therefore, the thermal gain in water is higher at high values of irradiations. Furthermore, declining trend in the thermal energy is seen which is because at high irradiations the temperature is higher at the system, therefore, some energy is lost into the environment before it gets transferred into the water. This is similar to the output hot water temperature described in Figure 4.50 the effect of the temperature gradient.

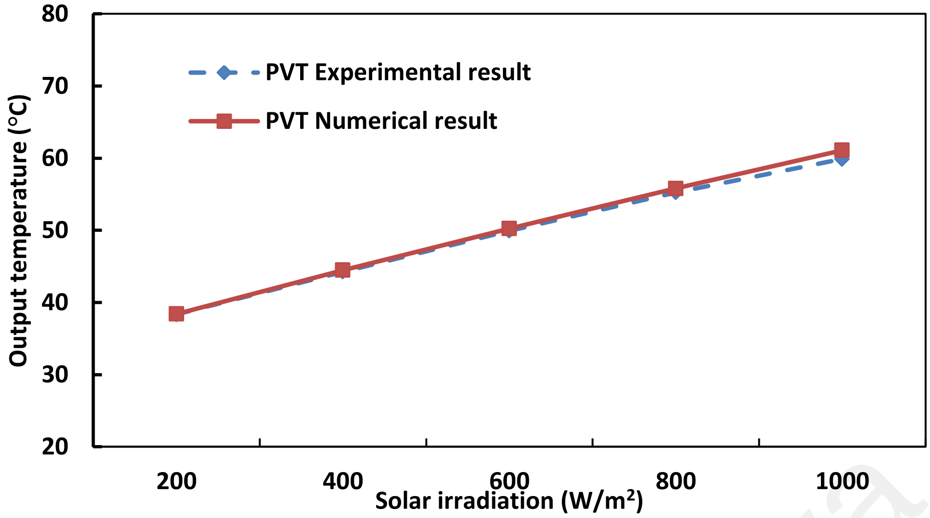

Figure 4.50: Solar irradiation effect on output temperature

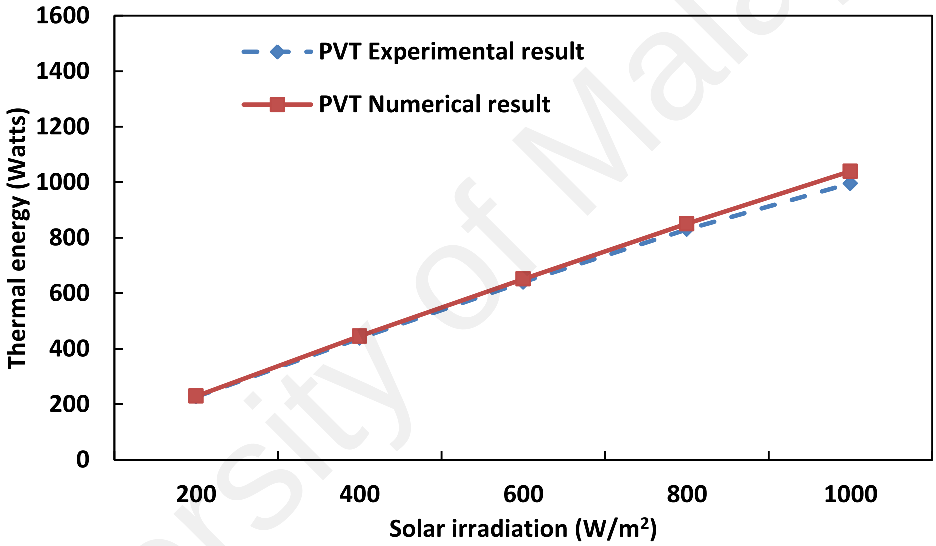

Figure 4.51: Solar irradiation effect on thermal energy

In Figure 4.52, the irradiation effect is shown on the thermal efficiency of the PVT system. Small deviations in the thermal efficiency are noticed after the 600 W/m^2 irradiations. This is due the reason that total of the energy is not efficiently converted into useful energy as some the energy is lost into the environment at higher temperatures due to a high temperature gradient. However, at low irradiation the losses are at a minimum as the maximum of the energy is transferred to flowing water but still, some energy is lost in this case. The effect of solar irradiation with other working conditions is also shown by (He et al., 2006), where 40% of thermal efficiency is achieved for PVT at working condition of the city of Hefai, China.

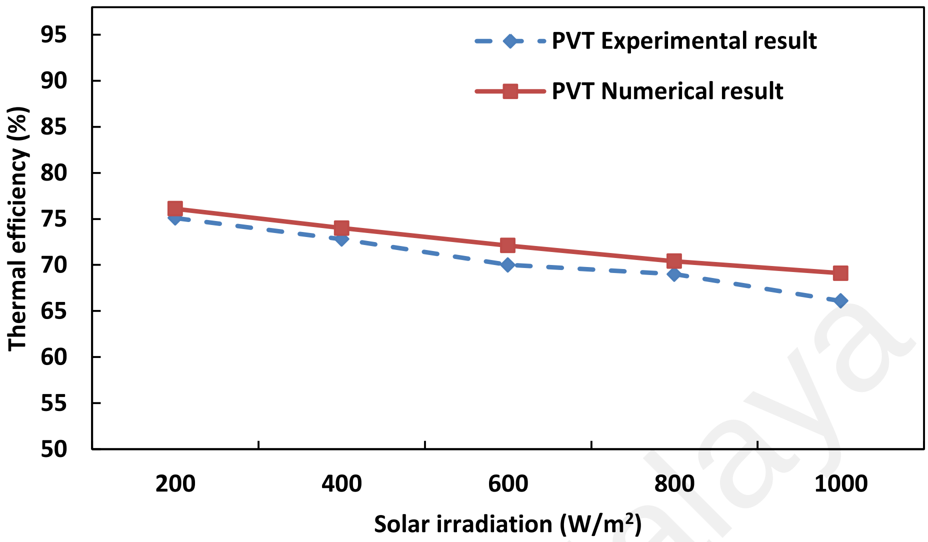

Figure 4.52: Solar irradiation effect on thermal efficiency

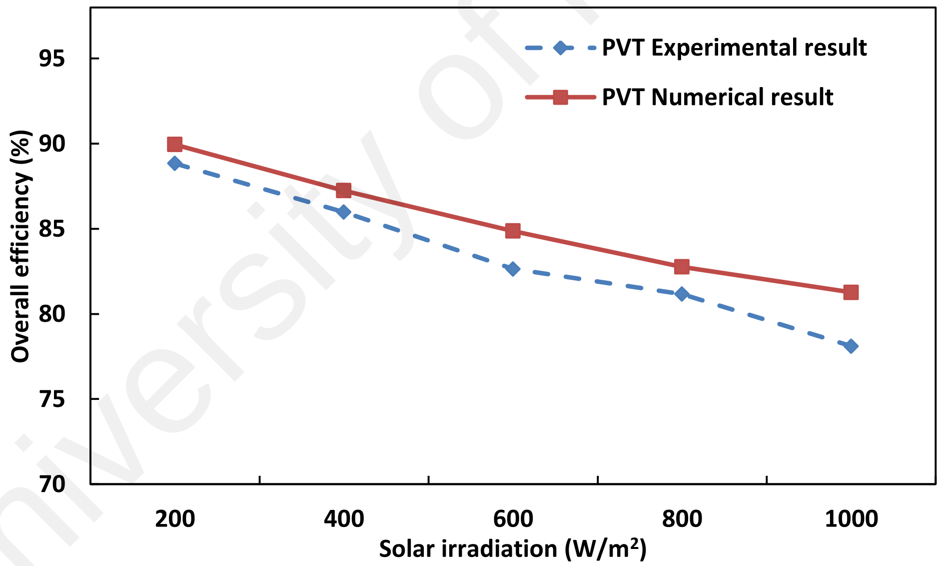

Figure 4.53: Solar irradiation effect on overall efficiency

Overall efficiency also decreases with increasing irradiation levels due to the effect of losses of energy back into environment as seen in Figure 4.53. Overall efficiency achieved at 200 W/m^2 is better than 1000 W/m^2 irradiations. The values of 89.95% and 88.84% are achieved for highest overall efficiency at 200 W/m^2 and 81.26% and

78.11% are obtained for minimum overall efficiency at 1000 W/m^2 for numerical and experimental results respectively.

4.4.4.3 Solar irradiation effect on PVT-PCM electrical performance

Figure 4.54 depicts the irradiation effect on cell temperatures of the PV and PVTPCM. The figure shows the clear relationship between the irradiations and cell temperature as the irradiation increase the cell temperature also increases. PCM (A44) plays role to absorb and store heat latently to further cool the PV module(Browne et al., 2016). However, this proportional relationship is not perfectly direct. At the higher irradiation levels, cell temperatures curves decline as compared to the radiations levels of 200 W/m^2 and 400 W/m^2. There is increase observed in the cell temperature due to the reason that higher irradiations have more energy to put into the PV and PVT-PCM but the declining behaviour of cell temperature at higher temperatures is because of the temperature gradient. The more the temperature gradient occurs the more heat flow from a hot body to the cold body.

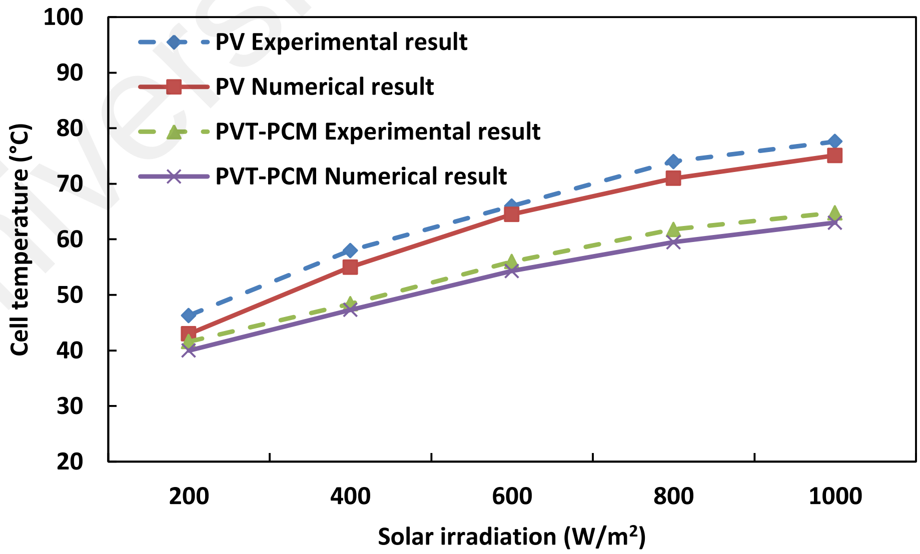

Figure 4.54: Solar irradiation effect on cell temperature

Effect of incident irradiation on power and electrical efficiency are shown in the Figures 4.55 and 4.56. This relationship shows that the irradiations have a proportional effect on the power as it increases the power also increases but not fully linearly. Power is increased with increase in irradiations but the current increases higher than voltage.

PVT-PCM system acquires higher values of power as compared to PV module because PVT-PCM system has cooling of PV through two ways of circulating water and PCM heat storage. Hence, it can also be concluded that this cooling is more effective than the PVT system as PVT doesn't have PCM, which is responsible for excessive heat absorption. Figure 4.56 shows that electrical efficiency relationship with cell temperature, where, it decreases with increase of cell temperature. More loss of electrical energy is observed in the case of PV as compared to PVT-PCM.

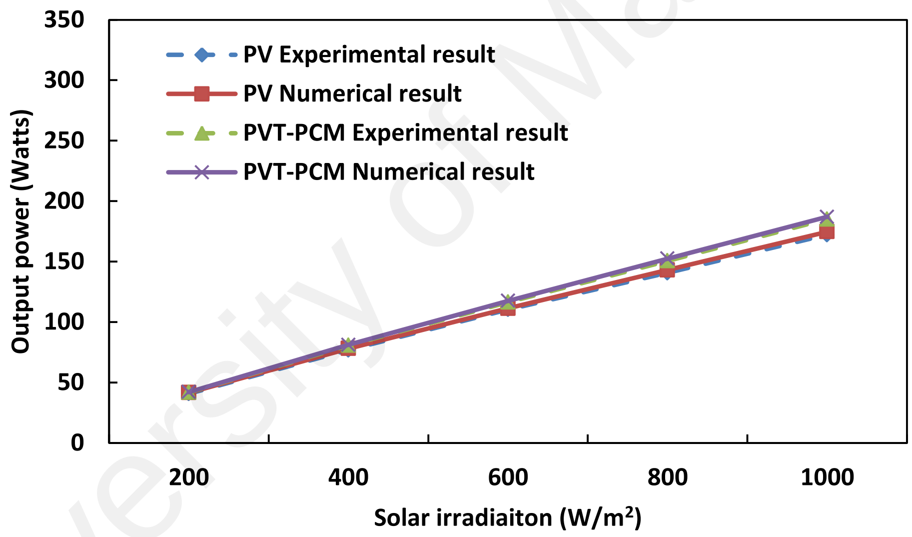

Figure 4.55: Solar irradiation effect on output power

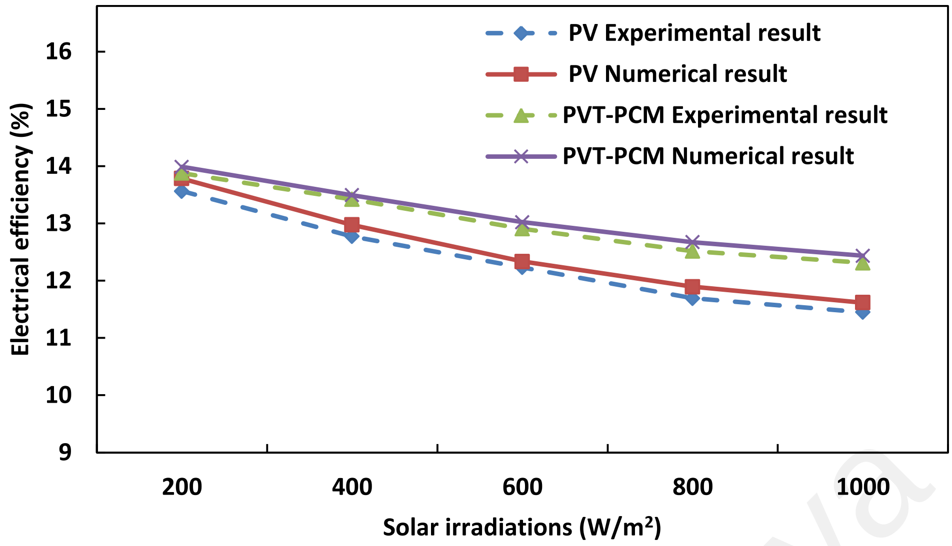

Figure 4.56: Solar irradiation effect on electrical efficiency

4.4.4.4 Solar irradiation effect on thermal performance of the PVT-PCM

The water outlet a temperature is increased due to increase in irradiations as observed in the Figures 4.57. The reason behind this increase in output temperature is the high energy input due to high intensity of irradiations incident on the system. The heat transfer phenomenon changes its pattern after the 600 W/m^2 and some of the heat starts to flow to the environment due to higher temperature difference in between PVT-PCM and environment (Browne, M.C. et al., 2015; Rohsenow et al., 1998).

Thus, the heat taken by the PVT-PCM is divided into heat carried by flowing water and the rest is stored in the PCM other than heat loss. Therefore, heat carried by water is lower in the PVT-PCM system as compared to only a PVT system (Gaur et al., 2017). In Figure 4.58, the effect of irradiation on the on the thermal energy is shown. Irradiation at higher levels put more energy into the systems and in result water circulating into thermal collector absorbs more energy. Therefore, the thermal gain in water is higher at high values of irradiations. Furthermore, declining trend in the thermal energy is seen which is because at high irradiations the temperature is higher at the system, therefore, some of the thermal energy is lost into the environment before it gets transferred into the water. This is similar to the output hot water temperature described in Figure 4.57 the effect of the temperature gradient. However, thermal energy obtained for PVT-PCM is lower than PVT case due to the reasons described in Figure 4.57.

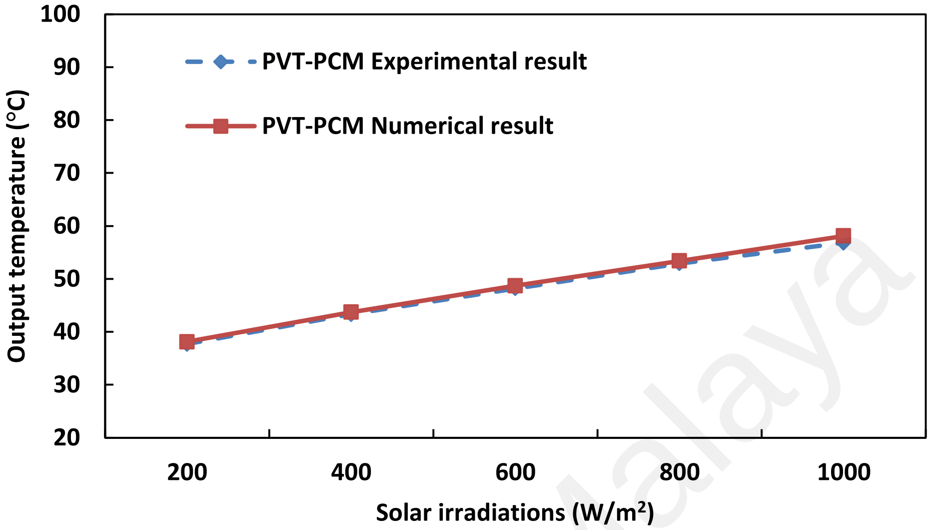

Figure 4.57: Output temperature of PVT-PCM at different solar irradiations

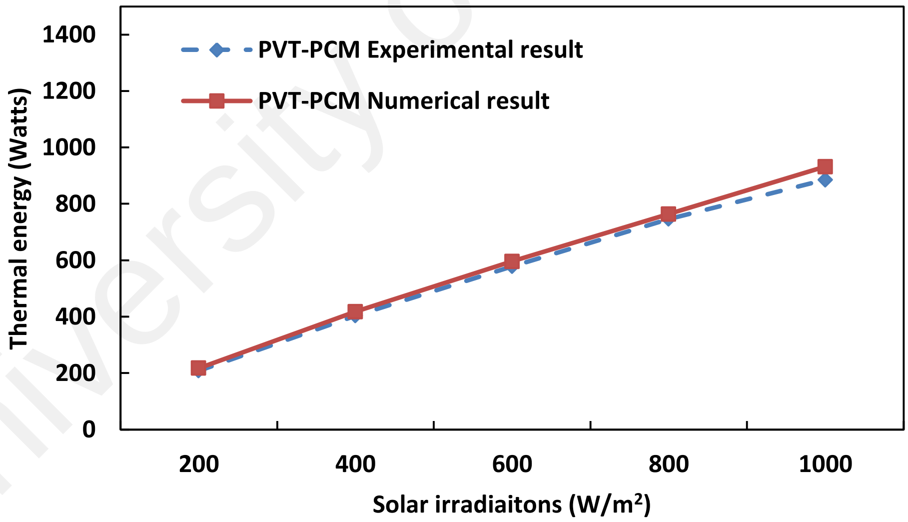

Figure 4.58: Thermal energy of PV and PVT-PCM at different solar irradiations

In Figure 4.59, the irradiation effect is shown on the PVT-PCM system thermal efficiency. The thermal efficiency is taken from the thermal energy obtained. It is observed that thermal efficiency reduces at higher irradiation levels especially after 600 W/m^2. This is due the reason that total of the energy is not efficiently converted into useful energy as some of the energy is lost into the environment at higher temperatures due to a high-temperature gradient. However, at low irradiation the losses are at a minimum as most of the energy is transferred to flowing water but still, some energy is lost in that case. In a cold environment of Ireland, phase change material based PVT was tested by (Browne et al., 2016) thermal efficiency of 25% is achieved due to lower environmental temperatures. It is to note that every PCM and design of thermal collector have a totally different effect on thermal efficiency output. Authors have examined the PVT-PCM systems in hot and cold environments and concluded that the PVT-PCM efficiency is better in hotter weather than colder ones. Similarly, this investigation is carried out in a hotter environment of 32°C.

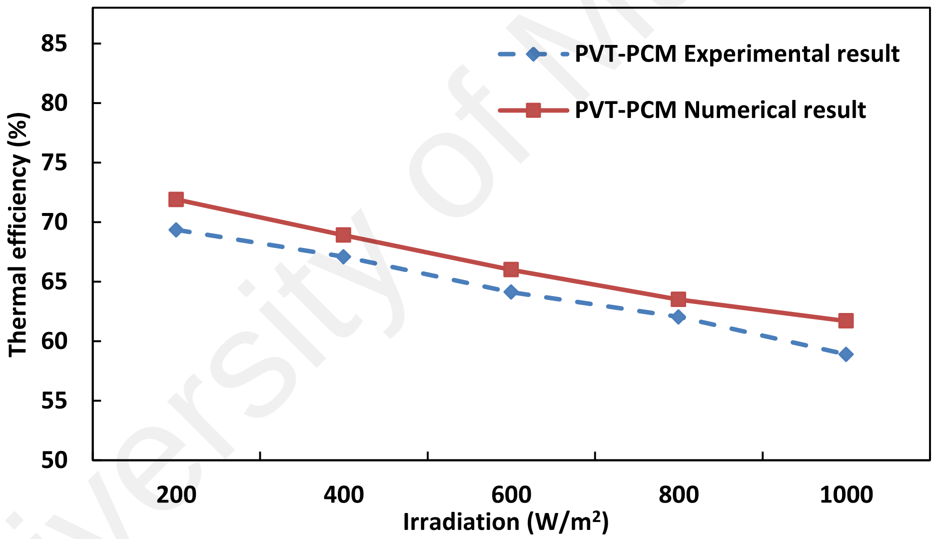

Figure 4.59: Thermal efficiency of PV and PVT-PCM at different solar irradiations

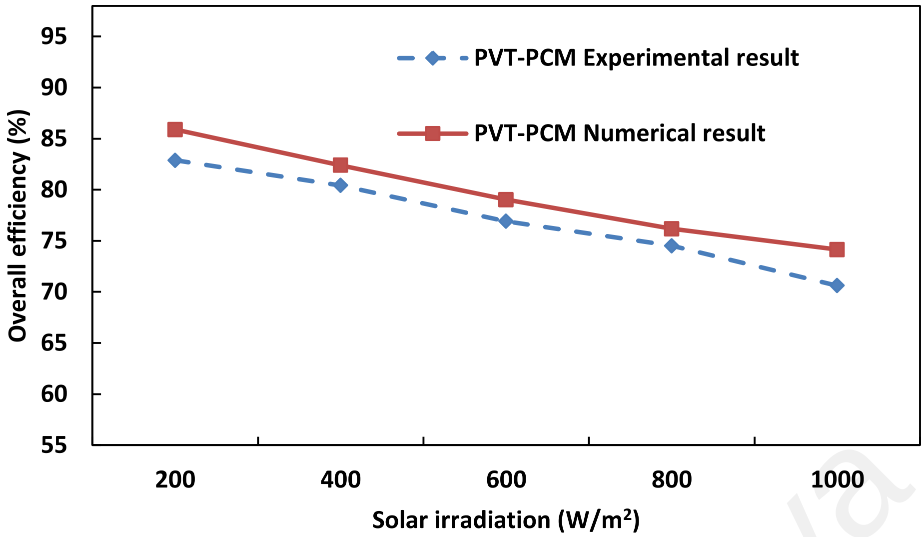

Figure 4.60: Overall efficinecy of PV and PVT-PCM at different solar irradiations

Overall efficiency also decreases with increasing irradiation levels due to the effect of losses of energy back into the environment as seen in Figure 4.60. Overall efficiency achieved at 200 W/m^2 is better than 1000 W/m^2 irradiations. The values of 85.88% and 82.87% are achieved for highest overall efficiency at 200 W/m^2 and 74.13% and 70.61% are obtained for minimum overall efficiency at 1000 W/m^2 for numerical and experimental results respectively.

4.4.5 Mass Flow rate Effect of on PVT and PVT-PCM Systems.

4.4.5.1 Mass flow rate effect on PVT electrical performance.

Mass flow rates of working fluids have prominent effects on the heat removal phenomenon in the system as observed in Figure 4.61. It is observed that the cell temperature of the PVT system reduces as the mass flow rate of water. As the inlet mass flow rate is increased the excessive heat is transferred to water from the module by convection phenomenon resulting in the reduction of cell temperature. There is a huge reduction in cell temperature at 0.5 LPM to 1 LPM but this trend reduces after 1 LPM (Wu et al., 2011). This is because of the reason that cell temperature is higher and the inlet mass flow rate is at a lower temperature, therefore, maximum heat is removed due to a higher temperature gradient. It can be noted that the numerical trend line is quite stable after 1 LPM but the experimental line is fluctuating through the course because of the reason of outdoor uncontrolled weather conditions. However, experimental and numerical values are almost the similar overall.

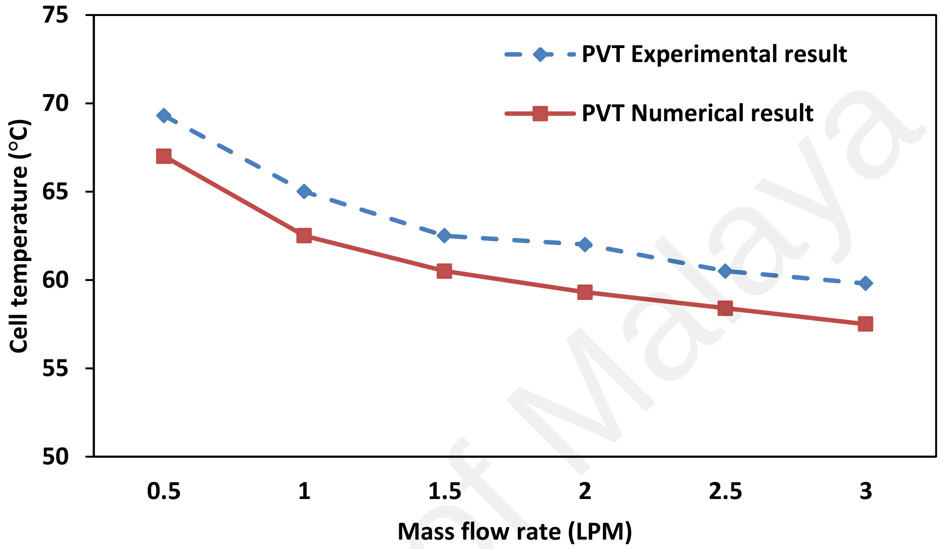

Figure 4.61: Mass flow rate effect on cell temperature of PVT

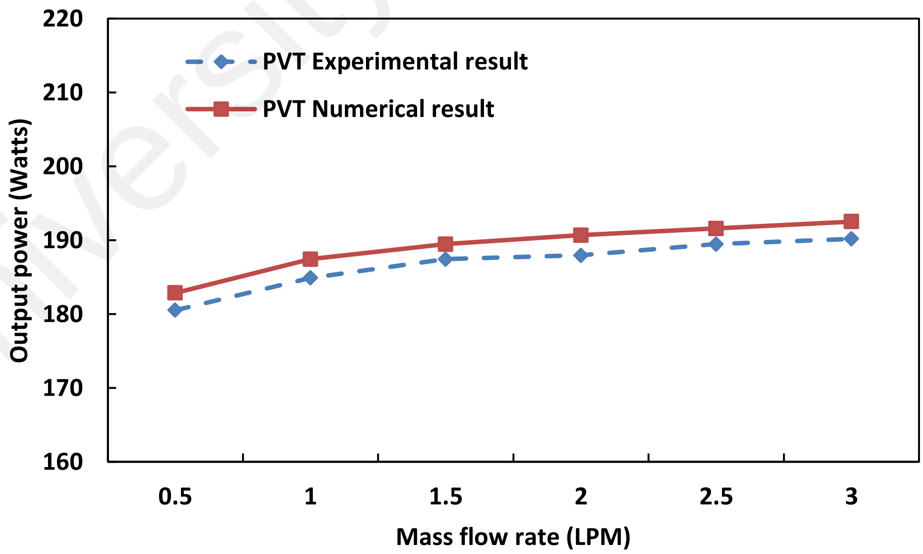

Figure 4.62: Mass flow rate effect on the output power of PVT

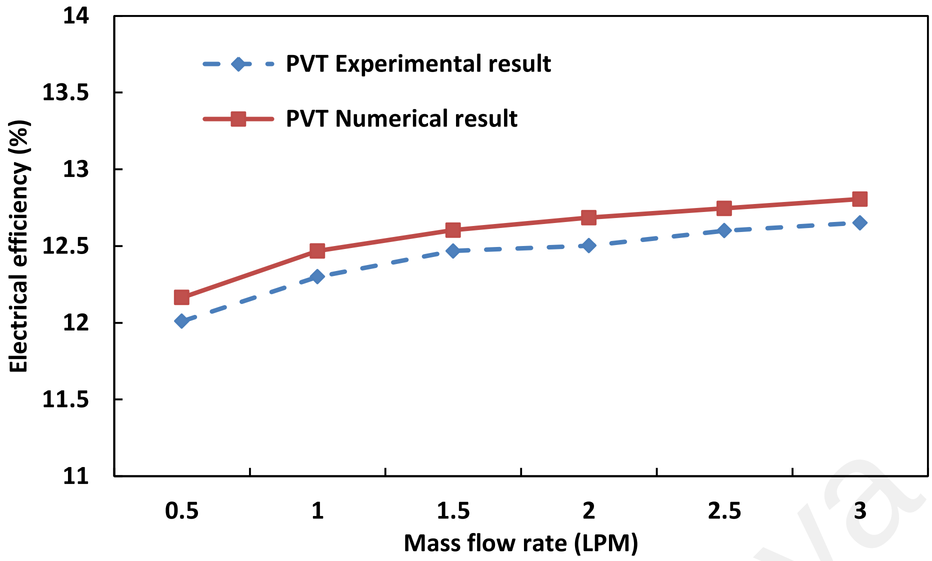

Figure 4.63: Mass flow rate effect on the electrical efficiency of PVT

Mass flow rate effect on electrical efficiency and power is depicted in Figures 4.62 and 4.63. Electrical performance increases as the cell temperature drops prominently due to the increase in mass flow rate, which transfers heat from the PV module. Consequently, PVT voltage increases noticeably while current reduces to some level, resulting in electrical efficiency and a power increase of the PVT. Highest values for the output power are achieved as 192.52W and 190.19W numerically and experimentally respectively. Whereas, the minimum output power is obtained as 182.88W and 180.54W numerically and experimentally respectively. Furthermore, on average output power increment is obtained as 1.25W and 1.58W per 0.5 LPM. Furthermore, on average output power increment is obtained as 1.60W and 1.61W per 0.5 LPM. Identically, the maximum values for electrical efficiency are obtained as 12.81% and 12.65% numerically and experimentally respectively. Further, the electrical efficiency with the minimum values is obtained as 12.16% and 12.12.01% numerically and experimentally respectively. Additionally, electrical efficiency increment per 0.5 LPM is observed as 0.108% and 0.106% for numerical and experimental results respectively. It is found that numerical values are higher to some value than the experimental values. These differences are due to the weather conditions, which are not fully in control and may deviate from a stable position. There is no ideal control of working parameters especially the ambient temperature in the experimental setup but 27°C ambient temperature is set for experimental and numerical investigation.

4.4.5.2 Mass flow rate effect on thermal performance of PVT

Figures 4.64 and 4.65 show the impact of mass flow rate on the output temperature and thermal energy of the PVT system. There is a reduction in water outlet temperature with increment in the inlet mass flow rate as seen in Figure 4.64. At lower mass flow rates more heat is occupied in the small mass of water, therefore, results in higher output temperature of water. Thus, the drop in output temperature with the rise in the mass flow rates determines that a huge mass of water accumulates higher heat but with less temperature. This is attributed to reason that a certain amount of heat absorbed by low mass have a higher temperature than the same amount of heat absorbed by huge mass. However, at higher mass flow rates more heat is transferred even though the output temperature is low as compared to 0.5 LPM. Therefore, the amount of heat removed is enhanced with the rise in mass flow rate with lesser time. Figure 4.64 also shows that the satisfactory agreement in results is achieved numerically and experimentally with small deviations in experimental data, which shows the validation of the numerical model confidently. Maximum output temperatures are observed as 61.11°C and 59.88°C numerically and experimentally respectively. Whereas, minimum output temperatures are 37.4°C and 37°C for numerically and experimentally respectively. Furthermore, on average 3.95°C and 3.81°C increment is achieved per 0.5 LPM numerically and experimentally respectively.

Achieved thermal energy versus mass flow rate shown in Figure. 4.65 enhances with increasing mass flow rate through the flow channel. Convective heat transfer rate increases at mass flow rate increases. However, it is noted that after 0.5 LPM it is slowed down as compared to an initial situation, which is due the reason discussed in the case of Figure 4.64, indicating the same trend for heat transfer rate for both Figures. Therefore, excessive heat is transferred under the similar conditions at higher mass flow rates.

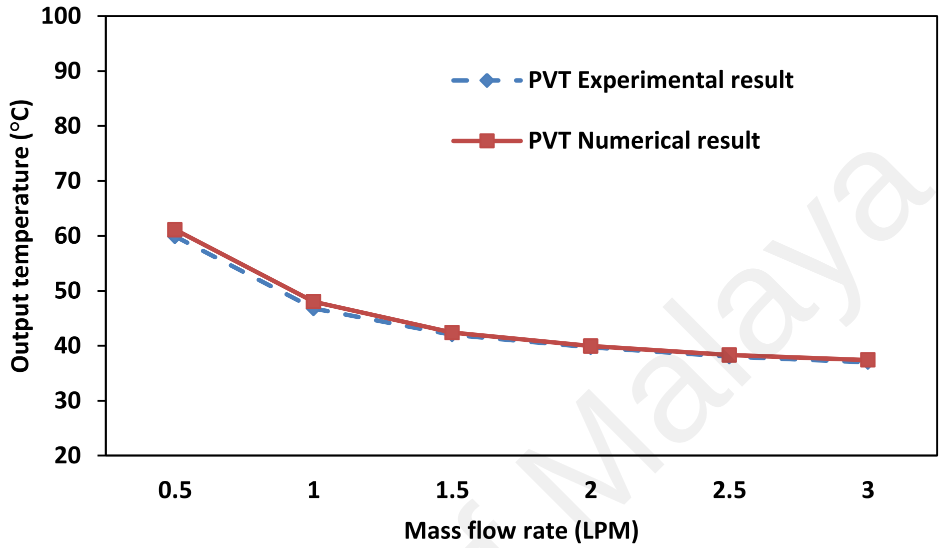

Figure 4.64: Mass flow rate effect on output temperature of PVT

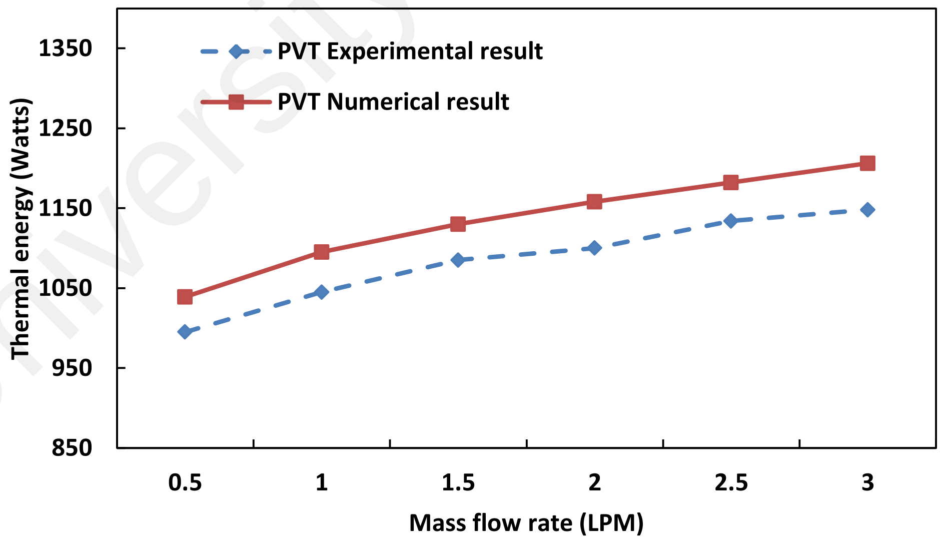

Figure 4.65: Mass flow rate effect on thermal energy PVT

Figures 4.66 shows that thermal efficiency enhances with the increment of water mass flow rate through the system. Increase in mass flow rate enhances the heat transfer through convection between water and thermal collector, which causes in excessive heat transfer at higher mass flow rates, resulting in enhancing the thermal efficiency. The highest values achieved for thermal efficiency are 76.8% and 75.3% numerically and experimentally respectively. Additionally, the lowest values are obtained as 69.13% and 66.2% numerically and experimentally. Furthermore, the rate of thermal efficiency increment is obtained as 1.27% and 1.51% per 0.5 LPM numerically and experimentally respectively. The overall system efficiency is shown in Figure 4.67. The thermal efficiency increases simultaneously with the increment in mass flow rates with the similar trend noted in electrical and thermal efficiency.

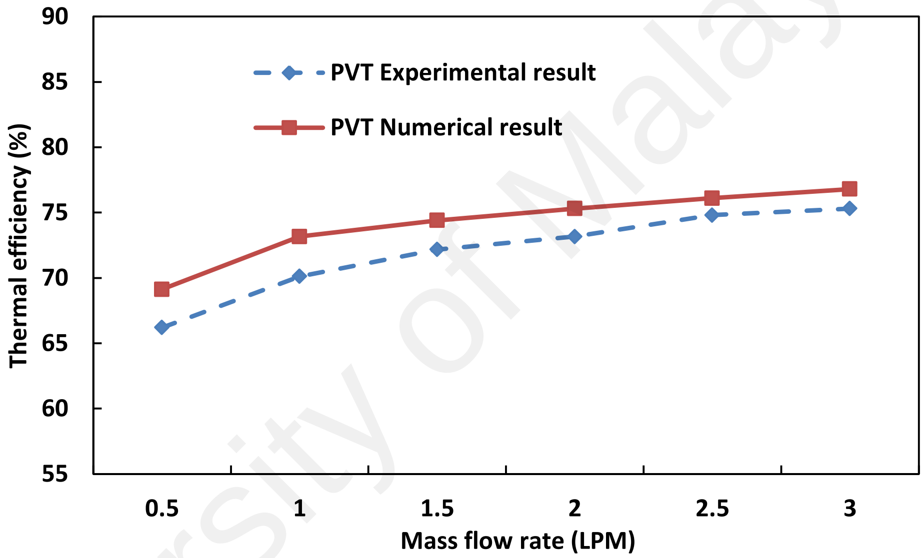

Figure 4.66: Mass flow rate effect on the thermal efficiency of PVT

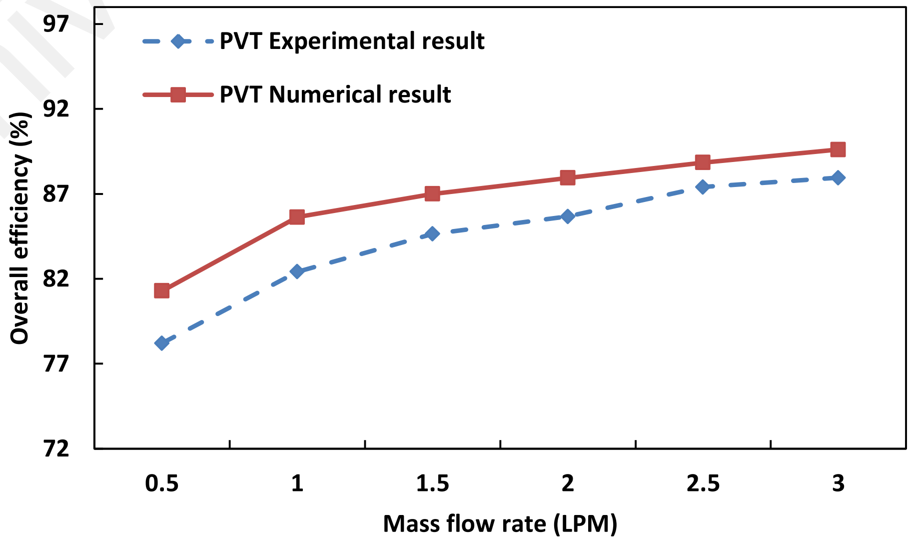

Figure 4.67: Mass flow rate effect on overall efficiency of PVT

4.4.5.3 Effect of mass flow rate on the electrical performance of the PVT-PCM system

The effect of the mass flow rate on the PVT-PCM cell temperature is shown in Figure 4.68. The cell temperature of the PVT system reduces as the mass flow rate of water increases. As the inlet mass flow rate is increased the excessive heat is transferred to water from the module by convection phenomenon resulting in the reduction of cell temperature. There is a huge reduction in cell temperature at 0.5 LPM to 1 LPM but this trend reduces after 1 LPM (Wu et al., 2011). This is because of the reason that cell temperature is higher and the inlet mass flow rate is at a lower temperature at first as well as PCM absorbs heat from cell simultaneously, therefore, maximum heat is removed due to a higher temperature gradient. It is noted that numerical trend line is quite stable after 1 LPM but the experimental line is fluctuating through the course because of the reason of indoor some out of controlled operating conditions or instrumental basic error percentage. However, experimental and numerical values are almost the similar overall.

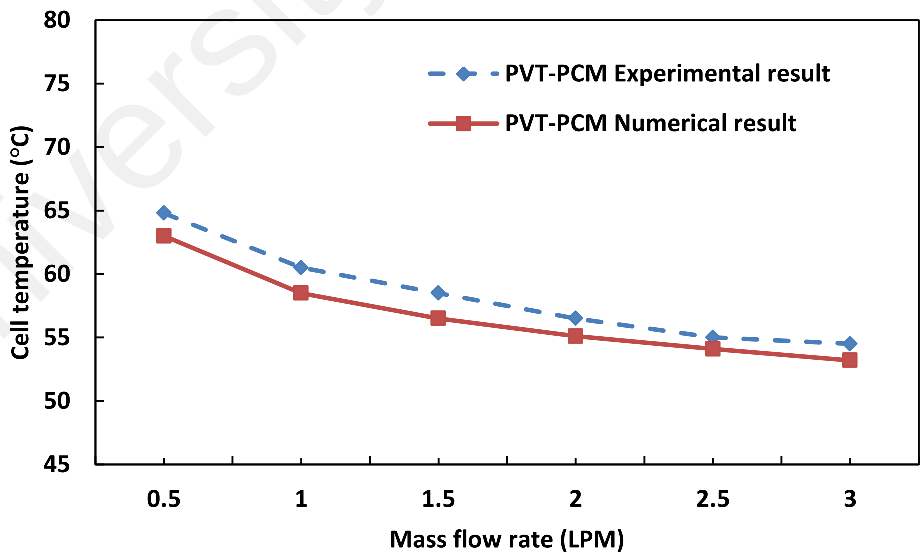

Figure 4.68: Mass flow rate effect on cell temperature of PVT-PCM

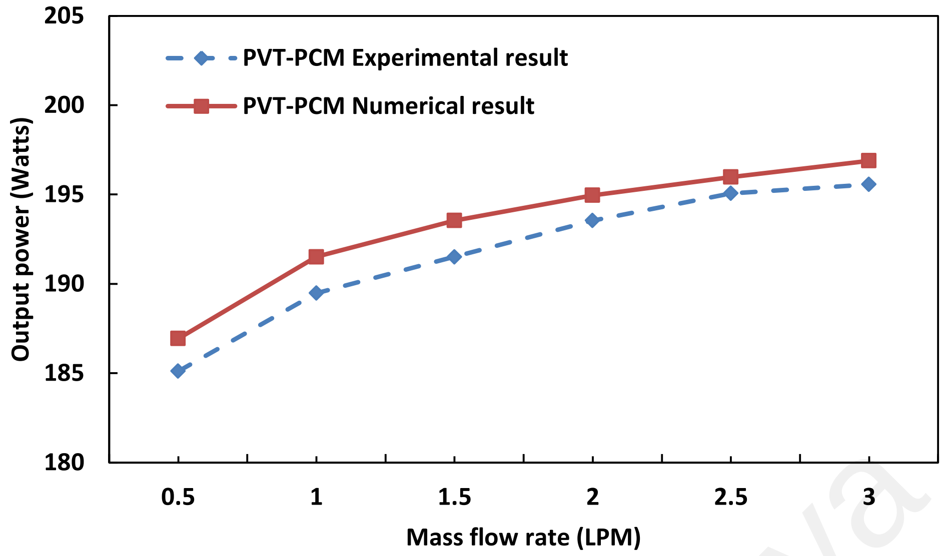

Figure 4.69: Mass flow rate effect on output power of PVT-PCM

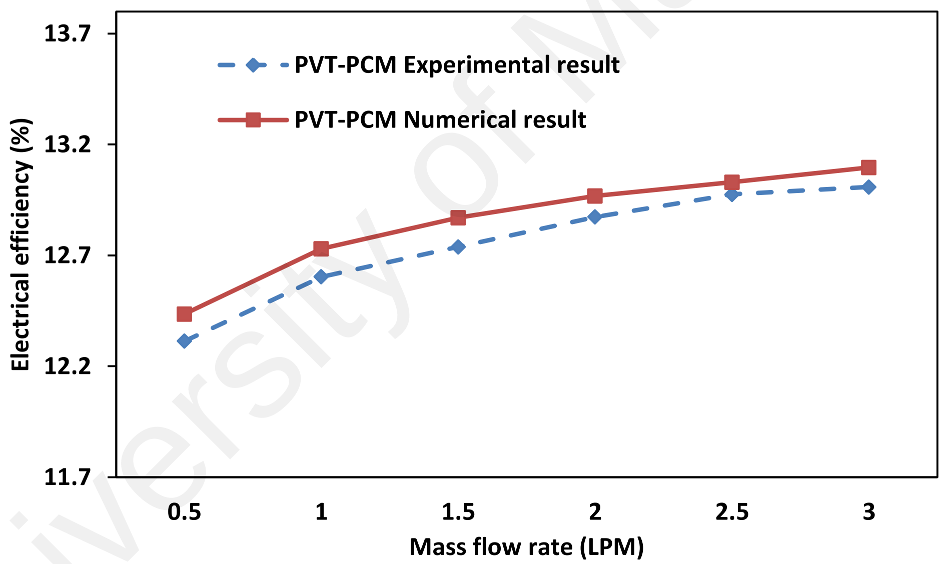

Figure 4.70: Mass flow rate effect on electrical efficiency of PVT-PCM

Mass flow rate effect on electrical efficiency and power is depicted in Figures 4.69 and 4.70. Electrical performance of PVT-PCM increases as the cell temperature drops prominently due to the increment in mass flow rate, which transfers heat form the PV module. Consequently, PVT voltage increases noticeably while current reduces to some level, resulting in electrical efficiency and a power increase of the PVT. The highest values for the power of PVT-PCM are achieved as 196.88W and 195.57W numerically and experimentally respectively. Whereas, the minimum output power is obtained as 186.94W and 185.12W numerically and experimentally respectively. Furthermore, on average output power increment is obtained as 1.65W and 1.74W per 0.5 LPM. Identically, the maximum values for electrical efficiency are obtained as 13.1% and 13.01% numerically and experimentally respectively. Whereas, the minimum electrical efficiency is achieved at about 12.43% and 12.31% numerically and experimentally respectively. Additionally, electrical efficiency increment per 0.5 LPM is observed as 0.111% and 0.116% for numerical and experimental results respectively. It is found that numerical values are higher to some value than the experimental values. These differences are due to the weather conditions, which are not fully in control and may deviate from a stable position. There is no ideal control of working parameters especially the ambient temperature in the experimental setup but 27°C ambient temperature is set for experimental and numerical investigation.

4.4.5.4 Thermal performance of the PVT-PCM system at varying mass flow rates

Figures 4.71 and 4.72 show the impact of mass flow rate on the output temperature and thermal energy of the PVT-PCM system. There is a drop in water outlet temperature with increment in the inlet mass flow rate as seen in Figure 4.35. At lower mass flow rates more heat is occupied in the small mass of water, therefore, results in higher output temperature of water, however, this value is smaller as compared to PVT because of the reason of incorporation of PCM some heat is absorbed in it. Thus, the drop in output temperature with an increment in the mass flow rates determines that a huge mass of water accumulates higher heat but with less temperature. This is attributed to the reason of a certain amount of heat absorbed by low mass have a higher temperature than the same amount of heat absorbed by huge mass and some amount absorbed by PCM as well. However, at higher mass flow rates more heat is transferred even though the output temperature is low as compared to 0.5 LPM of mass flow rate. Therefore, the amount of heat removed is enhanced with the increment in mass flow rate with lesser time. Figure 4.71 also shows that the satisfactory agreement in results is achieved numerically and experimentally with small deviations in experimental data, which shows the validation of the numerical model confidently. Maximum output temperatures are observed as 59.76°C and 58.64°C numerically and experimentally respectively. Whereas, minimum output temperatures are 37.39°C and 37.16°C for numerical and experimental cases respectively. Furthermore, on average 3.72°C and 3.58°C increment is achieved per 0.5 LPM for numerically and experimentally respectively. Thermal energy obtained versus mass flow rate shown in Figure. 4.72 enhances with an increase in mass flow rate through the flow channel. Convective heat transfer rate increases at mass flow rate increases. However, it is noted that after 0.5 LPM it is slowed down as compared to an initial situation which is due the reason discussed in the case of Figure 4.71, indicating the same trend for heat transfer rate for both Figures of PVT-PCM. Therefore, excessive heat is transferred under the similar conditions at higher mass flow rates.

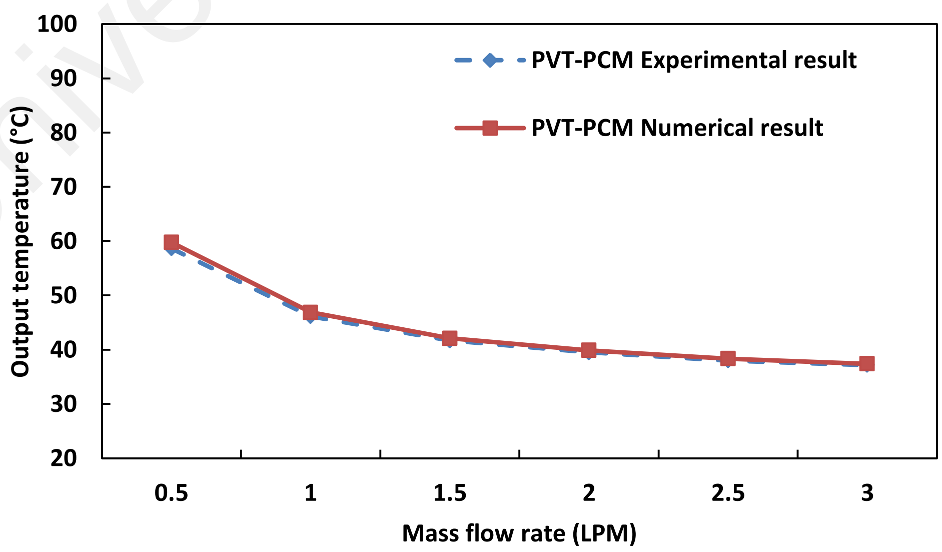

Figure 4.71: Mass flow rate effect on output temperature of PVT-PCM

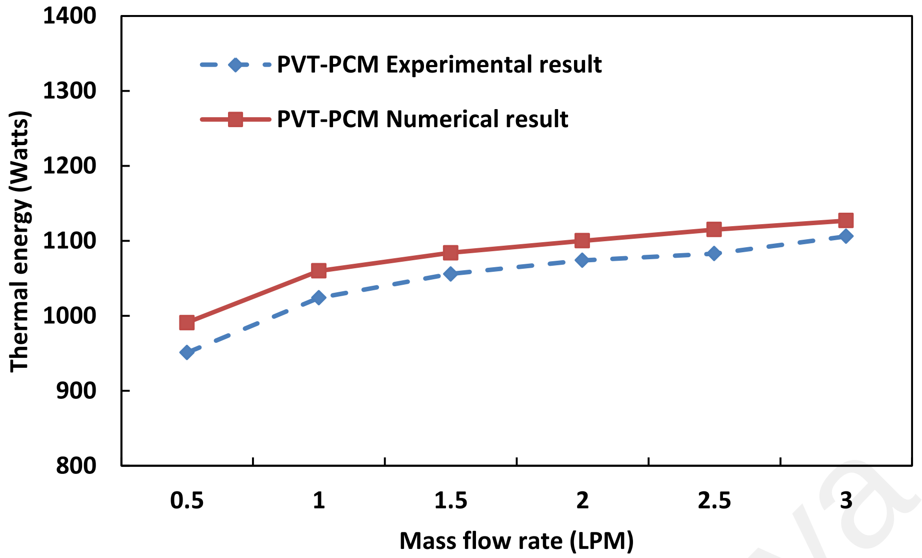

Figure 4.72: Mass flow rate effect on the thermal energy of PVT-PCM

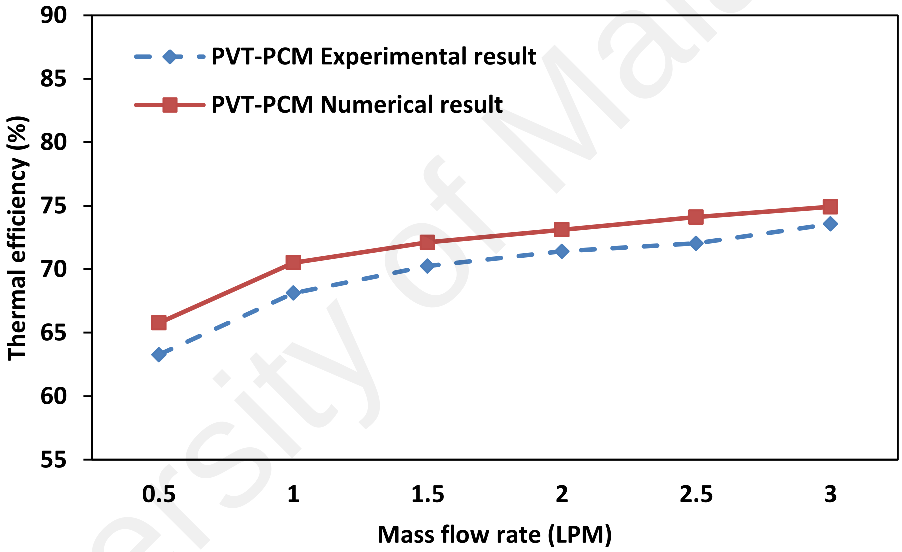

Figure 4.73: Mass flow rate effect on the thermal efficiency of PVT-PCM

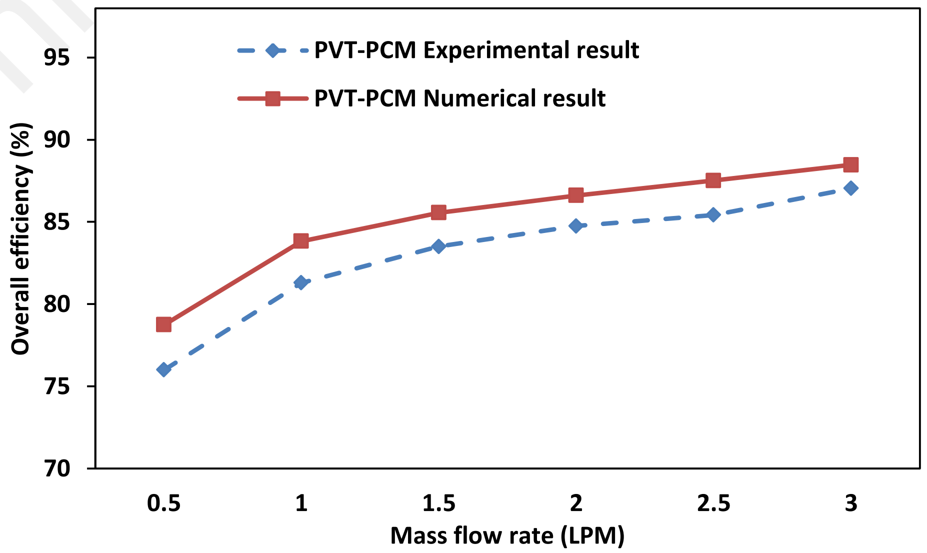

Figure 4.74: Mass flow rate effect on overall efficiency of PVT-PCM

Figures 4.73 shows that thermal efficiency enhances with increment in water mass flow rate through the system. Increase in mass flow rate enhances the heat transfer through convection between water and thermal collector as well as it gets less time for PCM to get heat form fast flowing water. It causes excessive heat transfer at increased mass flow rates, resulting in enhancing the thermal efficiency. The highest values achieved for thermal efficiency are 74.91% and 73.56% numerically and experimentally respectively. Additionally, lowest values are obtained as 65.77% and 63.26% for numerical and experimental results respectively. Figure 4.74 depicts the overall efficiency of the system PVT-PCM system. The overall efficiency increases simultaneously with the increment in mass flow rates with the similar trend noted in the electrical and thermal efficiency of the system. The values for the overall efficiency of PVT are achieved as 88.47% and 87.03%, numerically and experimentally respectively. Lowest values of the overall thermal efficiency are obtained as 78.74% and 76% numerically and experimentally. . Furthermore, the rate of efficiency increment is found as 1.62% and 1.83% for each mass flow rate of 0.5 LPM.

4.5 Performance Comparison Analysis of the Systems

In this section comparison of the thermal, electrical and overall performance of porposed systems is presented. Electrical results of PV are compared with PVT and PVT-PCM whereas; results with mass flow rates are only compared between PVT and PVT-PCM. Indoor and outdoor performance comparison is carried out separately in the following subsections.

4.5.1 Indoor Performance Comparison of PV, PVT and PVT-PCM Systems

4.5.1.1 Comparison of results for effect of irradiation

Comparison of PV, PVT and PVT-PCM is given in Tables 4.3, 4.4, 4.5 and 4.6 for electrical and thermal performances with the effect of irradiation and mass flow rate. However, a detailed analysis of these systems is done in previous sections individually. Whereas, Figures 4.75, 4.76 and 4.77 show the electrical thermal and overall performance comparison of the systems. It is noted from the values in tables and trend in figures that in terms of electrical performance PVT-PCM system is better. However, for thermal performance, PVT systems is efficient as compared to the PVT-PCM system. Many factors e.g. solar irradiation, ambient temperature, mass flow rate, the temperature of the inlet fluid etc. greatly affect the performance of the systems whether it is PV, PVT or PVT-PCM. The solar irradiation influence on cell temperature and electrical performance is shown in Table 4.3 and Figure 4.75. Cell temperature reduction between PV and PVT system is obtained as 8°C and 6.46°C in numerical case and 7.1°C and 6.51°C at maximum and minimum irradiations respectively in the experimental case.

Table 4.3: Comparison of indoor PV, PVT and PVT-PCM systems electrical performance for the effect of irradiation

System type	Irradiation level (W/m^2)	Solar irradiation effect					
		Cell temperature (°C)		Output power (Watts)		Electrical efficiency (%)	
		Numerical	Experimental	Numerical	Experimental	Numerical	Experimental
PV	1000	79	82	170.7	167.64	11.35	11.15
	200	44	46.9	41.24	40.65	13.71	13.52
PVT	1000	71	74.89	178.77	174.87	11.89	11.63
	200	37.54	40.39	42.55	41.97	14.15	13.96
PVT-PCM	1000	65	68.4	184.91	181.46	12.3	12.07
	200	34	37	43.27	42.66	14.39	14.19

Table 4.4: Comparison of indoor PVT and PVT-PCM systems thermal performance due to the effect of irradiation

Type	Irradiation level (W/m^2)	Solar irradiation effect							
		Output temperature (°C)		Thermal energy (Watts)		Thermal efficiency (%)		Overall efficiency (%)	
		Numerical	Experimental	Numerical	Experimental	Numerical	Experimental	Numerical	Experimental
PVT	**1000**	55.8	57.8	1085	1032	71.31	69.3	84.79	82.48
	200	34.9	36.5	236	230	78.46	76.42	94.49	92.24
PVT-PCM	**1000**	52.5	55	995	945	66	64.3	79.47	77.48
	200	32.8	33.8	231	207	73.5	72.5	89.54	88.32

It shows that a considerable amount of cell temperature reduction is achieved through PV cooling, which increases modules electrical performance in the result. For PV and PVT-PCM system, the cell temperature reduction is obtained as 21.5% and 29.4% at respective irradiations of 1000 W/m^2 and 200 W/m^2 in numerical case. Whereas, in the experimental case, 19.88% and 26.75% reduction in cell temperature is achieved at 1000 W/m^2 and 200 W/m^2 respectively. It is evident from the results obtained for PVT and PVT-PCM; the later system achieved higher performance in reducing cell temperature. Comparison between PVT and PVT-PCM cell temperature reduction is achieved as 75.2% and 54.7% numerically at respective irradiations of 1000 W/m^2 and 200 W/m^2. Whereas, in the experimental case, 91.2% and 52% for the PVT-PCM system, which is more efficient as compared to PVT at 1000 W/m^2 and 200 W/m^2 respectively. The cell temperature reduction analysis due to PVT and PVT-PCM shows that PVT-PCM is higher in performance as compared to PVT as it reduces maximum cell temperature from the PV module. Electrical efficiency increment between PV and PVT system is achieved as 4.75% and 3.25% at respective irradiations of 1000W/m^2 and 200 W/m^2 in numerical case. Whereas, 4.3% and 3.2% at respective irradiations of 1000 W/m^2 and 200 W/m^2 in experimental case. It shows that a considerable electrical efficiency is achieved in PV with cooling as PVT. Similarly, in the case of PV and PVT-PCM system, electrical efficiency increment is achieved as 8.3% and 4.96% at

1000 W/m^2 and 200 W/m^2 respectively in numerical case. Whereas, in the experimental case, 8.25% and 4.95% increment is achieved at 1000 W/m^2 and 200 W/m^2 respectively. It is clear from the results obtained for PVT and PVT-PCM, the latter system achieved higher performance in increasing electrical efficiency. Comparison between PVT and PVT-PCM electrical efficiency increment is achieved as 75.9% and 45.4% numerically at respective irradiations of 1000 and 200 W/m^2. Whereas, in experimental case, 91.6% and 52.2% more efficient PVT-PCM system as compared to PVT at respective irradiations of 1000 and 200 W/m^2. In case of electrical efficiency as well, the PVT-PCM system is higher in performance as compared to the PVT system. The thermal efficiency of PVT is higher than PVT-PCM as can be seen from Table 4.4. Similarly, overall efficiency of PVT is greater than PVT-PCM due to the major portion of overall efficiency consists of thermal efficiency, which is higher for PVT system as compared to PVT-PCM. The reason is that stored heat is not achieved on the time in flowing water and stored heat is not efficiently recovered at the times of irradiation absence as that energy is lost back to environment thought PV surface and other sides of PV module. However, the electrical efficiency of PVT-PCM is higher than PVT system. Whereas, in the experimental case, 6.4% and 4.4% more efficient at respective irradiations of 1000 W/m^2 and 200 W/m^2.

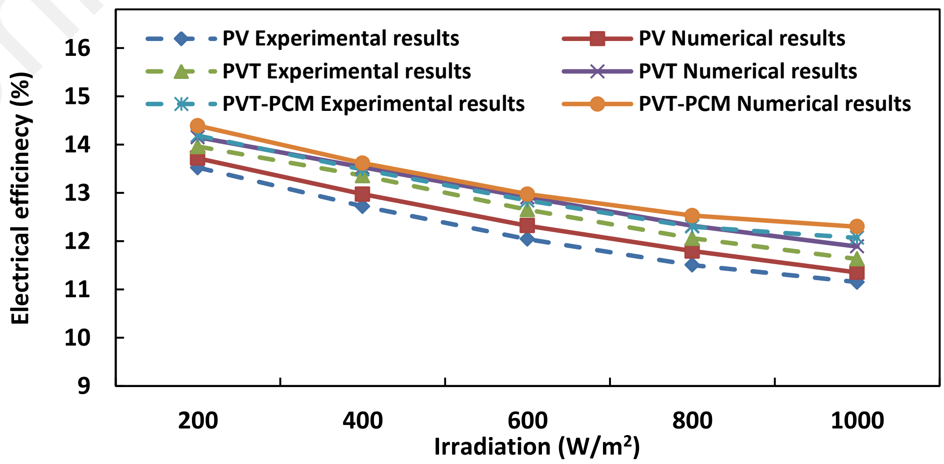

Figure 4.75: Electrical performance of all three systems at different solar irradiations and 0.5 LPM and 27°C ambient and inlet water temperature

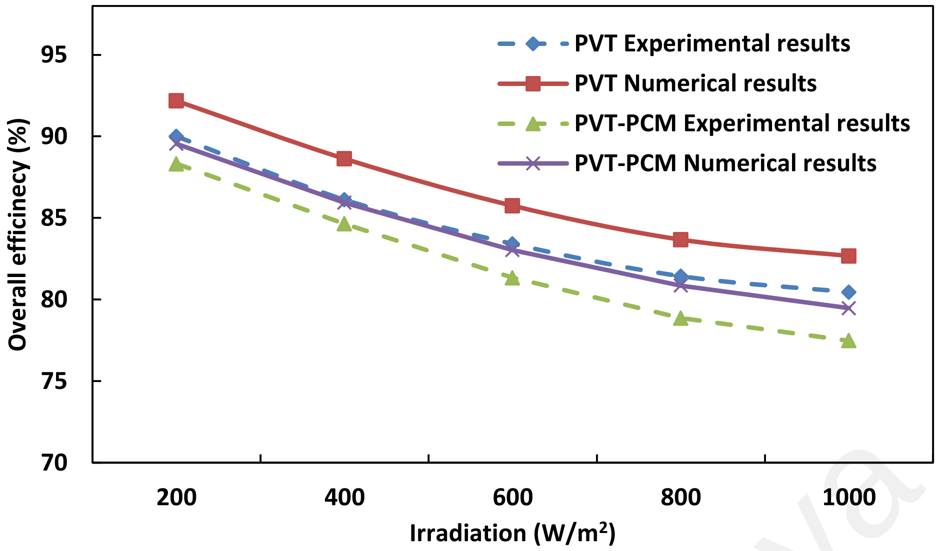

Figure 4.76: Overall performance of PVT and PVT-PCM at different solar irradiations and 0.5 LPM and 27°C ambient and inlet water temperature

Figure 4.75 shows the electrical efficiency of the systems with the effect of irradiations. Maximum electrical efficiency is obtained by the PVT-PCM system; consequently, PVT and PV follow the trend of efficiency in decreasing trend. Maximum electrical efficiency is obtained at 200 W/m^2 for all panels and minimum electrical efficiency obtained at 1000 W/m^2 because the reason of increased rate of heat transfer from the surfaces of panels as temperature gradient becomes high. Figure 4.76 depicts the overall efficiency of PVT and PVT-PCM systems versus the irradiation effect. Overall efficiency for PVT-PCM is lower than the PVT system due to the reason of higher contribution of thermal energy by PVT. However, the electrical efficiency of PVT-PCM is greater than PVT but due to a small percentage of electrical efficiency as compared to a thermal one, the overall efficiency of energy gain for PVT is higher. The maximum overall efficiency for both systems is obtained at 200 W/m^2, whereas, minimum overall efficiency is obtained at 1000 W/m^2.

4.5.1.2 Comparison of results for the effect of mass flow rate

Mass flow rate have an important effect on cell temperature of PVT and PVT-PCM. It has been noticed that the cell temperature directly drops with an increase in mass flow rate. Table 4.5 shows the effect of mass flow rate on the electrical performance of PVT and PVT-PCM. Comparative cell temperature reduction between PVT and the PVT-PCM system is achieved as 6% and 8.9% more for PVT-PCM at 0.5 LPM and 3 LPM respectively in numerical case. Whereas, 7.8% and 7.5% at 0.5 LPM and 3 LPM respectively in the experimental case. It shows that a considerable amount of cell temperature reduction is achieved more in PVT-PCM, which increases modules electrical performance in the result. Effect of cell temperature on electrical efficiency is direct in its increment. Electrical efficiency increment between PVT and the PVT-PCM system is achieved as 10.77% and 10.19% at 0.5 LPM and 3 LPM respectively in numerical case, whereas, 9.81% and 10.56% at 0.5 LPM and 3 LPM respectively in the experimental case. It shows that a considerable more amount of electrical efficiency is obtained in PVT-PCM in comparison with PVT.

Table 4.5: Comparison of indoor PVT and PVT-PCM systems electrical performance due to the effect of mass flow rate

System type	Mass flow rate (LPM)	Mass flow rate effect					
		Cell temperature (°C)		Output power (Watts)		Electrical efficiency (%)	
		Numerical	Experimental	Numerical	Experimental	Numerical	Experimental
PVT	0.5	71.05	74.59	178.77	174.87	13.47	13.2
	3	63.5	65.2	186.43	184.71	14.05	13.92
PVT-PCM	0.5	67	69.13	182.88	180.72	12.16	12.02
	3	58.3	60.6	191.71	189.37	12.75	12.59

Table 4.6: Comparison of indoor PVT and PVT-PCM systems thermal performance

Type	Mass flow rate (LPM)	Mass flow rate effect							
		Output temperature (°C)		Thermal energy (Watts)		Thermal efficiency (%)		Overall efficiency (%)	
		Numerical	Experimental	Numerical	Experimental	Numerical	Experimental	Numerical	Experimental
PVT	**0.5**	57.4	56	1069	1040.62	71	69	84.47	82.22
	3	33.1	32.43	1220	1163.1	81	77.36	95.05	91.11
PVT-PCM	**0.5**	54.58	53	965.91	938.91	64	62.45	76.16	74.47
	3	33	32	1085	1068	72	71	84.75	83.59

In the previous discussion, it is shown that the thermal energy of PVT is higher than the PVT-PCM Thermal efficiency of PVT is higher than PVT-PCM as can be seen from Table 4.6. Comparison between PVT and PVT-PCM thermal energy increment of PVT than PVT-PCM is achieved as 10.93% and 12.5% numerically at 0.5 LPM and 3 LPM respectively. Whereas, in the experimental case, 10.48% and 8.95% more efficient at 0.5 LPM and 3 LPM respectively. Similarly, the overall efficiency of PVT is greater than PVT-PCM due to the major portion of overall efficiency consists of thermal efficiency, which is higher for the PVT system as compared to PVT-PCM. However, the electrical efficiency of PVT-PCM is higher than PVT system. Comparative overall efficiency is achieved as 10.93% and 12.5% numerically at 0.5 LPM and 3 LPM respectively greater than PVT-PCM. Whereas, in the experimental case, 10.4% and 8.99% more efficient at 0.5 LPM and 3 LPM respectively.

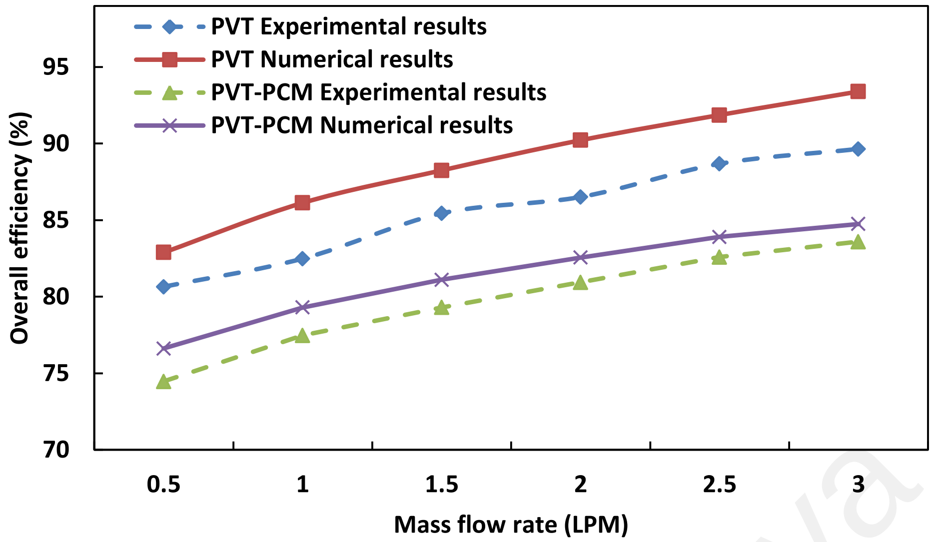

Figure 4.77: Effect of mass flow rate on the overall efficinecy of PV, PVT and PVT-PCM at 1000 W/m^2 and 27°C ambient and inlet water temperature

Figure 4.77 shows the effect of the mass flow rate ranging from 0.5 LPM to 3 LPM. The overall performance difference between PVT and PVT-PCM is very clear as experimental as well as numerical results are higher for PVT system. Hence, both systems follow a similar trend of energy gain from 0.5 LPM to 3 LPM. However, numerical and experimental agreement in case of PVT-PCM is better than PVT system.

4.5.2 Outdoor Performance Comparison of PV, PVT and PVT-PCM Systems

4.5.2.1 Comparison of results for the effect of solar irradiation

Each system is analyzed separately in previous sections. However, comparison of three systems is given in Tables 4.7, 4.8, 4.9 and 4.10 in terms of electrical and thermal performances with the effect of irradiation and mass flow rate. However, a detailed analysis of these systems is done in previous sections individually, whereas, Figures 4.78, Figure 4.79 and Figure 4.80 show the electrical thermal and overall performance comparison of the systems. It is noted from the values in tables and trend in figures that in terms of electrical performance PVT-PCM system is better. However, for thermal performance, a PVT system is efficient as compared to the PVT-PCM system. Many factors e.g. solar irradiation, ambient temperature, mass flow rate, the temperature of the inlet fluid etc. greatly affect the performance of the systems whether it is PV, PVT or PVT-PCM.

Table 4.7: Comparison of outdoor PV, PVT and PVT-PCM systems electrical performance due to the effect of irradiation

System type	Irradiation level (W/m^2)	Solar irradiation effect					
		Cell temperature (°C)		Output power (Watts)		Electrical efficiency (%)	
		Numerical	Experimental	Numerical	Experimental	Numerical	Experimental
PV	1000	75.1	77.6	174.66	17.13	11.62	11.45
	200	44	46.3	41.44	40.77	13.79	13.56
PVT	1000	67	69.3	182.88	180.55	12.16	12.01
	200	42	43.6	41.65	41.32	13.85	13.74
PVT-PCM	1000	63.1	64.8	186.94	185.11	12.43	12.31
	200	40	41.6	42.05	41.73	13.98	13.88

Table 4.8: Comparison of outdoor PVT and PVT-PCM systems thermal performance due to the effect of irradiation

Type	Irradiation level (W/m^2)	Solar irradiation effect							
		Output temperature (°C)		Thermal energy (Watts)		Thermal efficiency (%)		Overall efficiency (%)	
		Numerical	Experimental	Numerical	Experimental	Numerical	Experimental	Numerical	Experimental
PVT	1000	61.11	59.88	1039.23	995.32	66.1	66.1	81.26	78.11
	200	38.42	38.35	229.2	226.7	69.1	75	89.95	88.84
PVT-PCM	1000	58.1	56.8	931.77	885.36	61.7	58.89	74.14	70.61
	200	38.1	37.7	217.8	208.49	71.9	69.34	85.88	82.88

The solar irradiation impact on cell temperature and electrical of the systems is shown in Table 4.7 and Figure 4.78. Cell temperature reduction between PV and PVT system is achieved as 10.9% and 5.2% at 1000 W/m^2 and 200 W/m^2 respectively in numerical case. Whereas, 11.7% and 5.3% at 1000 W/m^2 and 200 W/m^2 respectively in the experimental case. It shows that a considerable amount of cell temperature reduction is achieved in PV cooling, which increases modules electrical performance in the result. In the case of PV and PVT-PCM system, cell temperature reduction is achieved as 18.9% and 8.5% at 1000 W/m^2 and 200 W/m^2 respectively in numerical case. Whereas, in the experimental case, 19.1% and 10.7% reduction in cell temperature is achieved at 1000 W/m^2 and 200 W/m^2 respectively. It is evident from the results obtained for PVT and PVT-PCM; the later system achieved higher performance in reducing cell temperature. Comparison between PVT and PVT-PCM cell temperature reduction is obtained as 48.1% and 100% numerically at 1000W/m^2 and 200 W/m^2 respectively. Whereas, in the experimental case, 54.21% and 42.55% for the PVT-PCM system, which is more efficient as compared to PVT at 1000 W/m^2 and 200 W/m^2 respectively. The cell temperature reduction analysis due to PVT and PVT-PCM shows that PVT-PCM is higher in performance as compared to PVT as it reduces maximum cell temperature from PV module.

Electrical efficiency increment between PV and PVT system is achieved as 3.7% and 1.01% at maximum and minimum irradiation respectively in numerical case. Whereas, 4.2% and 1.09% at maximum and minimum irradiation respectively in the experimental case. For electrical efficiency difference of PVT over PV is also shown by (Pathak et al., 2014) where 6.5% improvement in electrical efficiency achieved for weather conditions of the Detroit region, USA. It shows that a considerable electrical efficiency is obtained in PV with cooling as PVT. Similarly, in the case of PV and PVT-PCM system, electrical efficiency increment is achieved as 6% and 1.58% at 1000 W/m^2 and 200 W/m^2 respectively in numerical case. Whereas, in the experimental case, 6.4% and 2.03% increment is achieved at 1000 W/m^2 and 200 W/m^2 respectively. It is clear from the results obtained for PVT and PVT-PCM, the later system achieved higher performance in increasing electrical efficiency. Comparison between PVT and PVT-PCM electrical efficiency increment is achieved as 50% and 2.16% numerically at 1000 W/m^2 and 200 W/m^2 respectively. Whereas, in experimental case, 59.25% and 77.77% more efficient PVT-PCM system as compared to PVT at 1000 W/m^2 and 200 W/m^2 respectively. In case of electrical efficiency as well, the PVT-PCM system is higher in performance as compared to the PVT system. PVT thermal efficiency is greater than PVT-PCM as can be seen from Table 4.8. For PVT and PVT-PCM thermal energy comparison, increment of PVT than PVT-PCM is achieved as 4.8% and 4.4% numerically at 1000 W/m^2 and 200 W/m^2 respectively, whereas, in the experimental case, 4.5% and 5.6% more efficient at 1000 W/m^2 and 200 W/m^2 respectively.

Similarly, the overall efficiency of PVT is greater than PVT-PCM due to the major portion of overall efficiency consists of thermal efficiency, that is higher for PVT system in comparison with PVT-PCM. However, the electrical efficiency of PVT-PCM is higher than PVT system. Overall efficiency is achieved as 3.5% and 2.9% numerically at 1000 W/m^2 and 200 W/m^2 respectively, whereas, in the experimental case, 3.2% and 3.99% more efficient at 1000 W/m^2 and 200 W/m^2 respectively.

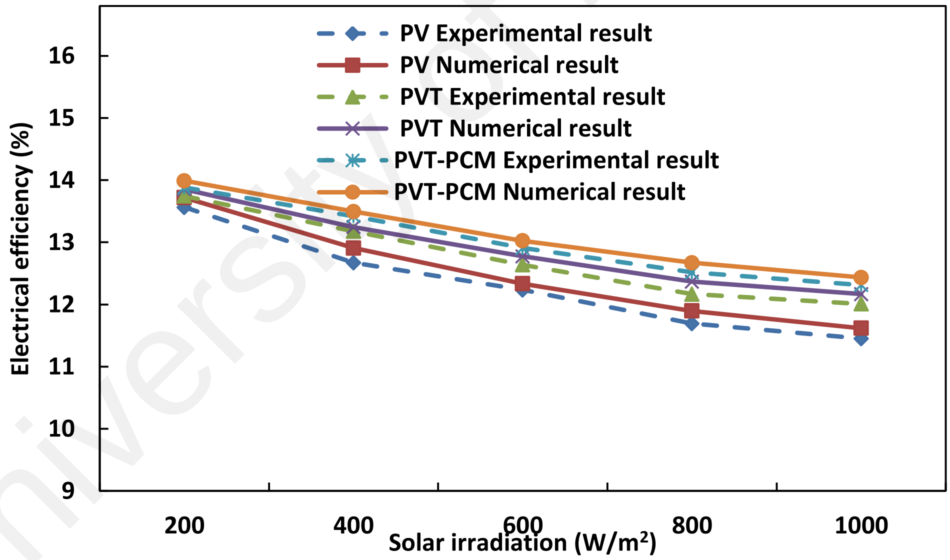

Figure 4.78: Electrical performance of all three systems at different solar irradiations

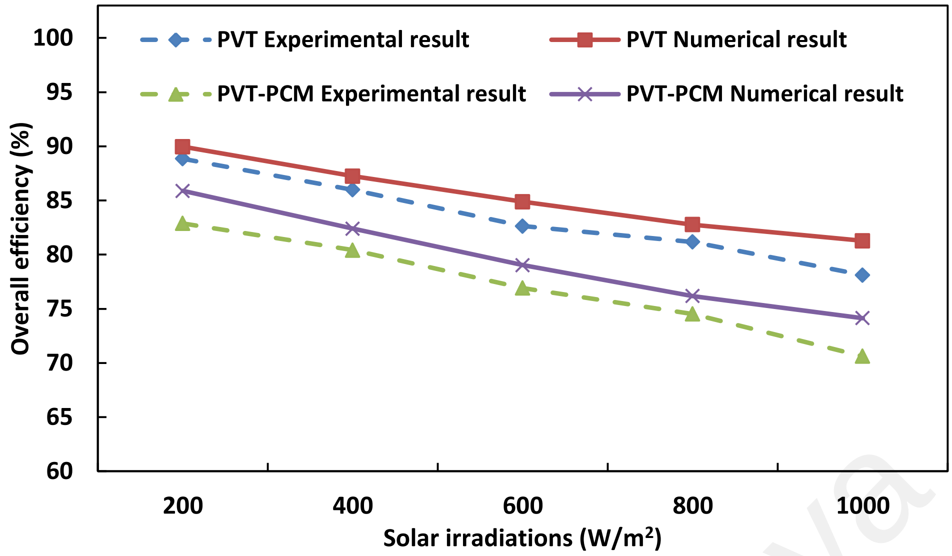

Figure 4.79: Overall performance at varying solar irradiations and 0.5 LPM and 32°C ambient and inlet water temperature

Figure 4.78 shows the electrical efficiency of the systems with the effect of irradiations. It is observed that maximum electrical efficiency is obtained by the PVT-PCM system; consequently, PVT and PV follow the trend of efficiency in decreasing trend. Maximum electrical efficiency is obtained at 200 W/m^2 for all panels and minimum electrical efficiency obtained at 1000 W/m^2 because the reason of increased rate of heat transfer from the surfaces of panels as temperature gradient becomes high. Figure 4.79 depicts the overall efficiency of PVT and PVT-PCM systems versus the irradiation effect. Overall efficiency for PVT-PCM is lower than the PVT system due to the reason of higher contribution of thermal energy by PVT. However, the electrical efficiency of PVT-PCM is greater than PVT but due to a small percentage of electrical efficiency as compared to a thermal one, the overall efficiency of energy gain for PVT is higher. The maximum overall efficiency for both systems is obtained at 200 W/m^2, whereas, minimum overall efficiency is obtained at 1000 W/m^2.

4.5.2.2 Comparison of results for the effect of mass flow rate

Mass flow rate plays important role in reducing cell temperature of PVT and PVT-PCM. It has been noticed that the cell temperature directly drops with an increase in mass flow rate. Table 4.9 shows the effect of mass flow rate on the electrical performance of PVT and PVT-PCM. Comparative cell temperature reduction between PVT and the PVT-PCM system is achieved as 8% and 2% more for PVT-PCM at 0.5 LPM and 3 LPM respectively in numerical case, whereas, 6.66% and 18.4% at 0.5 LPM and 3 LPM respectively in the experimental case. It shows that a considerable amount of cell temperature reduction is achieved more in PVT-PCM, which increases modules electrical performance in the result.

Effect of cell temperature on electrical efficiency is direct in its increment. Electrical efficiency increment between PVT and the PVT-PCM system is achieved as 2.38% and 6.3% at 0.5 LPM and 3 LPM respectively in numerical case. Whereas, 4.87% and 1% at 0.5 LPM and 3 LPM respectively in the experimental case. It shows that a considerable more amount of electrical efficiency is achieved in PVT-PCM in comparison with PVT.

Table 4.9: Comparison of outdoor electrical performance of systems due to the effect of mass flow rate

System type	Mass flow rate (LPM)	Mass flow rate effect					
		Cell temperature (°C)		Output power (Watts)		Electrical efficiency (%)	
		Numerical	Experimental	Numerical	Experimental	Numerical	Experimental
PVT	0.5	67	69.3	182.88	180.54	12.16	12.01
	3	57.5	59.8	192.52	190.19	12.81	12.65
PVT-PCM	0.5	63	64.8	186.94	185.12	12.43	12.31
	3	53.2	54.5	196.88	195.57	13.1	13.01

Table 4.10: Comparison of outdoor results for all three systems thermal performance for mass flow rate

Type	Mass flow rate (LPM)	Mass flow rate effect							
		Output temperature (°C)		Thermal energy (Watts)		Thermal efficiency (%)		Overall efficiency (%)	
		Numerical	Experimental	Numerical	Experimental	Numerical	Experimental	Numerical	Experimental
PVT	0.5	61.11	59.88	1039	995	69.1	66.2	81.42	78.23
	3	37.4	37	1206	1148	76.8	75.3	89.53	87.93
PVT-PCM	0.5	59.76	58.64	991.03	951.04	65.77	63.26	78.74	76
	3	37.39	37.16	1156.03	1106.12	74.91	73.56	88.47	87.03

In the previous discussion, it is shown that the thermal energy of PVT is higher than the PVT-PCM Thermal efficiency of PVT is higher than PVT-PCM as can be seen from Table 4.10. Similarly, the overall efficiency of PVT is greater than PVT-PCM due to the major portion of overall efficiency consists of thermal efficiency, which is higher for the PVT system as compared to PVT-PCM. However, the electrical efficiency of PVT-PCM is higher than PVT system. Comparative overall efficiency is obtained as 3.2% and 2.8% numerically at 0.5 LPM and 3 LPM respectively greater than PVT-PCM. Whereas, in the experimental case, 2.6% and 2.17% more efficient at 0.5 LPM and 3 LPM respectively. Figure 4.80 shows the mass flow rate effect ranging from 0.5 LPM to 3 LPM. The overall performance difference between PVT and PVT-PCM is very clear as experimental as well as numerical results are higher for PVT system. Hence, both systems follow a similar trend of energy gain from 0.5 LPM to 3 LPM. However, numerical and experimental agreement in case of PVT-PCM is better than PVT system.

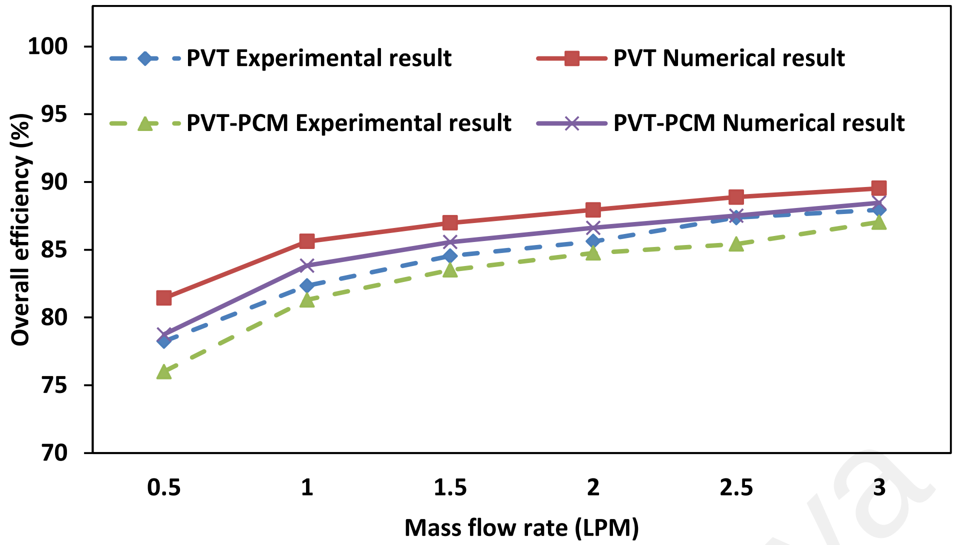

Figure 4.80: Effect of mass flow rate on the overall efficiency of PVT and PVT-PCM

It is observed that for electrical efficiency requirements PVT-PCM better candidate, whereas, PVT system is suitable where higher thermal energy is required as compared to electrical efficiency. While selecting the system type for the required application e.g. thermal energy requirement or higher output temperatures or electrical higher performance only regardless of hot water requirement, should really be taken into account. There is a compromise on either thermal performance or electrical efficiency of the system if it is about the selection of PVT or PVT-PCM systems.

4.6 Effect of Working Conditions on the Performance of PVT with Nanofluid as Working Fluid

Nanofluids play important role in the efficiency of heat transfer systems. Nanofluids are more efficient in performance as working fluid for heat transfer than water due to their good heat conductivity. Therefore, MWCNT as working fluid is used in this investigation is used additionally to further know the effect of nanofluids on the PVT overall performance as compared to water. In this section, the main findings of the effect of MWCNT water-based nanofluid are presented.

Figure 4.81 presents the effect the of weight fraction on the thermal efficiency of PVT. From the Figure 4.81, it is observed that there is the difference in output temperature due to weight fraction. It shows that the difference in output temperature does not greatly changes after 0.75 weight fraction. However, the overall difference can be seen from 0 means water to 1 weight fraction of MWNCT nanofluid, which is about 2°C temperature difference. Therefore, further study is carried out on the basis of 0.75% weight fraction of MWCNT as working fluid to avoid flow resistance due to the viscosity at a higher concentration of nanofluid (Fayaz et al., 2018).

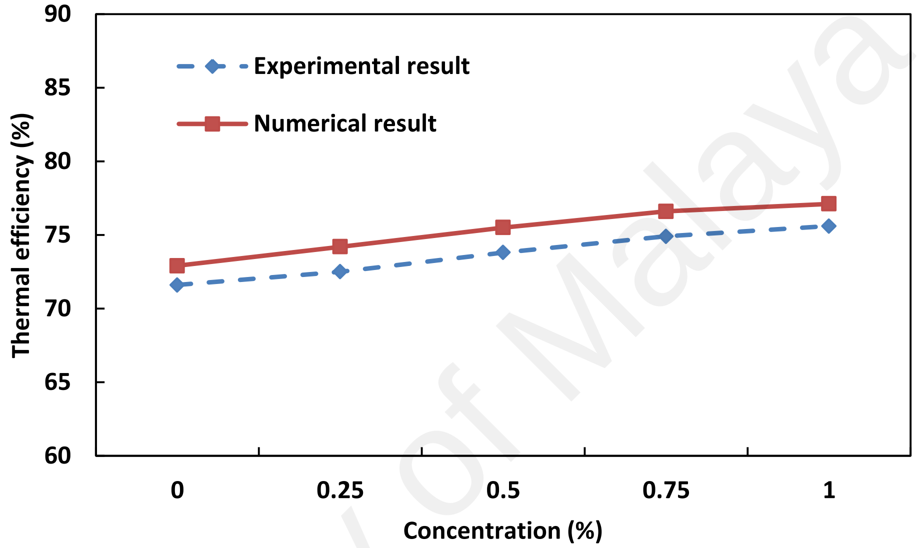

Figure 4.81: Effect of weight fraction on thermal efficiency of working fluid

Figure 4.82 depicts the effect of mass flow rate on the electrical efficiency of PVT. As seen from the figure, electrical efficiency enhances with the increment in mass flow rate in both numerical and experimental results. Nanofluid as working fluid in the PVT transfers heat effectively from PV module. Reduction in cell temperature causes the improved PV electrical performance. Therefore, electrical performance for PVT improves due to heat removal from the PV panel along with thermal energy gain. At each increase in 0.5 LPM of the mass flow rate, the increase in electrical efficiency is achieved as 0.42 and 0.43%. Similarly, (Sardarabadi and Passandideh-Fard, 2016) used water-based nanofluid such as ZnO/water for the enhancement of electrical efficiency of about 0.02% per 2% decrease in cell temperature. There is the difference in each nanofluid due to their different thermo-physical properties. Therefore, results are different but overall increase in efficiency is found due to a drop in cell temperature of the PV module.

The thermal efficiency of PVT with respect to the effect of mass flow rate is given in Figure 4.83. Significant gain of thermal efficiency is achieved at 0.5 to 1 LPM. However, gain in thermal efficiency continues further till 2 LPM but slightly lesser than 0.5 LPM to1 LPM. The effect of nanofluids use on thermal efficiency is also done by (Maadi et al., 2017) where 14.98% increase in thermal energy is achieved for TiO_2 as compared to pure water. These results show that nanofluids are always significant candidates for the enhanced thermal energy performance of the PVT systems. However, the rate of thermal energy achievement over pure water depends on the type of nanofluid and its weight fraction in the solution along with its base fluid.

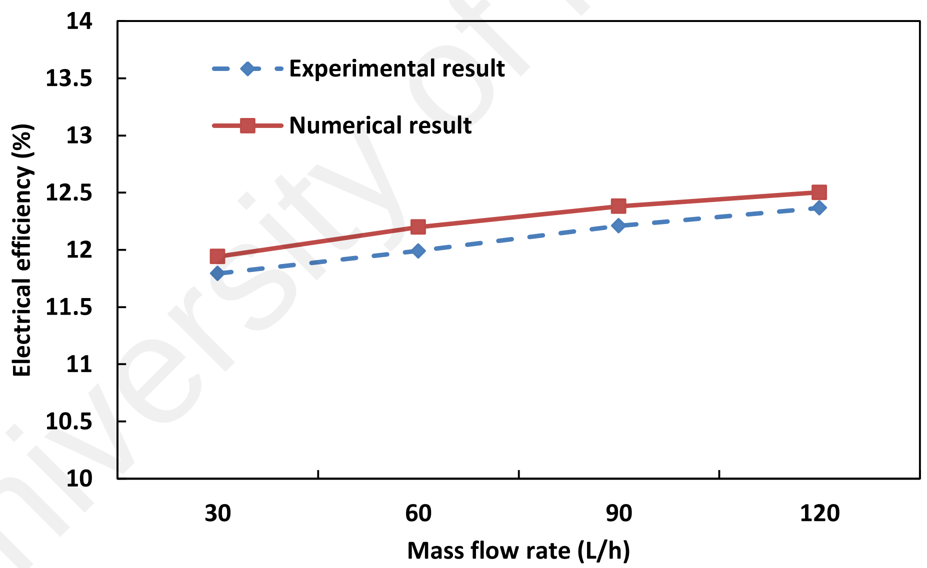

Figure 4.82: Mass flow rate effect on the electrical efficiency of PVT

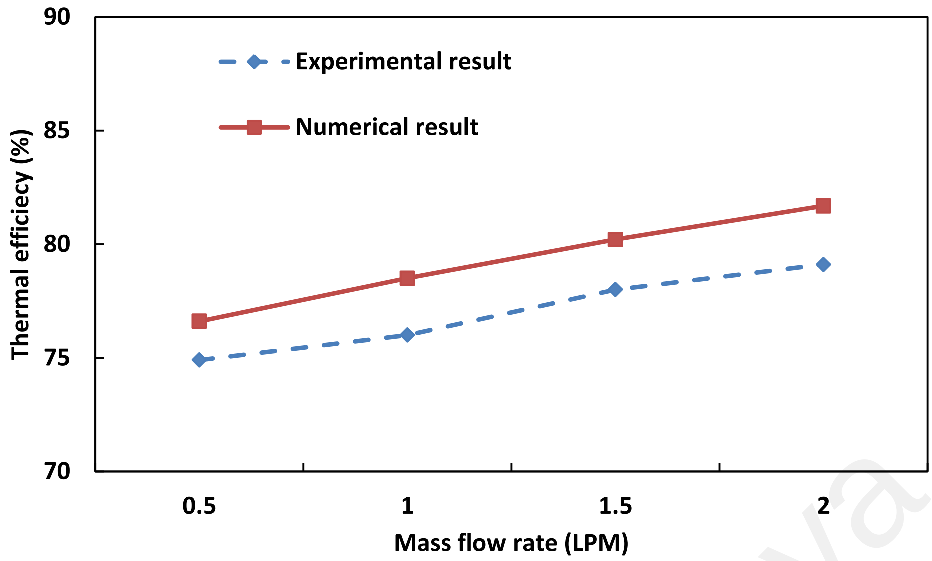

Figure 4.83: Effect of mass flow rate on the thermal efficiency of PVT

The PVT system overall efficiency run on nanofluid as working fluid is shown in figure 4.84. Results of the PVT overall efficiency run on working fluid as water is also added here to compare the results of nanofluid and water effect. The results indicate that prominent difference is gained by MWCNT nanofluid run PVT system than the PVT system using water as working fluid. Numerical maximum values for PVT run on water are 92% whereas, MWCNT based PVT system achieves 94% overall efficiency approximately (Fayaz et al., 2018).

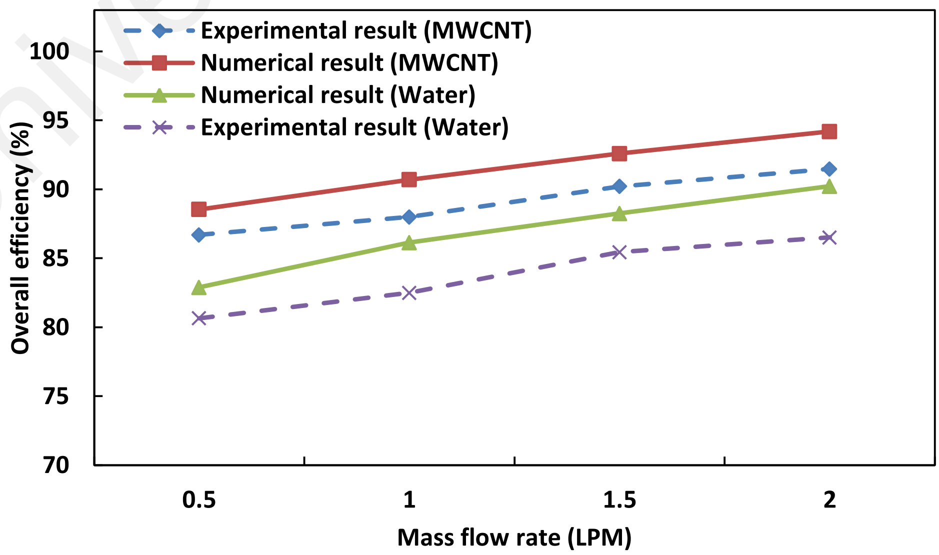

Figure 4.84: Mass flow rate effect on the overall efficiency PVT

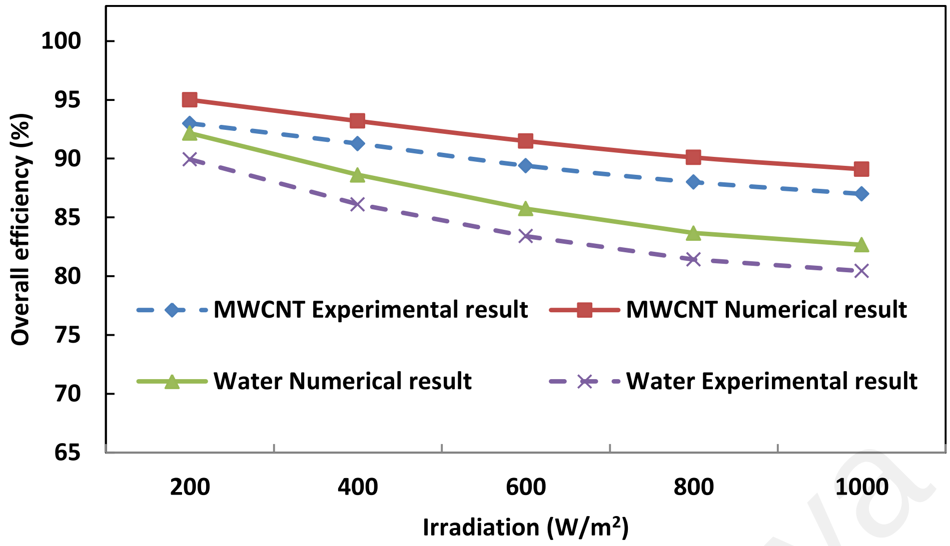

Figure 4.85: Irradiation effect on the overall efficiency

Figure 4.85 shows the results of overall efficiency of PVT run on nanofluid and water separately with respect to the effect of irradiations. Solar irradiations intensities are changed from 200 W/m^2 to 1000 W/m^2 for analysis of expected performance change of PVT system. It can be seen that at 200 W/m^2 results of nanofluid and water are not at the great difference. However, at increasing solar irradiations the difference little bit increases, which is due to the reason that nanofluids are more efficient and highly conductive as compared to simple water that they conduct heat from PVT to output source with lesser time and efficiency drop. It can be concluded that with nanofluid use in PVT, stable performance at higher solar irradiations can be achieved with less heat losses to the environment as compared to water (Nasrin et al., 2018b).

4.7 Conclusion

In this chapter, all the results achieved form numerical and experimental investigations after post-simulation processing and reduction of data are presented and discussed thoroughly. Effect of varying solar irradiations and mass flow rates on systems is investigated. The temperature profile of the systems is discussed in terms of surface and streamlines temperature of the collector. Electrical and thermal performances are investigated with the effect of solar irradiation and mass flow rates for both the indoor and outdoor cases. Firstly, the indoor investigation is presented, which shows the significant improvement of the electrical performance of PV after its cooling in terms of PVT and PVT. However, PVT-PCM provides better results of electrical performance of PV module than the PVT system. NWCNT/water used as working fluids yield better results as compared to water for the same working conditions. Secondly, outdoor investigation is also carried out where the results are different than the indoor investigation due to different environmental conditions. However, similar comparison results are achieved between the systems as compared to the indoor investigation. The detailed conclusion of the results and discussion is provided in the fifth chapter.

CHAPTER 5: CONCLUSION

5.1 Introduction

In this investigation, performance evaluation of all the systems has been done numerically and is validated experimentally. The experimental validation of numerical results is carried out at indoor controlled conditions and outdoor natural weather conditions with passive flow circuit of water employing overhead tank scheme at 27°C and 32°C ambient and inlet temperatures for indoor and outdoor cases respectively. The following findings have been concluded from the investigation:

5.1.1 Indoor Investigation

- Maximum cell temperature of the PV module is obtained as 79°C and 44°C in numerical case and in the experimental case, it is achieved as 82°C and 46.9°C for minimum and maximum irradiations set in this study.
- At above cell temperatures, numerical electrical efficiency is achieved as 11.35% and 13.71% and, experimentally, 11.15% and 13.52% electrical efficiency is achieved at minimum and maximum irradiations set in this study.
- Comparison between PVT and PVT-PCM cell temperature reduction is achieved as 91.9% and 70.9% numerically at 1000 W/m^2 and 200 W/m^2 respectively. Whereas, in the experimental case, 180% and 66% for the PVT-PCM system, which is more efficient as compared to PVT at 1000 W/m^2 and 200 W/m^2 respectively.
- The cell temperature reduction analysis due to PVT and PVT-PCM shows that PVT-PCM is higher in performance as compared to PVT as it reduces maximum cell temperature from the PV module.
- The overall efficiency of PVT is greater than PVT-PCM due to the major portion of overall efficiency consists of thermal efficiency, which is higher for

the PVT system as compared to PVT-PCM. However, the electrical efficiency of PVT-PCM is higher than PVT system. Overall efficiency is achieved as 6.6% and 5.5% numerically at 1000 W/m^2 and 200 W/m^2 respectively. Whereas, in the experimental case, 6.4% and 4.4% more efficient at 1000 W/m^2 and 200 W/m^2 respectively.

- In the case of mass flow rate effect, overall comparative efficiency is achieved as 10.93% and 12.5% numerically at 0.5 LPM and 3 LPM respectively greater than PVT-PCM. Whereas, in the experimental case, 10.4% and 8.99% more efficient at 0.5 LPM and 3 LPM respectively. The overall performance difference between PVT and PVT-PCM is very clear, as experimental as well as numerical results are higher for PVT system.
- In addition, the effect of MWCNT/water on PVT shows the better performance in comparison with PVT working with water as working fluid. The overall efficiency of PVT with MWCNT/water is found as 94 and 91.4% as compared to PVT run on water only which achieves overall efficiency as 90.22 and 86.51% for numerical and experimental results respectively.

5.1.2 Outdoor Investigation

- Maximum cell temperature of the PV module is obtained as 75.1°C and 44°C at 1000 W/m^2 and 200 W/m^2 respectively in numerical case. Whereas, in the experimental case, it is achieved as 77°C and 46.3°C at 1000 W/m^2 and 200 W/m^2 respectively.
- At above cell temperatures, numerical electrical efficiency is achieved as 11.62% and 13.79% at 1000 W/m^2 and 200 W/m^2 respectively. Whereas, experimentally, 11.45% and 13.56% electrical efficiency is achieved at 1000 W/m^2 and 200 W/m^2 respectively.

- Comparison between PVT and PVT-PCM cell temperature reduction is obtained as 48.1% and 100% numerically at 1000W/m^2 and 200 W/m^2 respectively. Whereas, in the experimental case, 54.21% and 42.55% for the PVT-PCM system, which is more efficient as compared to PVT at 1000 W/m^2 and 200 W/m^2 respectively.
- Comparison between PVT and PVT-PCM electrical efficiency increment is achieved as 50% and 2.16% numerically at 1000 W/m^2 and 200 W/m^2 respectively. Whereas, in experimental case, 59.25% and 77.77% more efficient PVT-PCM system as compared to PVT at 1000 W/m^2 and 200 W/m^2 respectively.
- For mass flow rate, overall efficiency difference between PVT and PVT-PCM is achieved as 2.9% and 1% numerically at 0.5 LPM and 3 LPM respectively greater than PVT-PCM. Whereas, in the experimental case, 3.4% and 1.2% more efficient at 0.5 LPM and 3 LPM respectively.

It can be concluded that for electrical efficiency requirements PVT-PCM is a better candidate, whereas, PVT system is suitable where higher thermal energy is required as compared to electrical efficiency. While selecting the system type for the required application, e.g. thermal energy requirement or higher output temperatures or only electrical higher performance regardless of hot water requirement, should really be taken into account. There is an unavoidable compromise on either thermal performance or electrical efficiency of the system if it is about the selection of PVT or PVT-PCM systems.

5.2 Recommendations

In the present investigation, two photovoltaic thermal systems; PVT and PVT-PCM were investigated regarding their competence in electrical and thermal performances in comparison with PV and with each other. After the investigation of the present work, following future work is advised for further research in the field.

- Serpentine design of heat exchanger with maximum length is investigated in the present investigation. However, the same design can be validated with different diameters experimentally along with other materials, e.g. copper, steel etc.
- In this investigation, paraffin wax (A44) PCM is used for heat absorption from PV module latently. There are many other phase change materials available in the market, which can be used to know their capability to store heat and reduce cell temperature of the PV module. Furthermore, aluminium sheets are used as the packaging of phase change materials for maximum heat transfer. However, the difficulty of packaging process is observed with maximum changes of leakage. Therefore, different methods and materials for packaging should be tested.
- Water is the working fluid in the present research. However, nanofluids can be employed as working fluid in the system for maximum heat transfer rate from the PV module in a closed circuit. Refrigerants can also be investigated for thermal performance, which may be used for direct solar refrigeration systems of closed-loop thermal systems only.
- Different thermal heat exchanger designs can be employed on concentrating photovoltaic thermal system for enhanced electrical and high-temperature thermal energy output applications.

5.3 Limitations of the Study

- 3D numerical analysis is for huge systems is time and energy taking. Computers with greater power as compared to commonly office computers are required to compute the huge calculations in time.

- Environmental instability and changing conditions require multiple repetitions of the same experiment and longer time period to validate and get better results.
- Experimental fabrication of PCM bags is a challenge to hold into proper packaging due to their greasy nature.
- Volume expansion of the PCM is another issue due to change temperatures and proper sealing and attachment of bags to the systems must be ensured.

References

Abdunnabi, M., 2012. Optimum values of tank volume to collector area ratios of thermosyphon solar water heaters for Libyan families. Solar Energy and Sustainable Development 1(1), 25-31.

Aelenei, L., Pereira, R., Gonçalves, H., Athienitis, A., 2014. Thermal performance of a hybrid BIPV-PCM: modeling, design and experimental investigation. Energy Procedia 48, 474-483.

Ahmed, F., Al Amin, A.Q., Hasanuzzaman, M., Saidur, R., 2013. Alternative energy resources in Bangladesh and future prospect. Renewable and Sustainable Energy Reviews 25, 698-707.

Al Imam, M., Beg, R., Rahman, M., Khan, M., 2016. Performance of PVT solar collector with compound parabolic concentrator and phase change materials. Energy and Buildings 113, 139-144.

Anderson, T.N., Duke, M., Carson, J.K., 2008. Designing photovolaic/thermal solar collectors for building integration. 16(2), 150-173.

Armstrong, S., Hurley, W., 2010. A thermal model for photovoltaic panels under varying atmospheric conditions. Applied Thermal Engineering 30(11), 1488-1495.

Başoğlu, M.E., Çakır, B., 2016. Comparisons of MPPT performances of isolated and non-isolated DC–DC converters by using a new approach. Renewable and Sustainable Energy Reviews 60, 1100-1113.

Bergene, T., Løvvik, O.M., 1995. Model calculations on a flat-plate solar heat collector with integrated solar cells. Solar energy 55(6), 453-462.

Bertram, E., Glembin, J., Rockendorf, G., 2012. Unglazed PVT collectors as additional heat source in heat pump systems with borehole heat exchanger. Energy Procedia 30(0), 414-423.

Bonyadi, N., Sömek, S.K., Özalevli, C.C., Baker, D., Tarı, İ., 2018. Numerical analysis of phase change material characteristics used in a thermal energy storage device. Heat Transfer Engineering 39(3), 268-276.

Brinkman, H., 1952. The viscosity of concentrated suspensions and solutions. The Journal of Chemical Physics 20(4), 571-571.

Browne, M., Norton, B., McCormack, S., 2015. Phase change materials for photovoltaic thermal management. Renewable and Sustainable Energy Reviews 47, 762-782.

Browne, M.C., Lawlor, K., Kelly, A., Norton, B., Cormack, S.J.M., 2015. Indoor Characterisation of a Photovoltaic/ Thermal Phase Change Material System. Energy Procedia 70, 163-171.

Browne, M.C., Quigley, D., Hard, H.R., Gilligan, S., Ribeiro, N.C.C., Almeida, N., McCormack, S.J., 2016. Assessing the Thermal Performance of Phase Change Material in a Photovoltaic/Thermal System. Energy Procedia 91, 113-121.

Budihardjo, I., Morrison, G.L., 2009. Performance of water-in-glass evacuated tube solar water heaters. Solar Energy 83(1), 49-56.

Cabeza, L.F., Castell, A., Barreneche, C., De Gracia, A., Fernández, A., 2011. Materials used as PCM in thermal energy storage in buildings: a review. Renewable and Sustainable Energy Reviews 15(3), 1675-1695.

Carriere, J., 2013. The Development and Application of a Simplified Thermal Performance Equation for a Sheet-and-tube Photovoltaic Thermal Combi-panel. Queens University, Kingston., 1-170.

Chandrasekar, M., Suresh, S., Senthilkumar, T., 2013. Passive cooling of standalone flat PV module with cotton wick structures. Energy conversion and management 71, 43-50.

Chapin, D.M., Fuller, C., Pearson, G., 1954. A new silicon p-n junction photocell for converting solar radiation into electrical power. Journal of Applied Physics 25(5), 676-677.

Chen, X., Omer, S., Worall, M., Riffat, S., 2013. Recent developments in ejector refrigeration technologies. Renewable and Sustainable Energy Reviews 19, 629-651.

Chong, K.K., Chay, K.G., Chin, K.H., 2012. Study of a solar water heater using stationary V-trough collector. Renewable Energy 39(1), 207-215.

Daghigh, R., Ruslan, M.H., Sopian, K., 2011. Advances in liquid based photovoltaic/thermal (PV/T) collectors. Renewable and Sustainable Energy Reviews 15(8), 4156-4170.

Dupeyrat, P., Ménézo, C., Fortuin, S., 2014. Study of the thermal and electrical performances of PVT solar hot water system. Energy and Buildings 68, Part C(0), 751-755.

Dupeyrat, P., Ménézo, C., Rommel, M., Henning, H.-M., 2011. Efficient single glazed flat plate photovoltaic–thermal hybrid collector for domestic hot water system. Solar Energy 85(7), 1457-1468.

Dwivedi, V., Tiwari, P., Tiwari, S., 2016. Importance of phase change material (PCM) in solar thermal applications: A review, Emerging Trends in Electrical Electronics & Sustainable Energy Systems (ICETEESES), International Conference on. IEEE, pp. 42-45.

Fayaz, H., Nasrin, R., Rahim, N.A., Hasanuzzaman, M., 2018. Energy and exergy analysis of the PVT system: Effect of nanofluid flow rate. Solar Energy 169, 217-230.

Fayaz, H., Rahim, N., Saidur, R., Solangi, K., Niaz, H., Hossain, M., 2011. Solar energy policy: Malaysia vs developed countries, Clean Energy and Technology (CET), 2011 IEEE First Conference on. IEEE, pp. 374-378.

Fayaz, H., Rahim, N.A., Hasanuzzaman, M., Rivai, A., Nasrin, R., 2019. Numerical and outdoor real time experimental investigation of performance of PCM based PVT system. Solar Energy 179, 135-150.

Fiorentini, M., Cooper, P., Ma, Z., 2015a. Development and optimization of an innovative HVAC system with integrated PVT and PCM thermal storage for a net-zero energy retrofitted house. Energy and Buildings 94, 21-32.

Fiorentini, M., Cooper, P., Ma, Z., Robinson, D.A., 2015b. Hybrid model predictive control of a residential HVAC system with PVT energy generation and PCM thermal storage. Energy Procedia 83, 21-30.

Garnett, J.M., 1906. Colours in metal glasses, in metallic films, and in metallic solutions. II. Philosophical Transactions of the Royal Society of London. Series A, Containing Papers of a Mathematical or Physical Character, 237-288.

Gaur, A., Ménézo, C., Giroux--Julien, S., 2017. Numerical studies on thermal and electrical performance of a fully wetted absorber PVT collector with PCM as a storage medium. Renewable Energy 109, 168-187.

Grant, C.D., Schwartzberg, A.M., Smestad, G.P., Kowalik, J., Tolbert, L.M., Zhang, J.Z., 2002. Characterization of nanocrystalline and thin film TiO 2 solar cells with poly (3-undecyl-2, 2′-bithiophene) as a sensitizer and hole conductor. Journal of electroanalytical Chemistry 522(1), 40-48.

Günther, E., Hiebler, S., Mehling, H., Redlich, R., 2009. Enthalpy of phase change materials as a function of temperature: required accuracy and suitable measurement methods. International Journal of Thermophysics 30(4), 1257-1269.

Hasan, A., McCormack, S.J., Huang, M.J., Norton, B., 2014. Energy and cost saving of a photovoltaic-phase change materials (PV-PCM) system through temperature regulation and performance enhancement of photovoltaics. Energies 7(3), 1318-1331.

He, W., Chow, T.-T., Ji, J., Lu, J., Pei, G., Chan, L.-s., 2006. Hybrid photovoltaic and thermal solar-collector designed for natural circulation of water. Applied Energy 83(3), 199-210.

Hinrichs-Rahlwes, R., 2013. Renewable energy: Paving the way towards sustainable energy security: Lessons learnt from Germany. Renewable Energy 49, 10-14.

Hollick, J., Barnes, B., 2007. PV Thermal Systems; Capturing the Untapped Energy, PROCEEDINGS OF THE SOLAR CONFERENCE. AMERICAN SOLAR ENERGY SOCIETY; AMERICAN INSTITUTE OF ARCHITECTS, p. 285.

Hosenuzzaman, M., Rahim, N., Selvaraj, J., Hasanuzzaman, M., Malek, A., Nahar, A., 2015. Global prospects, progress, policies, and environmental impact of solar photovoltaic power generation. Renewable and Sustainable Energy Reviews 41, 284-297.

Hosseinzadeh, M., Sardarabadi, M., Passandideh-Fard, M., 2018. Energy and exergy analysis of nanofluid based photovoltaic thermal system integrated with phase change material. Energy 147, 636-647.

Huang, M., Eames, P., Hewitt, N., 2006. The application of a validated numerical model to predict the energy conservation potential of using phase change materials in the fabric of a building. Solar Energy Materials and Solar Cells 90(13), 1951-1960.

Hust, J.G., Lankford, A.B., 1984. Thermal conductivity of aluminum, copper, iron, and tungsten for temperatures from 1 K to the melting point. National Bureau of Standards, Boulder, CO (USA). Chemical Engineering Science Div.

Ji, J., Pei, G., Chow, T.-t., Liu, K., He, H., Lu, J., Han, C., 2008. Experimental study of photovoltaic solar assisted heat pump system. Solar Energy 82(1), 43-52.

Joshi, A., Tiwari, A., Tiwari, G., Dincer, I., Reddy, B., 2009. Performance evaluation of a hybrid photovoltaic thermal (PV/T)(glass-to-glass) system. International Journal of Thermal Sciences 48(1), 154-164.

Joshi, R., Khandwawala, A., 2014. A comparative study of the effect of variation of inside diameter of condenser and mass flow rate on the heat transfer coefficient in a domestic refrigerator. Journal of Engineering Research and Applications 4(2), 514-518.

Kalogirou, S.A., Tripanagnostopoulos, Y., 2006. Hybrid PV/T solar systems for domestic hot water and electricity production. Energy Conversion and Management 47(18), 3368-3382.

Kamyar, A., Saidur, R., Hasanuzzaman, M., 2012. Application of computational fluid dynamics (CFD) for nanofluids. International Journal of Heat and Mass Transfer 55(15), 4104-4115.

Kazemian, A., Hosseinzadeh, M., Sardarabadi, M., Passandideh-Fard, M., 2018. Experimental study of using both ethylene glycol and phase change material as coolant in photovoltaic thermal systems (PVT) from energy, exergy and entropy generation viewpoints. Energy 162, 210-223.

Kreider, J.F., Kreith, F., 2011. Solar energy handbook. OSTI: 6408304. McGraw-Hill series in modern structures: systems and management, 1120.

Kreith, F., Black, W.Z., 1980. Basic heat transfer. Harper & Row New York.

Kumar, A., Baredar, P., Qureshi, U., 2015. Historical and recent development of photovoltaic thermal (PVT) technologies. Renewable and Sustainable Energy Reviews 42, 1428-1436.

Lausanne, M., Hedingen. , 2000. New generation of hybrid solar PV/T collectors/final report DIS 56360/16868. . Swiss Federal Office of Energy/ Active Solar energy, photovoltaics; .

Lin, W., Ma, Z., Sohel, M.I., Cooper, P., 2014. Development and evaluation of a ceiling ventilation system enhanced by solar photovoltaic thermal collectors and phase change materials. Energy conversion and management 88, 218-230.

Lu, Z., Yao, Q., 2007. Energy analysis of silicon solar cell modules based on an optical model for arbitrary layers. Solar Energy 81(5), 636-647.

Luna-Rubio, R., Trejo-Perea, M., Vargas-Vázquez, D., Ríos-Moreno, G.J., 2012. Optimal sizing of renewable hybrids energy systems: A review of methodologies. Solar Energy 86(4), 1077-1088.

Ma, T., Yang, H., Zhang, Y., Lu, L., Wang, X., 2015. Using phase change materials in photovoltaic systems for thermal regulation and electrical efficiency improvement: A review and outlook. Renewable and Sustainable Energy Reviews 43, 1273-1284.

Maadi, S.R., Kolahan, A., Passandideh-Fard, M., Sardarabadi, M., Moloudi, R., 2017. Characterization of PVT systems equipped with nanofluids-based collector from entropy generation. Energy Conversion and Management 150, 515-531.

Malvi, C., Dixon-Hardy, D., Crook, R., 2011. Energy balance model of combined photovoltaic solar-thermal system incorporating phase change material. Solar Energy 85(7), 1440-1446.

Mekhilef, S., Safari, A., Mustaffa, W.E.S., Saidur, R., Omar, R., Younis, M.A.A., 2012. Solar energy in Malaysia: Current state and prospects. Renewable and Sustainable Energy Reviews 16(1), 386-396.

Meyer, E.L., Busiso, M., 2012. Comparative study of a directly cooled PV water heating system to a naturally cooled module in South Africa, Photovoltaic Specialists Conference (PVSC), 2012 38th IEEE. IEEE, pp. 001296-001299.

Morrison, G.L., 1997. Developments in solar water heating. The Mechanical Engineer, ASME International 4.

Müller-Fürstenberger, G., Wagner, M., 2007. Exploring the environmental Kuznets hypothesis: Theoretical and econometric problems. Ecological Economics 62(3–4), 648-660.

N. Anderson, T., Duke, M., Carson, J., 2008. Designing photovolaic/thermal solar collectors for building integration, 16(2), 150-173 ed.

Nahar, A., Hasanuzzaman, M., Rahim, N.A., 2017. Numerical and experimental investigation on the performance of a photovoltaic thermal collector with parallel plate flow channel under different operating conditions in Malaysia. Solar Energy 144(Supplement C), 517-528.

Nasrin, R., Alim, M., 2014. Finite Element Simulation of Forced Convection in a Flat Plate Solar Collector: Influence of Nanofluid with Double Nanoparticles. Journal of Applied Fluid Mechanics 7(3).

Nasrin, R., Hasanuzzaman, M., Rahim, N.A., 2018a. Effect of high irradiation and cooling on power, energy and performance of a PVT system. Renewable Energy 116(Part A), 552-569.

Nasrin, R., Rahim, N.A., Fayaz, H., Hasanuzzaman, M., 2018b. Water/MWCNT nanofluid based cooling system of PVT: Experimental and numerical research. Renewable Energy 121, 286-300.

Ni, L., Qv, D., Yao, Y., Niu, F., Hu, W., 2016. An experimental study on performance enhancement of a PCM based solar-assisted air source heat pump system under cooling modes. Applied Thermal Engineering 100, 434-452.

Nishioka, K., Hatayama, T., Uraoka, Y., Fuyuki, T., Hagihara, R., Watanabe, M., 2003. Field-test analysis of PV system output characteristics focusing on module temperature. Solar Energy Materials and Solar Cells 75(3), 665-671.

Nordmann, T., Clavadetscher, L., 2003. Understanding temperature effects on PV system performance, Photovoltaic Energy Conversion, 2003. Proceedings of 3rd World Conference on. IEEE, pp. 2243-2246.

Othman, M.Y., Yatim, B., Sopian, K., Bakar, M.N.A., 2007. Performance studies on a finned double-pass photovoltaic-thermal (PV/T) solar collector. Desalination 209(1), 43-49.

Parida, B., Iniyan, S., Goic, R., 2011. A review of solar photovoltaic technologies. Renewable and sustainable energy reviews 15(3), 1625-1636.

Pathak, M.J.M., Sanders, P.G., Pearce, J.M., 2014. Optimizing limited solar roof access by exergy analysis of solar thermal, photovoltaic, and hybrid photovoltaic thermal systems. Applied Energy 120, 115-124.

PCMPRODUCTS, 2018. http://www.pcmproducts.net/

Qazi, A., Fayaz, H., Wadi, A., Raj, R.G., Rahim, N., Khan, W.A., 2015. The artificial neural network for solar radiation prediction and designing solar systems: a systematic literature review. Journal of Cleaner Production 104, 1-12.

Radziemska, E., 2003. The effect of temperature on the power drop in crystalline silicon solar cells. Renewable Energy 28(1), 1-12.

RETScreen, 2011. Solar water heating.

Rohsenow, W.M., Hartnett, J.P., Cho, Y.I., 1998. Handbook of heat transfer. McGraw-Hill New York.

Sandnes, B., Rekstad, J., 2002. A photovoltaic/thermal (PV/T) collector with a polymer absorber plate. Experimental study and analytical model. Solar Energy 72(1), 63-73.

Santbergen, R.Z., RJ Ch, 2008. The absorption factor of crystalline silicon PV cells: a numerical and experimental study. Solar energy materials and solar cells 92(4), 432-444.

Sardarabadi, M., Passandideh-Fard, M., 2016. Experimental and numerical study of metal-oxides/water nanofluids as coolant in photovoltaic thermal systems (PVT). Solar Energy Materials and Solar Cells 157, 533-542.

Sarı, A., Sarı, H., Önal, A., 2004. Thermal properties and thermal reliability of eutectic mixtures of some fatty acids as latent heat storage materials. Energy conversion and management 45(3), 365-376.

Sharma, A., 2011. A comprehensive study of solar power in India and World. Renewable and Sustainable Energy Reviews 15(4), 1767-1776.

Sharma, A., Tyagi, V.V., Chen, C., Buddhi, D., 2009. Review on thermal energy storage with phase change materials and applications. Renewable and Sustainable energy reviews 13(2), 318-345.

Sieminski, A., 2014. International energy outlook. Energy Information Administration (EIA).

Slimani, M.E.A., Amirat, M., Kurucz, I., Bahria, S., Hamidat, A., Chaouch, W.B., 2017. A detailed thermal-electrical model of three photovoltaic/thermal (PV/T) hybrid air collectors and photovoltaic (PV) module: Comparative study under Algiers climatic conditions. Energy Conversion and Management.

Stritih, U., 2016. Increasing the efficiency of PV panel with the use of PCM. Renewable Energy 97, 671-679.

Suganthi, L., Samuel, A.A., 2012. Energy models for demand forecasting—A review. Renewable and Sustainable Energy Reviews 16(2), 1223-1240.

Tian, Y., Zhao, C.-Y., 2013. A review of solar collectors and thermal energy storage in solar thermal applications. Applied Energy 104, 538-553.

Tiwari, G., Mishra, R., Solanki, S., 2011. Photovoltaic modules and their applications: a review on thermal modelling. Applied Energy 88(7), 2287-2304.

Tripanagnostopoulos, Y., Nousia, T., Souliotis, M., Yianoulis, P., 2002. Hybrid photovoltaic/thermal solar systems. Solar Energy 72(3), 217-234.

Tyagi, V.V., Kaushik, S.C., Tyagi, S.K., 2012. Advancement in solar photovoltaic/thermal (PV/T) hybrid collector technology. Renewable and Sustainable Energy Reviews 16(3), 1383-1398.

UFC, u.f.c., 2004. Design: solar heating of buildings and domestic hot water. U.S. ARMY CORPS OF ENGINEERS.

Watson, D., 2011. Designing and building a solar house: your place in the sun. OSTI: 7084852. Book, 282.

Wu, S.-Y., Zhang, Q.-L., Xiao, L., Guo, F.-H., 2011. A heat pipe photovoltaic/thermal (PV/T) hybrid system and its performance evaluation. Energy and buildings 43(12), 3558-3567.

Zakharchenko, R., Licea-Jiménez, L., Pérez-Garcıa, S., Vorobiev, P., Dehesa-Carrasco, U., Pérez-Robles, J., Gonzalez-Hernandez, J., Vorobiev, Y., 2004. Photovoltaic solar panel for a hybrid PV/thermal system. Solar Energy Materials and Solar Cells 82(1), 253-261.

Zalba, B., Marín, J.M., Cabeza, L.F., Mehling, H., 2003. Review on thermal energy storage with phase change: materials, heat transfer analysis and applications. Applied thermal engineering 23(3), 251-283.

Zhangbo, Y., Qifen, L., Qunzhi, Z., Weiguo, P., 2009. The cooling technology of solar cells under concentrated system, Power Electronics and Motion Control Conference, 2009. IPEMC'09. IEEE 6th International. IEEE, pp. 2193-2197.

Zondag, H., Van Helden, W., Bakker, M., Affolter, P., Eisenmann, W., Fechner, H., Rommel, M., Schaap, A., Soerensen, H., Tripanagnostopoulos, Y., 2006. PVT roadmap. A European guide for the development and market introduction of PVT technology.

List of publications and papers

Journal Articles:

1. **Fayaz, H.,** Rahim, N.A., Hasanuzzaman, M., Rivai, A., Nasrin, R., 2019. Numerical and outdoor real time experimental investigation of performance of PCM based PVT system. Solar Energy 179, 135-150. *(Published in Q1)*
2. **Fayaz, H**., Nasrin, R., Rahim, N.A., Hasanuzzaman, M., 2018. Energy and exergy analysis of the PVT system: Effect of nanofluid flow rate. Solar Energy 169, 217-230. *(Published in Q1)*
3. Nasrin, R., Rahim, N.A., **Fayaz, H**., Hasanuzzaman, M., 2018. The water/MWCNT nanofluid based cooling system of PVT: Experimental and numerical research. Renewable Energy 121, 286-300. *(Published in Q1)*
4. **H. Fayaz**, Rahim, N.A, H., Hasanuzzaman. Ahmed Rivai, Rehena Nasrin. Numerical and Experimental Investigation of the Effect of Operating Conditions on Performance of PVT and PVT-PCM. Renewable Energy. *(Under revision in Renewable Energy Journal Q1)*

Conferences Proceedings:

5. **H. Fayaz**, N. A Rahim, R. Saidur, M Hasanuzzaman. Techno-economic Analysıs of Evacuated Tube Solar Water Heater usıng F-chart Method IOP Conference Series: Materials Science and Engineering 358 (1), 012016.
6. **H. Fayaz**, M Hasanuzzaman, N. A Rahim. Solar Energy Transition In Malaysia Through Implementation of PV and PVT Technologies. CEAT2018 International Conference on Clean Energy and Technology.
7. Presented the PVT and PVT-PCM project at UMPEDAC Renewable energy symposium 2017.
8. Presented the PVT and PVT-PCM project at mini-conference at UMPEDAC in 2017 .